Hydrological now- and forecasting

Nederlandse Geografische Studies / Netherlands Geographical Studies

Redactie / Editorial Board
Drs. J.G. Borchert (Editor in Chief)
Prof. Dr. J.M.M. van Amersfoort
Dr. P.C.J. Druijven
Prof. Dr. A.O. Kouwenhoven
Prof. Dr. H. Scholten

Plaatselijke Redacteuren / Local Editors
Dr. R. van Melik,
Faculteit Geowetenschappen Universiteit Utrecht
Dr. D.H. Drenth,
Faculteit der Managementwetenschappen Radboud Universiteit Nijmegen
Dr. P.C.J. Druijven,
Faculteit der Ruimtelijke Wetenschappen Rijksuniversiteit Groningen
Drs. F.J.P.M. Kwaad,
Fysich-Geografisch en Bodemkundig Laboratorium Universiteit van Amsterdam
Dr. L. van der Laan,
Economisch-Geografisch Instituut Erasmus Universiteit Rotterdam
Dr. J.A. van der Schee,
Centrum voor Educatieve Geografie Vrije Universiteit Amsterdam
Dr. F. Thissen,
Afdeling Geografie, Planologie en Internationale Ontwikkelingsstudies Universiteit van Amsterdam

Redactie-Adviseurs / Editorial Advisory Board
Prof. Dr. G.J. Ashworth, Prof. Dr. P.G.E.F. Augustinus, Prof. Dr. G.J. Borger, Prof. Dr. K. Bouwer, Prof. Dr. J. Buursink, Dr. J. Floor, Prof. Dr. G.A. Hoekveld, Dr. A.C. Imeson, Prof. Dr. J.M.G. Kleinpenning, Dr. W.J. Meester, Prof. Dr. F.J. Ormeling, Prof. Dr. H.F.L. Ottens, Dr. J. Sevink, Dr. W.F. Sleegers, T.Z. Smit, Drs. P.J.M. van Steen, Dr. J.J. Sterkenburg, Drs. H.A.W. van Vianen, Prof. Dr. J. van Weesep

ISSN 0169-4839

Netherlands Geographical Studies 379

Hydrological now- and forecasting

Integration of operationally available remotely sensed and forecasted hydrometeorological variables into distributed hydrological models.

J. M. Schuurmans

Utrecht 2008

Royal Dutch Geographical Society /
Faculty of Geosciences, Utrecht University

This publication is identical to a dissertation submitted for the title of Doctor at Utrecht University, The Netherlands. The public defence of this thesis took place on November 28, 2008.

Promotor
Prof. dr. ir. M.F.P. Bierkens, Utrecht University / Deltares, The Netherlands

Co-promotor
Dr. ir. F.C. van Geer, Deltares, The Netherlands

Examination committee
Prof. Dr. W.G.M. Bastiaanssen, Technical University of Delft, The Netherlands
Prof. Dr. G. Blöschl, University of Vienna, Vienna
Prof. Dr. S.M. de Jong, Utrecht University, The Netherlands
Prof. Dr. ir. R. Uijlenhoet, Wageningen University, The Netherlands
Dr. ir. A.H. Weerts, Deltares, The Netherlands

ISBN 978-90-6809-422-0

Copyright © J.M. Schuurmans p/a Faculty of Geosciences, Utrecht University, 2008.

Niets uit deze uitgave mag worden vermenigvuldigd en/of openbaar gemaakt door middel van druk, fotokopie of op welke andere wijze dan ook zonder voorafgaande schriftelijke toestemming van de uitgevers.

All rights reserved. No part of this publication may be reproduced in any form, by print or photo print, microfilm or any other means, without written permission by the publishers.

Printed in the Netherlands by A-D Druk - Zeist.

Contents

Figures **7**

Tables **9**

1 Introduction **11**
1.1 Background 11
1.2 Problem outline and research questions 12
1.3 Thesis focus 14
1.4 Method 15
1.5 Thesis outline 16

2 Automatic prediction of high-resolution daily rainfall fields **17**
2.1 Introduction 18
2.2 Data and data processing 19
2.2.1 Rain gauge network 19
2.2.2 Radar data 21
2.2.3 Event selection 21
2.2.4 Data transformation 22
2.3 Methods 22
2.3.1 Variogram estimation 22
2.3.2 Prediction methods 24
2.3.3 Back transformation and zero Rainfall 27
2.4 Results 29
2.4.1 Variograms 29
2.4.2 Rainfall prediction 34
2.5 Discussion 38
2.6 Conclusions 44

3 Effect of spatial distribution of daily rainfall on interior catchment response of a distributed hydrological model **45**
3.1 introduction 46
3.2 Model and data 47
3.2.1 Study area 47
3.2.2 Hydrological model 48
3.2.3 Meteorological input data 49
3.3 Methods 51
3.3.1 Introduction 51
3.3.2 Rainfall prediction 52
3.3.3 Rainfall scenarios 52
3.4 Results 56
3.4.1 Discharge 56

3.4.2 Groundwater 57
3.4.3 Soil moisture 58
3.5 Conclusions and discussion 61

4 Remotely sensed latent heat fluxes for improving modelled soil moisture predictions: a case study 69
4.1 Introduction 70
4.2 Study area and data 71
4.2.1 Study area 71
4.2.2 Data 72
4.3 Methods 74
4.3.1 Hydrological model 74
4.3.2 SEBAL 78
4.3.3 Data assimilation 79
4.4 Results 84
4.4.1 ET_{act} comparison 86
4.4.2 soil moisture update 86
4.5 Discussion 91
4.6 Conclusions and recommendations 92
4.6.1 Conclusions 92
4.6.2 Recommendations 92

5 Ability to forecast regional soil moisture with a distributed hydrological model using ECMWF rainfall forecasts 95
5.1 Introduction 96
5.2 Method and data 97
5.2.1 Ensemble soil moisture prediction system 97
5.2.2 Study area 97
5.2.3 Hydrological model 98
5.2.4 rainfall data 99
5.3 Results and Discussion 100
5.3.1 ECMWF rainfall accuracy 100
5.3.2 Soil moisture accuracy 105
5.4 Conclusions and outlook 109

6 Synthesis 113
6.1 Added value of meteorological radar 113
6.2 Remotely sensed latent heat fluxes for improving model predictions of soil moisture 115
6.3 Forecasting spatially-distributed soil moisture 117
6.4 HNFS: applications and considerations 118

Appendices 123

Summary 137

Samenvatting 139

Bibliography 142

Dankwoord 149

Publications 152

Curriculum Vitae 154

Figures

1.1	The hydrologic cycle	12
1.2	Spatial and temporal scales of hydrological processes	13
1.3	Hydrological Now- Forecasting System (HNFS)	15
1.4	Location of the two study areas	16
2.1	Locations of weather radars and rain gauges in The Netherlands	20
2.2	Gaussian quantile-quantile plots of normalized non-zero rainfall data	23
2.3	Box-and-whisker plots of the standard deviation of non-zero rainfall	28
2.4	Small-extent normalized variograms of square-root transformed daily rainfall	30
2.5	Medium-extent normalized variograms of square-root transformed daily rainfall	31
2.6	Large-extent normalized variograms of square-root transformed daily rainfall	32
2.7	Automatically fitted ranges of spherical variogram models for all extents	33
2.8	Pooled variogram models of small-, medium-, and large extent	33
2.9	Total rainfall (March-Oct 2004) at small extent according to radar	34
2.10	Composite range corrected radar fields of 4 April 2004 and 1 May 2004	35
2.11	Prediction of rainfall at small extent for 4 April and 1 May 2004	36
2.12	Prediction of rainfall for The Netherlands at 1 May 2004	37
2.13	Box-and-whisker plots of the RMSE for radar and all used kriging methods	39
2.14	Ratio of the RMSE as function of the correlation between rain gauges and radar	40
2.15	Box-and-whisker plots of the mean z-score from the cross validation	41
2.16	Box-and-whisker plots of the variance of the z-score from the cross validation	42
3.1	Location of Lopikerwaard catchment within the Netherlands	48
3.2	Locations of rain gauges and weather radars in the Netherlands	50
3.3	Range of values of total rainfall (March-Oct 2004) for all 8 scenarios	52
3.4	Spatial distribution of total rainfall (March-Oct 2004) of spatial variable scenarios	53
3.5	Hydrographs of pumping station Koekoek for all the rainfall scenarios	54
3.6	Hydrographs of pumping station Hoekse Molen for all the rainfall scenarios	55
3.7	Mean and sd of the average daily discharge for all 4 pumping stations	58
3.8	Development of groundwater level in time of one node for all rainfall scenarios	59
3.9	Spatial pattern of mean groundwater level (March-Oct 2004)	60
3.10	Spatial pattern of temporal sd of groundwater level (March-Oct 2004)	63
3.11	Spatial pattern of rainfall on 1 May 2004 for all rainfall scenarios	64
3.12	Spatial variation of groundwater level on 1 May 2004	65
3.13	Development of soil moisture content in time of one node	66
3.14	Spatial pattern of soil moisture content on 1 May 2004	67
4.1	Surface level, land use and soil types of Langbroekerwetering	72

4.2	Spatial distribution of total rainfall (March-Nov 2006) and time series of the spatial mean of rainfall and the reference evapotranspiration	73
4.3	Feddes evaporation reduction function	76
4.4	Time series of modelled and measured VMC per location	77
4.5	Bubble plot of bias in phreatic and confined groundwater during 2001 - 2006	78
4.6	Time series of error in ET_{act} for each soil moisture measurement location	85
4.7	Example of the critical threshold of FR_{new}	85
4.8	Spatial plot of $ET_{act}$and ET_{pot} as derived by SEBAL and by METASWAP for 8 June 2006	87
4.9	Same as Figure 4.8 but for 17 July 2006	87
4.10	Spatial plot of update scenarios of our data assimilation method	89
4.11	Spatial difference of the root zone storage between unperturbed and updated model run	90
5.1	Surface level, land use and soil types of Langbroekerwetering	98
5.2	Spatial distribution of total rainfall (March-Nov 2006) and time series of the spatial mean rainfall and the reference evapotranspiration	100
5.3	Difference in rainfall due to the difference in time span between the forecasts and the measured rainfall	101
5.4	Cumulative rainfall distribution of the measured (spatial mean) and the forecasted (ensemble mean) rainfall per lead time	101
5.5	Percentage of days as function of rainfall amount for the measured (spatial mean) and forecasted rainfall per lead time	102
5.6	Rainfall forecast statistics per lead time	103
5.7	Categorical measures of skill for detecting rainfall	104
5.8	Temporal mean bias in root zone storage during March-Nov for soil moisture forecast system 1	106
5.9	Same as Figure 5.8 but then for soil moisture forecast system 2	107
5.10	Box-and-whisker plots of spatial distribution of bias in root zone storage per lead time	107
5.11	Time series of root zone storage for one SVAT-unit for 4 lead times	108
5.12	Schematic representation of the loss of information content in forecasts	111
6.1	Example of practical application HNFS	119
2	Photo of rain gauge calibration.	123
3	Calibration of rain gauges	124
4	Simulated rainfall fields	127
5	Cumulative distribution function of simulated rainfall and rain gauges	128
6	Photo of soil moisture sensor calibration.	130
7	Calibration of soil moisture sensors	130
8	Transmissivity (kD) and resistance (c) values of hydrological model	132

Tables

2.1	Parameters of fitted pooled spherical variogram models	29
3.1	Percentage of days (March-Oct 2004) the discharge threshold value is exceeded	56
4.1	Description of soil types within study area	71
4.2	Root zone thickness, crop factors and predefined pressure heads of Feddes curve for the land use types within the study area	76
4.3	Soil physical (Van Genuchten) parameters of the soils in the study area	84
4.4	Standard error of the model based ET_{act} per measurement location	84
4.5	Comparison between ET as derived by SEBAL and METASWAP	88
4.6	Percentage METASWAP nodes for each soil moisture update scenario	88
5.1	Description of soil types within study area	99
5.2	Total rainfall (March-Nov 2006) according to measurements and forecasts for lead time 1-9 days	102
5.3	Categories of rainfall prediction used to calculate categorical measures of skill	104
5.4	Spatial mean bias, RMSE and MAE for both soil moisture forecast systems	109

What we're talking about is late night and early morning low clouds
with a chance of fog, chance of showers into the afternoon
with variable high cloudiness and gusty winds
Gusty winds at times around the corner of Sunset and Alvorado
Yeah, I know, things are tough all over
When the thunder storms start increasing over the
Southeast and South Central portions of my apartment, I get upset
And a line of thunderstorms was developing in the early morning
ahead of a slow moving coldfront, cold blooded
with tornado watches issued shortly before noon Sunday
for the areas including the western region of my mental health
and the northern portions of my ability to deal rationally
with my disconcerted precarious emotional situation
It's cold out there
Colder than a ticket taker's smile at the Ivar Theatre, on a Saturday night
Flash flood watches covered the southern portion of my disposition, yeah
There was no severe weather well into the afternoon
except for kind of a lone gust of wind in the bedroom
A high pressure zone covering the eastern portion of a small
suburban community with a 1034 millibar high pressure zone
and a weak pressure ridge extending from my eyes down to my cheeks
cause since you left me baby and put the vice grips on my mental health
well, the extended outlook for an indefinite period of time
until you come back to me, baby, is high tonight, low tomorrow
and precipitation is expected
Emotional Weather Report-Tom Waits

1 Introduction

1.1 Background

The hydrologic - or water– cycle is the continuous movement of water between the earth and the atmosphere, which plays an important role in our climate system (Figure 1.1). When precipitation (e.g. rain, snow) reaches the land surface, it becomes of interest for hydrologists. On the land surface it can either collect on the land and become surface water (e.g. streams, rivers, lakes) or infiltrate to become soil moisture or even percolate further to the groundwater reservoir. Continuously, water is also released back to the atmosphere via evapo(transpi)ration (from soil, vegetation, streams and oceans). How precipitation is distributed over the different hydrological variables (e.g. surface water discharge, soil moisture, groundwater) depends on the spatial and temporal variability of precipitation, the land surface characteristics and on the current hydrological state of the land surface. All these hydrological processes have their own spatial and temporal scale (Figure 1.2). Considering the hydrologic cycle, the linkage between hydrology and meteorology is evident. As science moves on and new techniques are developed within both disciplines, continuous feedback between them is of great importance and can be mutually beneficial. Meteorologists need expertise from hydrologists about the unsaturated zone to improve their climate models. On the other hand meteorologists can provide hydrologists with valuable hydrometeorological information like precipitation fields from radar, evapotranspiration fields from satellites and weather (temperature, rainfall, wind) forecasts.

Computer simulation models that simulate (part of) the hydrological cycle are an important tool for hydrologists to understand and describe the hydrological system. If these models succeed in achieving accurate results, they can predict what happens to the hydrological system if for example climate (e.g. precipitation, evaporation) or water management and land use changes: the so-called scenario analysis. In the last 30 years the number but also the complexity of hydrological computer models has grown tremendously, due to more powerful computers, geographical information systems (GIS) and remote sensors (Bergström and Graham, 1998). Catchment models can be classified as physically-based or conceptual (semi-empirical), depending on the degree of complexity and physical completeness in the formulation of the structure (Beven, 1989; Refsgaard, 1996, 1997; Refsgaard and Henriksen, 2004). Furthermore, models are classified as lumped or distributed depending on the degree of discretisation when describing the terrain in the basin. A distributed hydrological model

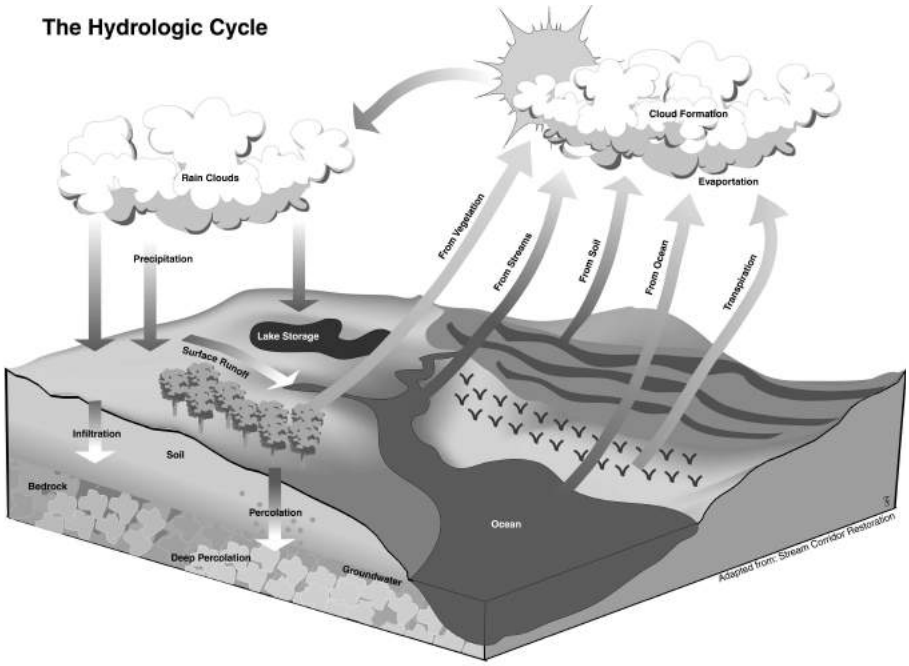

Figure 1.1 The hydrologic cycle, a schematic overview of the continuous movement of water between earth and atmosphere (by Tom Schultz, Department of Natural Resource Ecology and Management (NREM), Iowa State University).

is defined by Reed et al. (2004) as "any model that explicitly accounts for spatial variability inside a basin and has the ability to produce simulations at interior points without explicit calibration at these points". Today, most hydrological models are distributed to some degree.

1.2 Problem outline and research questions

As more spatially-distributed information about land surface characteristics becomes available and computer capacity increases, the distributed hydrological models are also developed at higher spatial resolutions. Potentially, these high resolution models can give us insight into the hydrological processes in more detail. However, a major problem plaguing these high-resolution models is over-parameterization and lack of validation resources. At the same time, hydrometeorological information based on remote sensing techniques like meteorological rainfall radar and evapotranspiration derived from satellites has become more easily available and its quality has greatly improved over the years. These operational spatially-distributed data can serve as improved input and validation data for distributed hydrological models and could improve the accuracy of these models. Accuracy in this thesis is defined as "faithful measurement" or "representation of the truth", not in the mathematical sense of precision.

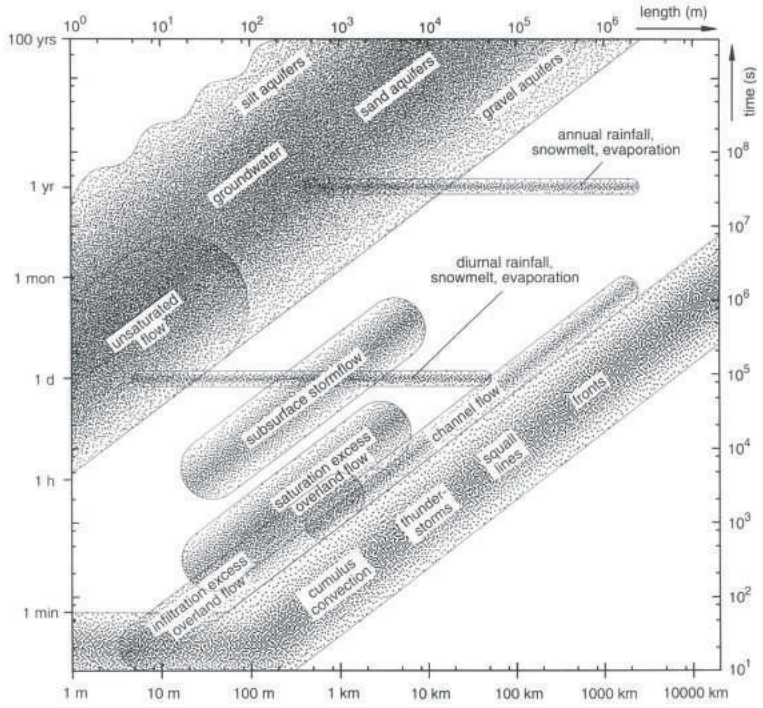

Figure 1.2 Schematic relationship between spatial and temporal process scales for a number of hydrological processes (Blöschl and Sivapalan, 1995; Grayson and Blöschl, 2000)

Meteorologists are also developing and improving numerical weather prediction models (NWPs) that provide (among other variables like wind, temperature) rainfall forecasts. Typical of these forecast data is that they consist of a number of model outcomes that are all equally likely to occur (Persson, 2001). These so called "ensemble members" provide insight into the reliability of the model outcomes. Reliability is this thesis is defined as "trustworthy" or "consistency": if the ensemble members show a small spread they are more reliable than if they show a large spread. The ensemble members of NWPs could be used by hydrologists to make forecasts of the hydrological system and provide insight into the reliability of the model outcomes. However, in practice these data are not commonly used by hydrologists. Reasons for this lack of use are outstanding questions of which the following form the *research questions* of this thesis:

1. What is the added value of meteorological radar with respect to rain gauges?
2. What is the effect of spatial variability of daily rainfall on modelled interior catchment response?
3. Can remotely sensed evapotranspiration improve the accuracy of the prediction of spatially-distributed soil moisture by a distributed hydrological model?
4. Is it feasible to accurately predict the spatial distribution of soil moisture by using rainfall forecasts of a numerical weather prediction model as input for a

distributed hydrological model, and, if so, up to how many days?

Furthermore a coherent framework to integrate hydrometeorological variables into spatially-distributed models does not exist. Therefore the Hydrological Now- And Forecasting System (HNFS) was developed (Figure 1.3). Three major parts can be distinguished within this system.

- improved model input (e.g. high resolution distributed rainfall)
- assimilation of observed hydrological variables that are available on an irregular basis in order to improve the accuracy of the model (e.g. remotely sensed data from satellites)
- implementation of forecasted input variables (e.g. rainfall forecasts) in order to obtain forecasts of the hydrological system.

To answer the research questions fieldwork had to be done in order to obtain input as well as validation data. Besides, software tools for the HNFS system had to be developed.

1.3 Thesis focus

This thesis focusses on physically based spatially-distributed hydrological models. Moreover, existing model codes are used and models which are operational. It is the scope of this thesis to investigate (i) whether operational remote sensing data that provide spatially-distributed hydrological information can improve the accuracy of these models and (ii) whether rainfall forecasts could provide accurate forecasts of the hydrological model. It is not the scope of this thesis to calibrate these models.

Within the hydrological system, this thesis focusses on soil moisture as hydrological variable. Insight into the spatial distribution of soil moisture within a catchment is of great interest for e.g. farmers and water boards. Accurate prediction of its current and short- to medium- term ($\sim$ 9 days) spatial distribution (i.e. now- and forecasting), is helpful for optimizing irrigation gifts, hydrological drought forecasting and the assessment of catchment wetness for flood control. Moreover, for climate models insight into the spatial distribution of soil moisture is of importance because of its influence on the partition of the components of the energy balance of the earth surface.

Operational remote sensing data embraces an enormous amount of data. In this thesis we focus on (i) daily rainfall fields from meteorological radar and (ii) thermal satellite images in association with a surface-energy-balance-algorithm that provides daily fields of latent heat flux (i.e. evapotranspiration).

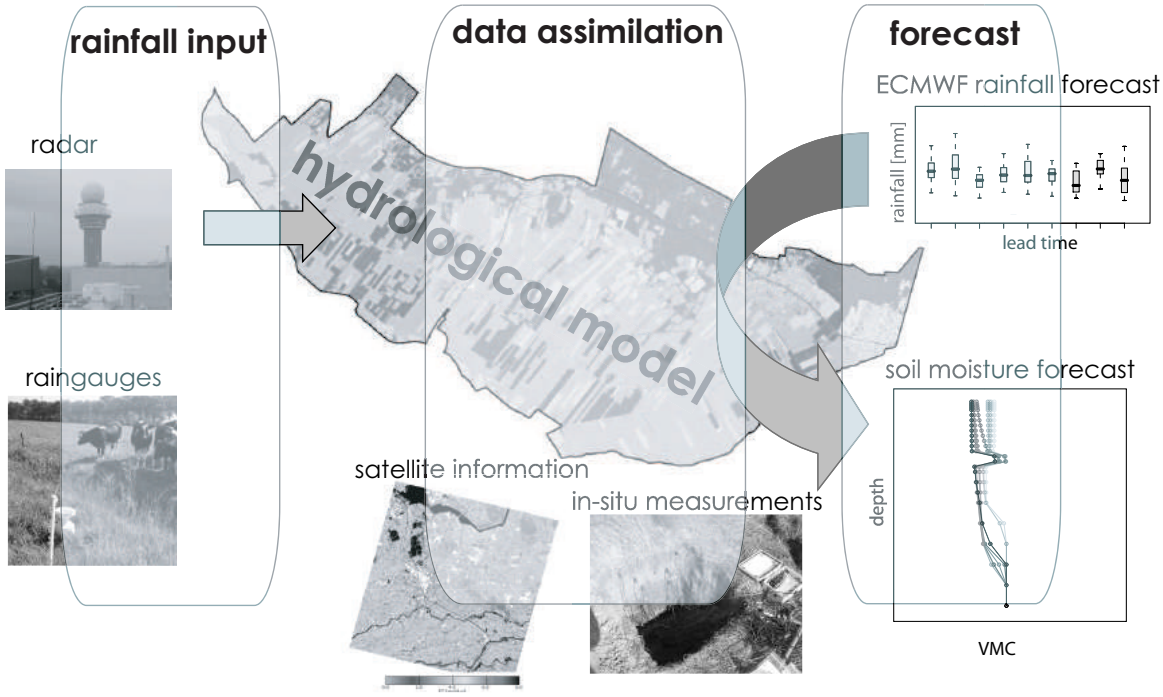

Figure 1.3 Hydrological Now- Forecasting System (HNFS)

1.4 Method

To be able to answer the research questions 1 and 2, the spatial small scale variability of daily rainfall was studied during 2004 within the area "Lopikerwaard" (135 km^2: Figure 1.4), using a dense network of 30 rain gauges. Meteorological radar data, as well as data from the country wide network of rain gauges were supplied by the Royal Netherlands Meteorological Institute (KNMI). To investigate the added value of meteorological radar, we applied three different geostatistical methods to develop high-resolution daily rainfall fields with either rain gauges only or a combination of rain gauges and meteorological rainfall radar. The effect of spatial variability of daily rainfall on modelled interior catchment response was studied by applying several rainfall input scenarios to an operational distributed hydrological model of the Lopikerwaard. Because the Lopikerwaard has homogenous land surface characteristics and due to shallow groundwater tables evapotranspiration reduction rarely occurs, this area was less interesting to investigate research question 3. Therefore, the area "Langbroekerwetering" (70 km^2: Figure 1.4) was chosen. This area is located along the rim of the Holocene Rhine-Meuse delta (Berendsen and Stouthamer, 2000), which onlaps coversands and sandur outwash deposits in front of a Saalian ice-pushed ridge (Busschers et al., 2007). Within this area there is a large variability in elevation, soil type and land use. To be able to generate accurate high-resolution rainfall fields a network of 15 rain gauges was set up within this area. To investigate whether remotely sensed evapotranspiration can improve the prediction of spatially-distributed soil moisture by a distributed hydrological model, we used an operational hydrological model that

Figure 1.4 Location of the two study areas within The Netherlands: Lopikerwaard (135 km^2) and Langbroekerwetering (70 km^2).

was based on a recently developed model code (METASWAP) and satellite images (from two different satellites for the same two days in 2006) that were transformed into evapotranspiration fields using an often-used surface energy balance algorithm (SEBAL). At 5 locations the soil moisture was measured at variable depth in order to retrieve validation data for METASWAP. To study the feasibility to accurately predict the spatial distribution of soil moisture by using rainfall forecasts of a NWP, we used ensemble rainfall forecasts from the European Centre for Medium-Range Weather Forecasts (ECMWF) during the period March-November 2006 that were provided by the KNMI. These rainfall forecasts were used as input for the hydrological model of the Langbroekerwetering. Model outcomes of the forecasted spatially-distributed soil moisture up to 9 days ahead were compared with model runs that used measured rainfall as input.

1.5 Thesis outline

The formulated four research questions are addressed in subsequent chapters. Each chapter is based on an article that has been published or submitted to an international peer reviewed journal. This means that the chapters have their own introduction and end with conclusions. In Chapter 6 the main results of this dissertation are given and these are placed and discussed in a broader perspective. Also some practical applications of the HNFS are shown and some considerations about future catchment modelling are given. This introduction together with Chapter 6 can be read independently and should provide the reader with the main results of this dissertation.

2 Automatic prediction of high-resolution daily rainfall fields for multiple extents: the potential of operational radar

Schuurmans, J.M, M.F.P. Bierkens, E.J. Pebesma & R. Uijlenhoet (2007), Automatic prediction of high-resolution daily rainfall fields for multiple extents: the potential of operational radar. Journal of Hydrometeorology 8, pp. 1204 - 1224

Abstract

This study investigates the added value of operational radar with respect to rain gauges in obtaining high-resolution daily rainfall fields as required in distributed hydrological modelling. To this end we combine data from the Netherlands operational national rain gauge network (330 gauges nation wide) with our own experimental network (30 gauges within 225 km^2). Based on 74 selected rainfall events (March-October 2004) the spatial variability of daily rainfall is investigated at three spatial extents: small (225 km^2), medium (10,000 km^2) and large (82,875 km^2). From this analysis it is shown that semivariograms show no clear dependence on season. Predictions of point rainfall are performed for all three extents using three different geostatistical methods: (i) ordinary kriging (OK; rain gauge data only), (ii) kriging with external drift (KED) and (iii) ordinary colocated cokriging (OCCK), the latter two using both rain gauge data and range-corrected daily radar composites - a standard operational radar product from the Royal Netherlands Meteorological Institute (KNMI). Focus here is on automatic prediction. For small extent rain gauge data alone perform better than radar while for larger extents with lower gauge densities radar performs overall better than rain gauge data alone (OK). Methods using both radar and rain gauge data (KED and OCCK) prove to be more accurate than using either rain gauge data alone (OK) or radar, in particular for larger extents. The added value of radar is positively related to the correlation between radar and rain gauge data. Using a pooled semivariogram is almost as good as using event-based semivariograms, which is convenient if the prediction is to be automated. An interesting result is that the pooled semivariograms perform better in terms of estimating the prediction error

(kriging variance) especially for the small- and medium extent, where the number of data points to estimate semivariograms is small and event-based semivariograms are rather unstable.

2.1 Introduction

Rainfall is the main input variable for hydrological models. Hydrologists use spatially-distributed hydrological models to gain insight into the spatial variability of soil moisture content, groundwater level as well as the discharge of catchments. As the spatial information on surface elevation, land use and soil properties increases, hydrologists increase the spatial resolution of these models. However, up to now the spatial resolution of the rainfall input information lags behind. To properly model soil moisture content and groundwater level at high-resolution, hydrologists require rainfall information to be at high-resolution as well.

The rainfall information that is readily available for hydrologists in The Netherlands comes from both rain gauges and meteorological radar. All the rainfall data are collected and distributed by the Royal Netherlands Meteorological Institute (KNMI). There are two rain gauge networks, of which the network with the highest density has approximately 1 gauge per 100 km^2 with daily rainfall measured. The operational radar product employed in this research is a processed composite field of daily rainfall with a resolution of 2.5 km $\times$ 2.5 km from two C-band Doppler radars.

If *operationally available* rainfall data, i.e. rainfall fields from radar and rain gauge data, could be used to predict high-resolution rainfall automatically, hydrologists would probably be more willing to use these in their modelling. In this study we therefore focus on using operational radar products that can be readily obtained from the KNMI over the internet. Moreover, we concentrate on prediction procedures that can be *automated*, i.e. they have to be reliable and robust such that without additional intervention daily predictions are guaranteed. Of course, at the same time the resulting predictions have to be sufficiently accurate to be of any use.

Consequently, the main objective of this study is to provide for automatic prediction of rainfall at a high (within a radar pixel) spatial resolution using operational daily rainfall products. Our most important research question is: what is the added value of operational radar with respect to rain gauges in terms of rainfall prediction?

To predict at a high spatial resolution we need information about the spatial variability of daily rainfall at a small extent. Therefore we have set up an experimental high density rain gauge network of 30 rain gauges within an area of 225 km^2 in the middle of the Netherlands. Although we know that there is a space-time correlation in rainfall we restrict ourselves to daily rainfall for two reasons. First, within the Netherlands we have a relatively slow hydrological response to stratiform-dominated rainfall, which means that a temporal resolution of one day is already very informative. Second, the operational radar products we use in this study are available at a daily time step. We selected 74 rainfall events and studied for each event the spatial

variability of rainfall at three different extents: the small- (225 km^2), medium- (10,000 km^2) and large- (82,875 km^2) extent, i.e. the meso-γ and meso-β scale (Orlanski, 1975). We used three geostatistical prediction methods, one using rain gauge data only and the other two combining rain gauge and radar data, and compared the results.

The organization of this chapter is as follows. In Section 2.2 we describe the data and the event selection procedure. In Section 2.3 the methods are described, starting with variogram modelling, followed by the three geostatistical prediction methods used. The results are given in Section 2.4, starting with the variography (i.e. spatial variability) of rainfall, followed by a case study to show the prediction methods used and finally the cross-validation results are shown. Section 2.5 deals with the uncertainties of this study. In Section 2.6 we summarize the main conclusions.

2.2 Data and data processing

2.2.1 Rain gauge network

We used two different kinds of rain gauge networks; one permanent network which is operated by the Royal Netherlands Meteorological Institute (KNMI) and one experimental network. Figure 2.1 shows the location of all the rain gauges of these two networks. The largest network consists of 330 stations and has a density of approximately 1 station per 100 km^2. This network is maintained by volunteers who report the rainfall depth daily at 0800 UTC. These data are available on-line at the KNMI .

The experimental high-density network consists of 30 tipping bucket rain gauges within an area of 225 km^2 in the central part of the Netherlands. The choice for this particular area was based on the fact that several other hydro-meteorological experiments are ongoing within this area as well (Cabauw Experimental Site for Atmospheric Research-CESAR), which may be mutually beneficial. Different from the HYREX (HYdrological Radar EXperiment), which took place in the UK between May 1993 and April 1997 (Moore et al., 2000), the purpose of our network was not to give the best estimate of mean rainfall over a radar pixel but in addition to asses the small-extent variability of rainfall, i.e. to estimate the semivariograms of the rain fields, in particular for short lag distances. Therefore, at five locations two rain gauges were placed at very close distance (1-5 meter) from each other, a setup that is also recommended by Krajewski et al. (2003). The rest of the gauges were set up in such a way that we had many different inter-gauge distances. Krajewski et al. (2003) state that knowledge of rainfall structure at spatial extents between a few meters and a few kilometers is still poor. The operational rain gauge network in the Netherlands only gives information for distances larger than approximately 10 km, which implies that prediction of high-resolution rainfall fields (smaller than 10 km) is very uncertain. Our high density experimental network can be compared with the high density networks of HYREX, which had 49 tipping bucket rain gauges within 132 km^2 (Moore et al., 2000), and the network of Iowa Institute of Hydraulic Research, which has 15

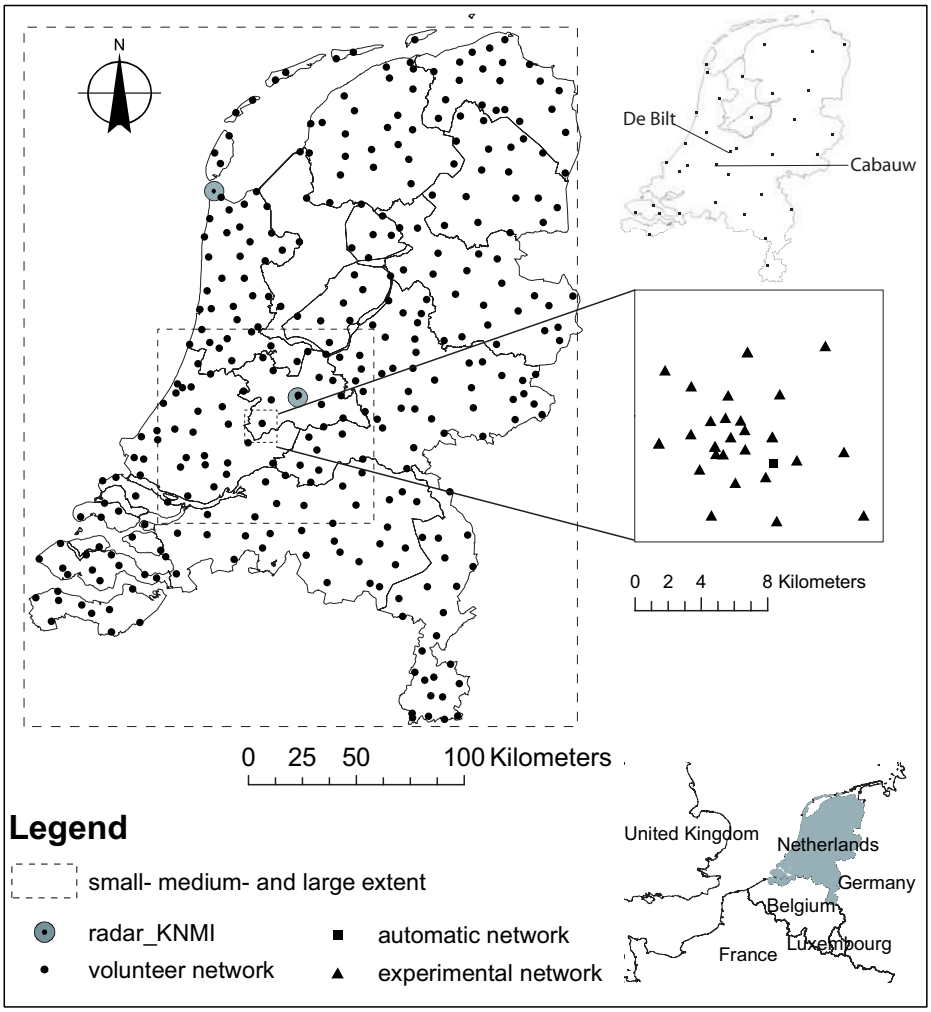

Figure 2.1 Locations of weather radars and rain gauges in The Netherlands: 2 C-band Doppler radars, volunteer network with 330 rain gauges (temporal resolution of 1 day), automatic network with 35 tipping bucket rain gauges (temporal resolution of 10 minutes) and experimental network with 30 tipping bucket rain gauges (equipped with event loggers). The three spatial extents studied are also shown.

rain gauges with separation distances ranging from 10-1000 meters (Krajewski et al., 1998). Our network is therefore unique in The Netherlands and provides valuable information on the spatial structure of rainfall at short distances.

For the experimental network we used ARG100 tipping buckets (developed by the Centre for Ecology and Hydrology in the UK), which are designed to reduce their sensitivity to wind speed and direction, through their aerodynamic design. We placed the rain gauges in open area, free from obstacles. All gauges were equipped with event loggers, that record the momentary tipping event, storing the time and date of each event with a time resolution of 0.5 seconds. The nominal rainfall accumulation per tipping was 0.2 mm, but a laboratory-derived intensity dependent correction was made (Appendix 1). Approximately every month the loggers were read out and the rain gauges maintained.

2.2.2 Radar data

The KNMI operates two C-band Doppler radars, one at De Bilt and one at Den Helder (Figure 2.1), which both record 288 pseudo CAPPI (800 m) reflectivity fields each day (i.e. every 5 minutes) after removal of groundclutter (Wessels and Beekhuis, 1997). The resolution of these fields is 2.5 km × 2.5 km. The measured radar reflectivity factor Z [mm^6 m^{-3}] of each resolution unit is converted to surface rainfall intensity R [mm h^{-1}] using the Marshall-Palmer Z-R relationship, which has been found to be most suitable for stratiform dominated rainfall events (Battan, 1973):

$$Z = 200 \cdot R^{1.6} \tag{2.1}$$

For both radars, the surface rainfall intensities are accumulated from 0800 UTC until 0800 UTC the next day, for each pixel. It is known that there is a distance-related underestimation of surface rainfall by weather radars due to spatial expansion of the radar beam and due to attenuation of the radar signal. Also overestimation due to the bright band (vertical profile of reflectivity) may occur. Therefore, data from the rain gauges of the volunteer network, from the same period, are used to perform a range correction for each radar separately every day (Holleman, 2004). This is a range dependent bias correction and is done as follows (Holleman, 2003). Colocated radar (R) and gauge (G) observations form the variable RG, which is only calculated if both the radar and rain gauge measured more than 1 mm rainfall.

$$RG \equiv 10 \log(\frac{R}{G}) \tag{2.2}$$

The available RG values are plotted as a function of distance from the radar (r) and a parabola is fitted through these data:

$$RG(r) = a + b \cdot r + c \cdot r^2 \tag{2.3}$$

with a, b and c being the fitting parameters After the range correction, a composite field is constructed by averaging the pixel values of the two radars up to a radius of 200 km away from each radar. Within a radius of 15 km from one radar, the information of the other radar is used. This composite radar field is an operational product of the KNMI and is used in this study.

2.2.3 Event selection

The rain gauges of the experimental network were installed at the beginning of 2004. Between March and October 2004 we selected the 74 events with mean daily rainfall depth of all rain gauges of the experimental network exceeding 1 mm. Rainfall was accumulated from 0800 UTC until 0800 UTC the next day to match the measuring period of the volunteer network and the weather radar. Krajewski et al. (2003) and Steiner et al. (1999) have already mentioned the problems that can occur with rain gauges and we experienced these same problems, resulting in the fact that seldom all

30 rain gauges of the experimental network yielded reliable data simultaneously. We performed a quality check to filter outliers. For each event we made box-and-whisker plots, showing the distribution of the data. Data from rain gauges further than 1.5 times the interquartile range from the nearest quartile were marked as "suspicious" points. Only if it was clear from the fieldwork that these rain gauges showed problems (e.g. clogged up, problems with logger) they were removed from the data set, otherwise the outlier was attributed to spatial variability of the true rainfall field.

2.2.4 Data transformation

For kriging a (multivariate) Gaussian distribution of the data is preferred. In that case the kriging predictor is the same as the conditional mean and the kriging variance is the same as the variance of the conditional distribution, which makes it possible to calculate exceedence probabilities from kriging predictions (Goovaerts, 1997). To approximate a Gaussian distribution, we tried both a log-transformation and a square-root transformation on the data. Only measurements with non-zero rainfall were taken into account and were normalized for each event. Figure 2.2 shows these transformations for the three different extents.As the square-root transformation gave the best results in approximating a Gaussian distribution at all three extents, we chose this transformation for further study.

2.3 Methods

2.3.1 Variogram estimation

The semivariogram, from now on simply called the variogram, describes in terms of variances how spatial variability changes as a function of distance and direction (Isaaks and Srivastava, 1989). The variogram is needed for kriging. To get insight in the multi-extent spatial variability, we distinguished three different spatial extents (Figure 2.1); small extent (225 km^2), medium extent (10,000 km^2) and large extent (82,875 km^2). The extent is defined in this study as the area over which predictions are made, following Bierkens et al. (2000).

In case of no failure, we had data from 30 rain gauges at the small extent, 103 rain gauges at the medium extent (including the 30 from the small extent network) and 330 rain gauges at the large extent (including the 103 from the medium extent network).

Individual variograms
For each of the 74 events we calculated the experimental variogram of the square-root transformed rain gauge data. The experimental variogram is calculated as half the average squared difference between the paired data values, so in case of square-root

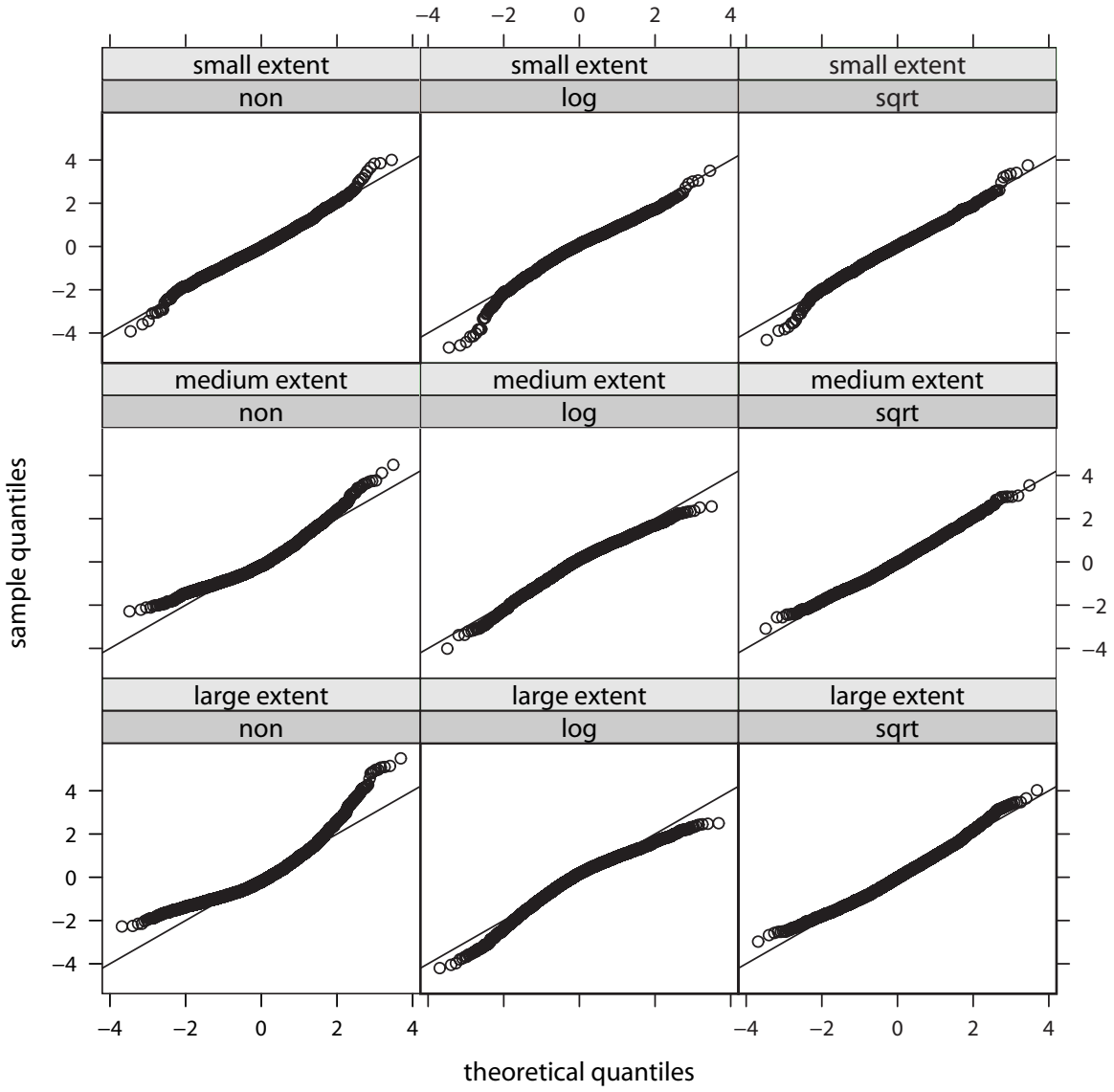

Figure 2.2 Gaussian quantile-quantile plots of normalized non-zero rainfall data of the 74 events for three different extents (small-, medium-, and large extent) and for three transformation scenarios: no transformation (non), log transformation (log) and square-root transformation (sqrt).

transformed rain gauge measurements $G(x_i)$:

$$\hat{\gamma}(h) = \frac{1}{2N(h)} \sum_{i=1}^{N(h)} (G(x_i) - G(x_i + h))^2, \tag{2.4}$$

in which $N(h)$ is the number of point pairs and h the separation distance. The maximum separation distance considered is taken as 1/3 of the extent, i.e. 8, 50 and 150 km for the small-, medium-, and large extent respectively. The reason for that is that point pairs with a larger separation distance are too highly correlated (Journel and Huijbregts, 1978). Up to the maximum separation distance we chose 15 distance intervals into which data point pairs were grouped for semivariance estimates. To assure that the kriging equations have a unique and stable solution, i.e. to force the variogram to be semi-positive definite, we have to fit a suitable variogram model (Isaaks and Srivastava, 1989) to the experimental variogram. Among several models, we chose the widely used spherical variogram model, defined as:

$$\gamma(h) = \begin{cases} C_0 \left(1 - \delta_k \left(h\right)\right) + C \left(\frac{3h}{2a} - \frac{h^3}{2a^3}\right) & 0 \leq h \leq a \\ C_0 + C & h > a, \end{cases} \tag{2.5}$$

in which the Kronecker delta function $\delta_k \left(h\right)$ is 1 for $h = 0$ and 0 for $h > 0$. The parameter C_0 is the nugget variance, C is the partial sill and a is the range of the spherical variogram model. The parameters of the spherical variogram models were fitted automatically with non-linear regression, using weights $N(h)/h^2$ with $N(h)$ the number of point pairs and h the distance. This criterion is partly suggested by theory, and partially by practice (Pebesma, 2004). When it was not possible to fit a unique variogram model, the range was forced to be beyond the extent. All geostatistical operations were carried out using the package *gstat* (Pebesma, 2004) within R (R Development Core Team, 2004).

Pooled variograms
Without the experimental rain gauge network, hydrologists should extract information about the small scale rainfall variability from the KNMI network. As mentioned in Section 2.2 these networks do not give insight into the spatial variability of rainfall at distances smaller than approximately 10 kilometers. To be able to make high-resolution predictions of rainfall in spite of that, we computed a single pooled variogram for each extent based on all the 74 selected events, including the information of the experimental rain gauge network. For each event we performed kriging predictions using both the individual variogram model for that event as well as the pooled variogram model and compared the results. This way we can draw conclusions whether it is permitted to use one standard variogram model, which would be helpful for automated prediction.

2.3.2 Prediction methods

This section introduces briefly three geostatistical prediction methods that were used for this study. The first method uses only rain gauge information while the second and

third method use both rain gauges and radar information but in a different manner. For more detailed information readers are referred to Isaaks and Srivastava (1989), Goovaerts (1997) and Cressie (1993).

Ordinary kriging
Geostatistical prediction is based on the concept of a random function, whereby the unknown values are regarded as a set of spatially dependent random variables. Kriging is a generalized least-squares regression technique that allows one to account for the spatial dependence between observations, as revealed by the variogram, in spatial prediction. Kriging is associated with the acronym B.L.U.P., meaning "best linear unbiased predictor" (Cressie, 1993). It is "linear" as the estimated values are weighted linear combinations of the available data. It is "unbiased" because the expectation of the error is 0 and it is "best" as it minimizes the variance of the prediction errors. The ordinary kriging prediction of square-root rainfall ($\widehat{R}_{OK}$) at the unsampled location x_0 is a linear combination of the n neighboring square-root transformed rain gauge observations $G(x_i)$:

$$\widehat{R}_{OK}(x_0) = \sum_{i=1}^{n} \lambda_i G(x_i) \tag{2.6}$$

The weights λ_i must be such that the predictor $\widehat{R}_{OK}$ is (1) unbiased, i.e. giving no systematic under- or over-estimation, and (2) optimal, i.e. with a minimal mean squared error. These weights are obtained by solving:

$$\begin{cases} \sum_{j=1}^{n} \lambda_j \gamma(x_i - x_j) - \mu = \gamma(x_i - x_0) \quad i = 1, \ldots, n \\ \sum_{j=1}^{n} \lambda_j = 1, \end{cases} \tag{2.7}$$

with μ being the Lagrange parameter accounting for the unbiasedness constraint on the weights. The only information needed to solve the kriging system (Eq. 2.7) are the semivariogram values, which can be calculated from the fitted variogram model (Eq. 2.5).

Kriging with external drift
Beyond using information from the rain gauges $G(x_i)$ only, kriging can use secondary information to improve the kriging prediction (Goovaerts, 1997). In case of rainfall, an informative secondary data source is the square-root rainfall estimated by the weather radar (R). We used two kriging algorithms that incorporate exhaustively sampled secondary data:(1) kriging with external drift (KED) and (2) ordinary colocated cokriging (OCCK).

KED is comparable to universal kriging (kriging with a trend): we assume that we know the shape of the trend and kriging is then performed on the residuals while the trend parameters are implicitly estimated. In universal kriging the trend is often a function of internal variables (coordinates) while in KED the trend surface is based on a trend through the secondary data (external variables). Mathematically they are identical. Although the trend can be a polynomial regression through several external

variables, we only considered radar $R(x)$ as secondary data in a linear trend model:

$$m(x) = a_0 + a_1 R(x) \tag{2.8}$$

The trend coefficients (a_0 and a_1) are implicitly estimated through the kriging system within each search neighborhood using generalized least squares. In our case the search neighborhood was not fixed but depended on the available data points. At maximum 40 neighboring points are taken into account. The kriging with external drift prediction of square-root rainfall ($\widehat{R}_{KED}$) at the unsampled location x_0 is:

$$\widehat{R}_{KED}(x_0) = \sum_{i=1}^{n} \lambda_i G(x_i), \tag{2.9}$$

The weights of kriging with external drift are obtained by solving the system:

$$\begin{cases} \sum_{j=1}^{n} \lambda_j \, \gamma_{res}(x_i - x_j) + \mu_0 + \mu_1 R(x_i) = \\ \quad \gamma_{res}(x_i - x_0) & i = 1, \ldots, n \\ \\ \sum_{j=1}^{n} \lambda_j = 1 \\ \\ \sum_{j=1}^{n} \lambda_j R(x_j) = R(x_0), \end{cases} \tag{2.10}$$

with μ_0 and μ_1 being the Lagrange parameters accounting for the unbiasedness constraints on the weights. Kriging with external drift is performed using γ_{res} being the variogram of the residuals from the trend.

Ordinary colocated cokriging
Another algorithm for taking into account secondary information is ordinary colocated cokriging (OCCK). Different from KED in which the secondary data provide information on the trend only, in OCCK the secondary data, which are now considered as a random variables as well, influence the kriging prediction directly. In addition, OCCK accounts for the global linear correlation between primary and secondary variables, whereas with KED the secondary information tends to influence strongly the prediction, especially when the estimated slope or intercept of the local trend model is large.

A more or less similar and more well-known kriging method using secondary information is ordinary cokriging (OCK). Several studies have used OCK to merge rain gauge and radar rainfall, e.g. Creutin et al. (1988); Fiorucci et al. (2001); Krajewski (1987); Seo et al. (1990a); Seo et al. (1990b). Goovaerts (2000) incorporated elevation as secondary information and tested several kriging methods that account for secondary data. OCCK is preferred to OCK for the following four reasons (Goovaerts, 1997): (1) OCCK avoids instability caused by highly redundant secondary data; (2) OCCK is faster than OCK as it calls for a smaller cokriging system; (3) OCCK does not call for a secondary covariance function at distances larger than 0; (4) OCCK does not require modelling of the cross covariance function by using the Markov-type approximation, i.e. dependence of the secondary variable on the primary is limited to the colocated primary datum.

The ordinary colocated cokriging prediction of square-root rainfall ($\widehat{R}_{OCCK}$) at the unsampled location x_0 is a linear combination of the n neighboring square-root transformed rain gauge observations G and one colocated square-root transformed radar observation R:

$$\widehat{R}_{OCCK}(x_0) = \sum_{i=1}^{n} \lambda_i G(x_i) + \xi R(x_0), \tag{2.11}$$

with the constraint that the weights ($\sum_{i=1}^{n} \lambda_i + \xi$) sum to one.

In case the expected value of the primary and secondary data are not equal, Eq. 2.11 must be adjusted, so the secondary data are bias corrected. In our case we assumed the expected values of the rain gauges and radar to be the same because the operational radar are already bias corrected (Section 5.22.2.2). The ordinary colocated cokriging weights are obtained by solving the system:

$$\begin{cases} \sum_{j=1}^{n} \lambda_j \, \gamma_{GG}(x_i - x_j) + \xi \, \gamma_{GR}(x_i - x_0) + \\ \quad \mu = \gamma_{GG}(x_i - x_0) & i = 1, \ldots, n \\ \\ \sum_{j=1}^{n} \lambda_j \, \gamma_{GR}(x_0 - x_j) + \xi \, \gamma_{RR}(0) + \\ \quad \mu = \gamma_{GR}(0) \\ \\ \sum_{j=1}^{n} \lambda_j + \xi = 1, \end{cases} \tag{2.12}$$

with μ being the Lagrange parameter accounting for the unbiasedness constraints on the weights, γ_{GG} the direct variogram of the rain gauge data, γ_{GR} the cross variogram of rain gauge and radar data and γ_{RR} the direct variogram of the radar data.

The three variograms are modelled as a linear combination of the same basic model, the fitted spherical variogram model of the normalized square-root transformed rain gauge data (Eq. 2.5). The direct variogram of the rain gauges (γ_{GG}) was calculated by multiplying the standardized variogram with the variance of the square-root transformed rain gauge measurements. The direct variogram of the radar data (γ_{RR}) was calculated by multiplying the standardized variogram by the variance of the square-root transformed radar data. The cross variogram (γ_{GR}) was calculated by multiplying the direct variogram of the rain gauges (γ_{GG}) with the correlation between the colocated square-root transformed rain gauge and radar data, assuming the Markov-type approximation (Goovaerts, 1997).

2.3.3 Back transformation and zero Rainfall

Rainfall can be considered as a binary process, it either rains or it does not. As shown in Figure 2.2 the measurements of non-zero daily rainfall closely follow a Gaussian distribution after a square-root transformation. Kriging performs best when data are (multivariate) Gaussian distributed and we therefore applied kriging to the non-zero, square-root transformed (non-standardized) rainfall measurements. This means that the ordinary kriging prediction and colocated cokriging prediction are "best" in

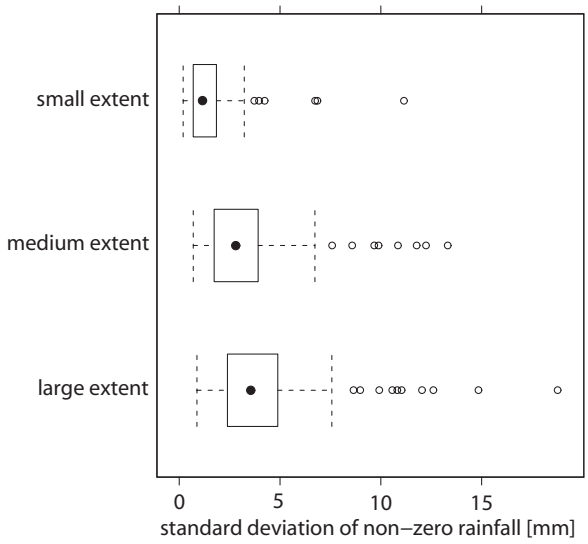

Figure 2.3 Box-and-whisker plots of the standard deviation of non-zero rainfall at the three spatial extents for the 74 events. The black dot denotes the median, solid boxes range from the lower to the upper quartile, dashed whiskers show the data range. Data that are further than 1.5 times the interquartile range from the nearest quartile are shown as open bullets.

predicting the square-root rainfall given that it rains. To obtain back-transformed rainfall values we cannot simply take the square of the kriging prediction based on the square-root transformed rainfall data. The reason for this is that if a Gaussian distribution is squared, it becomes positively skewed, resulting in a mean larger than the median. Simply squaring the kriging prediction of square-root transformed rainfall data would underestimate the conditional mean of rainfall, especially in case of large kriging variances. In order to backtransform prediction values we therefore calculated the percentiles of the conditional distribution of square-root transformed rainfall, assuming this distribution to be Gaussian with mean equal to the kriging prediction and variance equal to the kriging variance. After that we backtransformed (squared) these percentiles, whose rank and percentile value do not change with transformation. From this new distribution function we calculated the mean and the variance.

By not considering the number of zeroes in the data set valuable information would be lost. Therefore we forced the predicted rainfall values to contain the same percentage of zero's as in the data set. The predicted rainfall amounts were arranged in increasing order and a threshold was calculated that corresponded with the percentage of zeroes in the rainfall data set. All the prediction locations with rainfall smaller than this threshold were set to zero.

2.4 Results

2.4.1 Variograms

To compare the spatial structure of each event in one plot we calculated the variograms of the normalized (i.e. variance equals one) square-root transformed rainfall data. The variance in rainfall however, differs between both the events and extents. Figure 2.3 shows in a box-and-whisker plot for each extent the standard deviation of non-zero (non-normalized and non-transformed) rainfall for all the 74 events. This figure shows a positive trend in the variability of non-zero rainfall from small to larger extent.

Figure 2.4, 2.5 and 2.6 show for each event the normalized experimental variograms of the square-root transformed daily rainfall, as well as the automatically fitted spherical variogram model of respectively the small-, medium-, and large extent. In Figure 2.4 the fitted variogram model for 17 and 21 August (0817 resp. 0821) is outside the plotted semivariance range. During those days there was a high semivariance between point pairs with the smallest separation distance, causing our automated procedure to fit a variogram model with a large nugget. Due to the larger data availability at larger extents, the experimental variograms become less ambiguous and the variogram models fit better. Figure 2.7 shows the fitted ranges of the spherical variogram models for each event for the small-, medium-, and large extent. This figure shows a large variability in fitted ranges across events, but a seasonal effect is not clear. Figure 2.7 also shows the fitted range of the spherical variogram model for the small- and medium- extent to be often 25 and 150 km respectively, which are the values that were enforced when the non-linear variogram fitting procedure was not successful.

Figure 2.8 shows the experimental pooled variograms as well as the fitted spherical variogram models of the small-, medium-, and large extent. For the medium- and large extent we fitted a nested spherical variogram model, i.e. a sum of two spherical variogram models (Deutsch and Journel, 1998). The parameters of the fitted spherical variogram models are given in Table 2.1.

The pooled variogram model was calculated using normalized square-root transformed daily rainfall data. For the kriging prediction, the nugget and sill of the variogram model should be multiplied by the variance of the square-root transformed daily rainfall data.

Table 2.1: Parameters of fitted pooled spherical variogram models. C_1 and a_1 are resp. the partial sill and range of the first variogram model. In case of a nested variogram model C_2 and a_2 are resp. the partial sill and range of the second variogram model (see Eq. 3.2).

Parameter	Small Extent	Medium Extent	Large Extent
C_0	0.172	0.035	0.053
C_1	1.270	0.473	0.281
C_2	–	8.994	0.795
a_1 [km]	10	20	23
a_2 [km]	–	1040	156

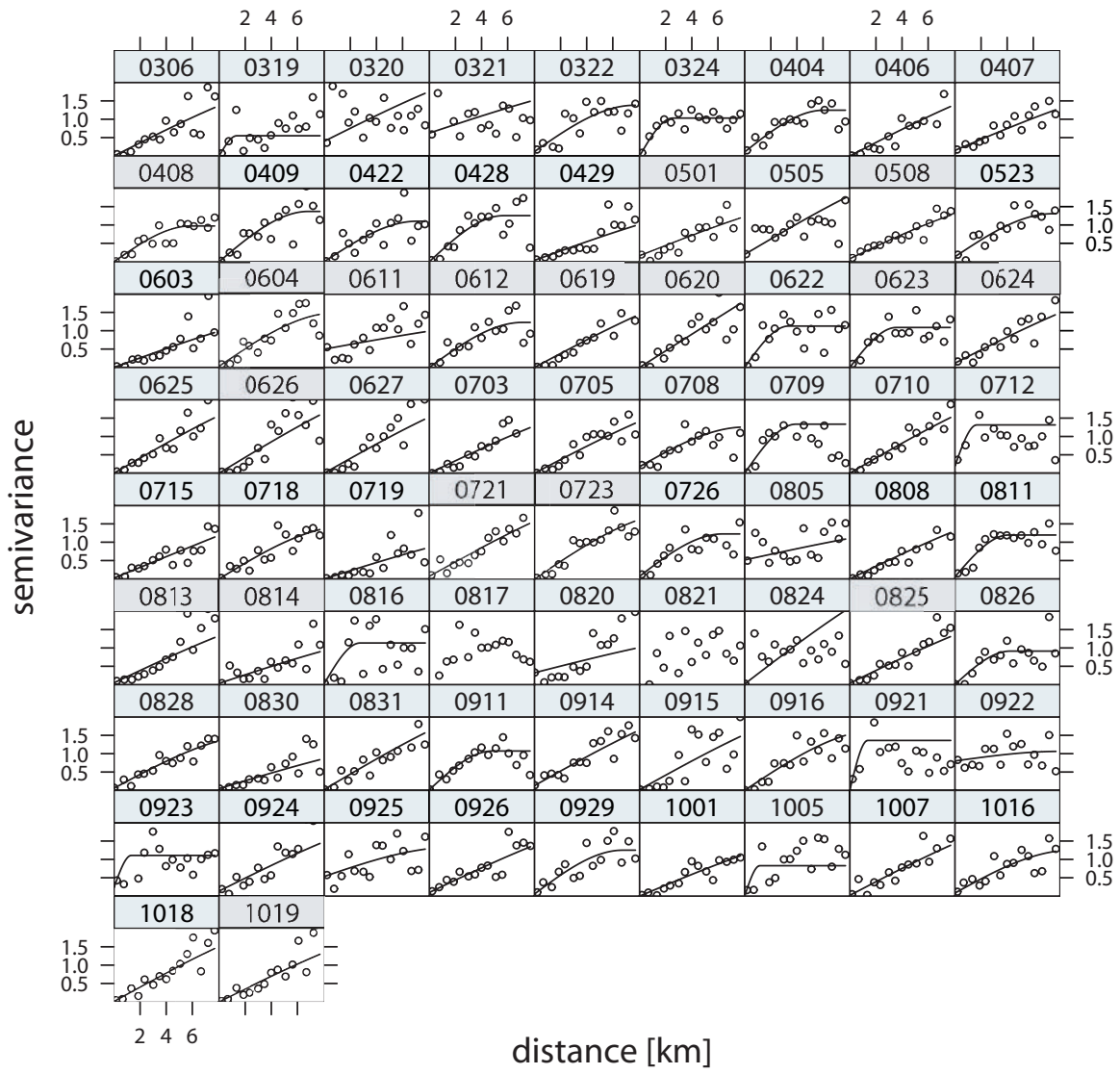

Figure 2.4 Small-extent normalized variograms of square-root transformed daily rainfall with fitted spherical model for each of the 74 events in 2004 (header in "month month day day", e.g. 0306 means 6 March). For 17 and 21 August 2004 the automatically fitted variogram model is outside the plotted semivariance range.

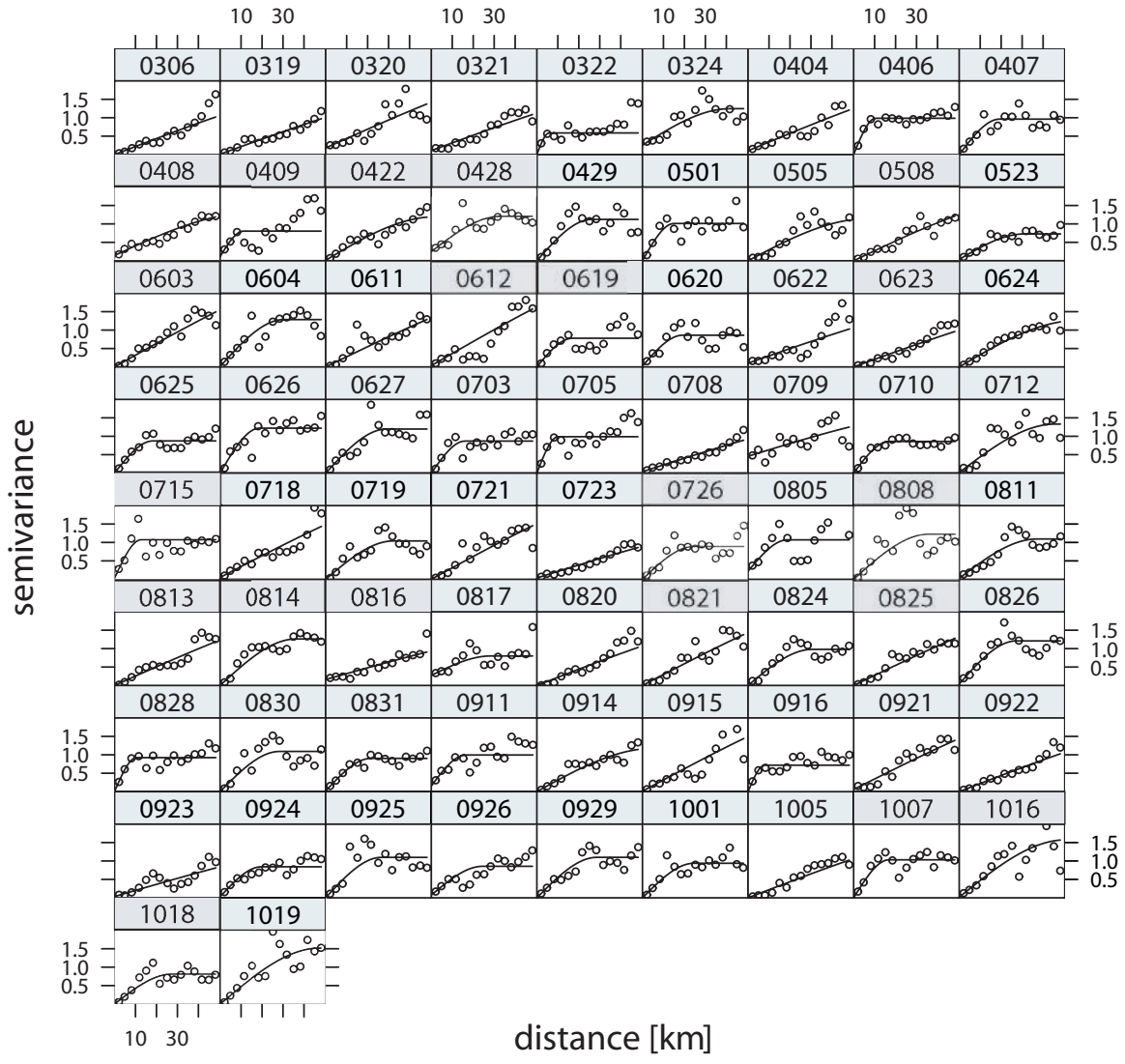

Figure 2.5 Medium-extent normalized variograms of square-root transformed daily rainfall with fitted spherical model for each of the 74 events in 2004 (header in "month month day day", e.g. 0306 means 6 March).

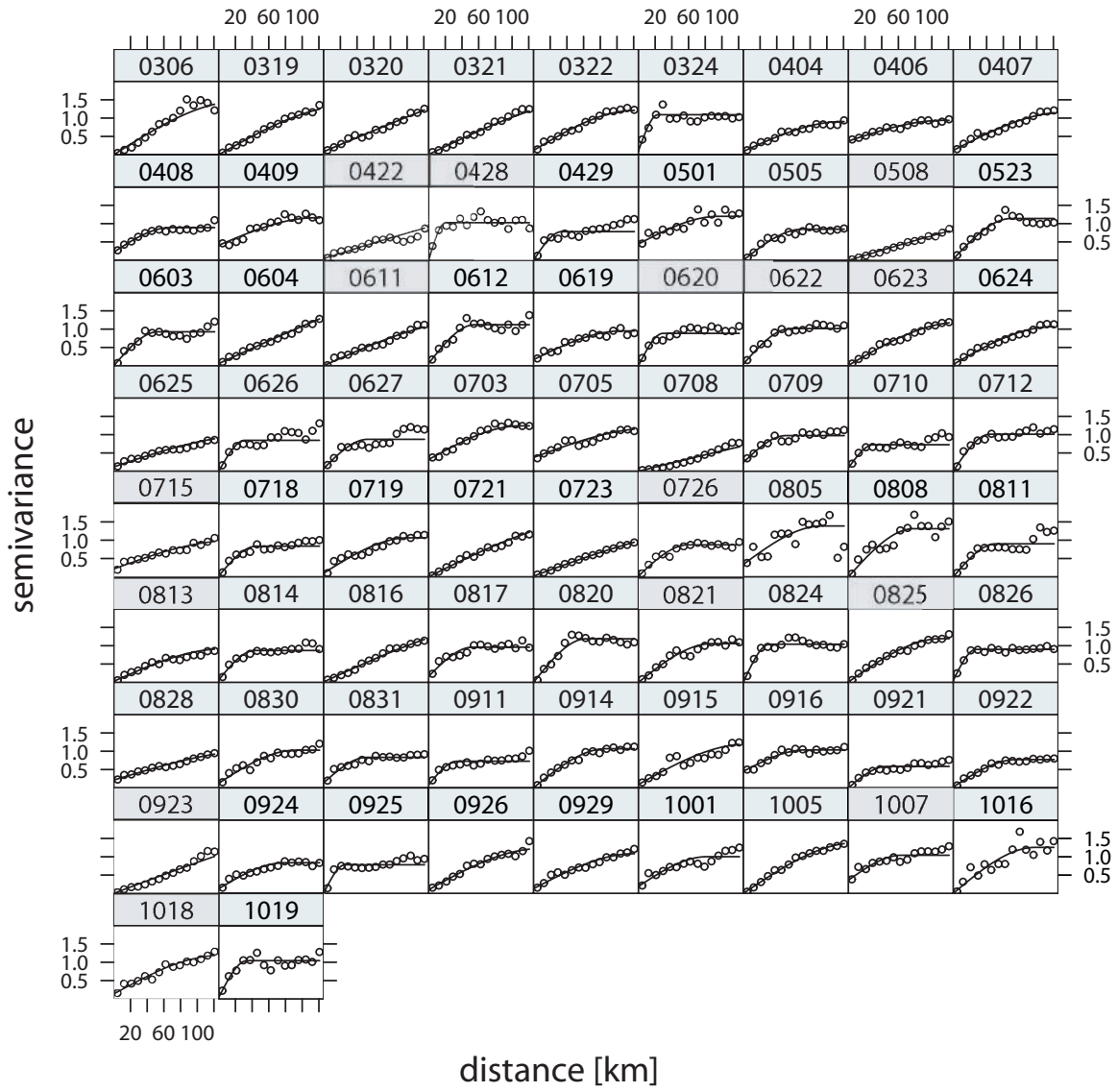

Figure 2.6 Large-extent normalized variograms of square-root transformed daily rainfall with fitted spherical model for each of the 74 events in 2004 (header in "month month day day", e.g. 0306 means 6 March).

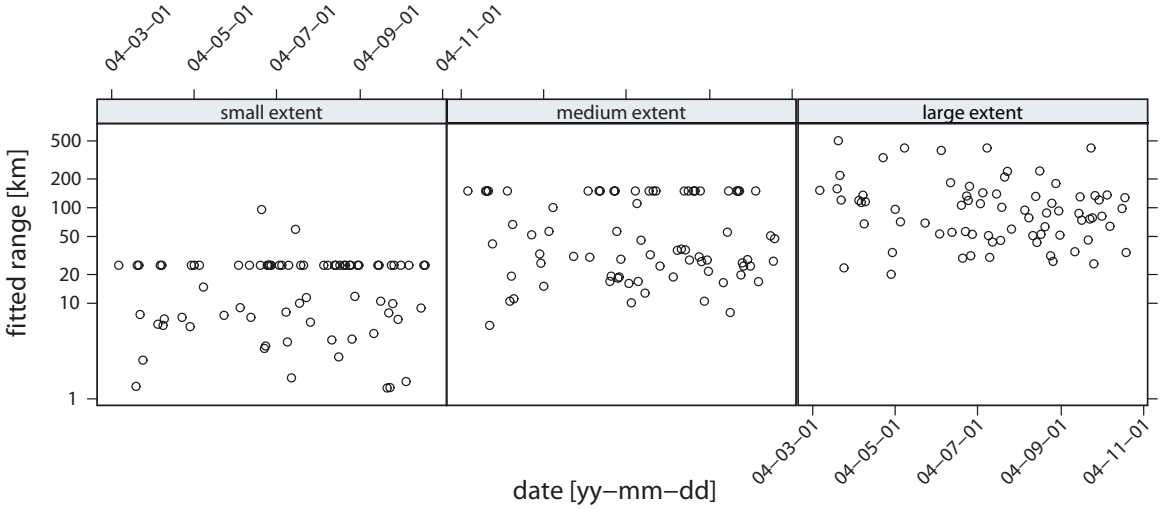

Figure 2.7 Automatically fitted ranges (km) of spherical variogram models for small-, medium-, and large extent as function of event date.

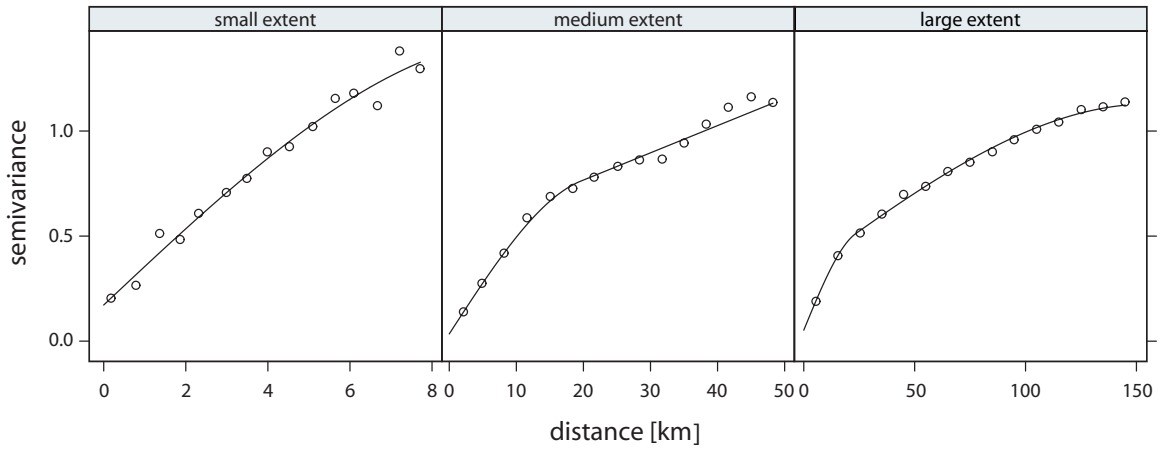

Figure 2.8 Pooled variogram models of small-, medium-, and large extent, calculated from the standardized non-zero square-root transformed daily rainfall data. For the medium- and large extent a nested spherical variogram model is fitted.

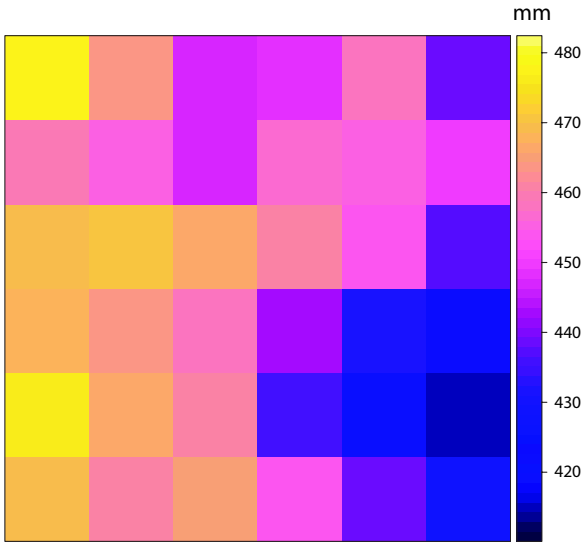

Figure 2.9 Total rainfall [mm] during March-October 2004 at small extent according to daily range corrected radar.

2.4.2 Rainfall prediction

Case study
Figure 2.9 shows the accumulated daily composite range corrected radar field for the period March-October 2004 at the small extent. During this period, 22 radar images were either missing or incomplete. From this figure is can be seen that even for an accumulation period of 7 months, there still is a difference of 10% rainfall within the small extent. This corroborates our argument that for The Netherlands a temporal resolution of one day is important even at small extent.

To demonstrate the kriging methods described in the preceding paragraphs we selected two of the 74 rainfall events, 4 April 2004 and 1 May 2004. Figure 2.10 shows the composite range corrected radar fields for the selected dates. These two events were chosen because they represent two different rainfall types with different correlation between rain gauge data and radar. The event of 4 April 2004 is an example of a stratiform event as it rains over a large area and extremely high rainfall areas can not be detected. The event of 1 May 2004 is an example of a convective event as the rainfall area is smaller and high rainfall values are present.

Figure 2.11A shows the prediction of rainfall depth at the small extent for 4 April 2004 according to respectively the range corrected radar, the ordinary kriging prediction, kriging with external drift prediction and the ordinary colocated cokriging prediction. The kriging predictions are made at a high-resolution point grid with distances of 100 meters. For the medium- and large extent we only used the 40 nearest data points instead of the complete data set for kriging. For this event the correlation between the rainfall measured by the rain gauges and the colocated radar at the small extent was 0.16. Because of this low correlation, the trend surface of the radar has a very small effect on the KED prediction. For the ordinary colocated

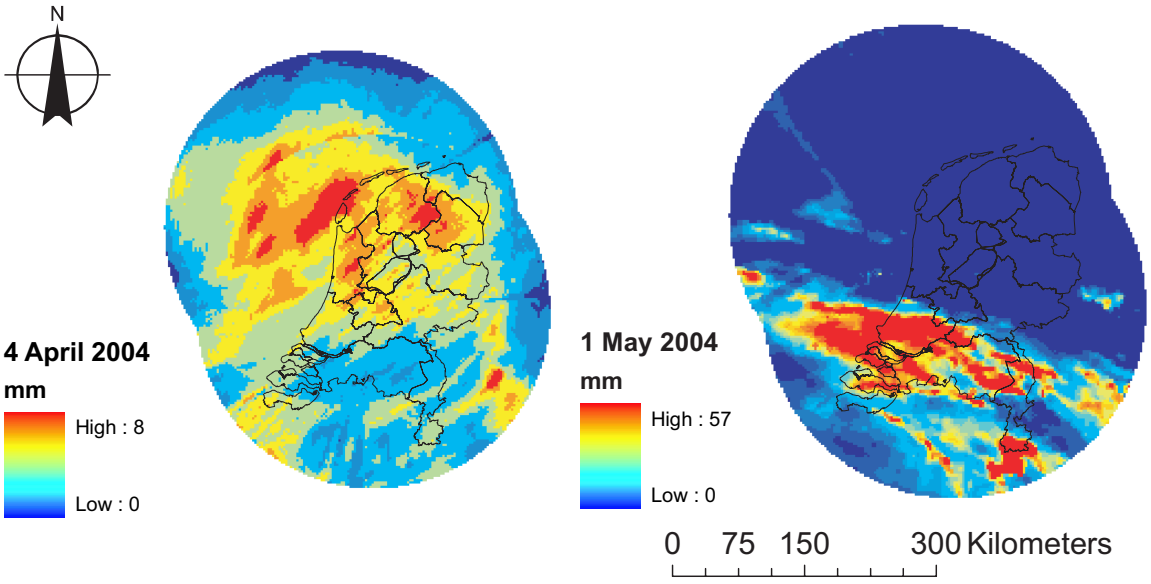

Figure 2.10 Composite range corrected radar fields of 4 April 2004 (left) and 1 May 2004 (right).

cokriging prediction however, the radar field can be clearly seen. This is due to the fact that for each prediction location within a radar pixel this same colocated radar value is taken into account (Eq. 2.11). Within the radar pixel itself, the rainfall depths are interpolated. To overcome the problem of sudden transitions in rainfall depth from one radar pixel to the other, the radar field can be pre-smoothed before executing the KED or OCCK. We retrieved good results by smoothing the radar with inverse distance interpolation using the four closest grid cell center points of the radar field.

Figure 2.11B shows the rainfall fields using the same kriging methods for the 1 May 2004 event. For this event the correlation between the rainfall measured by the rain gauges and the colocated radar at the small extent was 0.84.

In the Figures 2.11A and B we show the predicted rainfall depths using OK, KED and OCCK for the small extent. We assumed that for all events it rained throughout the whole small extent so we did not have to cope with the problem of zero rainfall.

To illustrate how our method deals with zero rainfall, we show the rainfall depths of the different methods for 1 May 2004 at the large extent in Figure 2.12. During this event 114 rain gauge stations out of the 211 reported zero rainfall. We forced the same percentage (54 %) of the prediction locations to have zero rainfall. From this figure it can be seen that with using ordinary kriging (OK) rainfall is predicted in the northern part of the Netherlands where the radar did not detect rainfall, whereas in the southern part ordinary kriging does not predict rainfall where the radar does detect rainfall. KED and OCCK combine the two sources of information, but in a slightly different manner. In this case, the predictions of both methods follow the spatial rainfall structure as shown by the radar. The rainfall measured by the rain

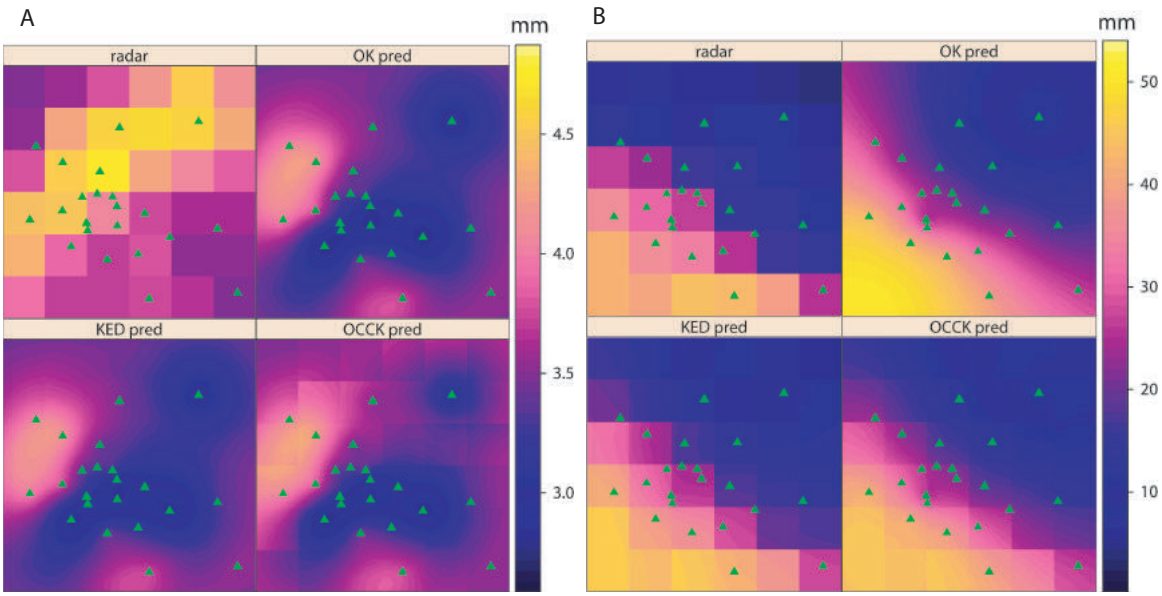

Figure 2.11 Prediction of rainfall depth at small extent according to the range corrected radar (radar), ordinary kriging (OK pred), kriging with external drift (KED pred) and ordinary colocated cokriging (OCCK pred) for A: 4 April 2004 (radar-rain gauge correlation is 0.16) and B: 1 May 2004 (radar-rain gauge correlation is 0.84). Green triangles show the rain gauge locations.

gauges in the northern part of the Netherlands was so low that it was set to zero.

Cross validation

To compare the accuracy of the three different kriging forms (OK, OCCK and KED) as well as the use of either the individual variogram models or pooled variogram models, we used cross-validation. The idea of cross-validation is to remove one data point at a time from the data set and re-predict this value from the remaining data. For each extent and event we performed cross-validation, using the three different kriging forms. For ordinary kriging as well as ordinary colocated cokriging we used both the individual variogram model of that event (Figure 2.4) as well as the pooled variogram model (Figure 2.8) of that extent. Finally, we calculated for each event the root mean squared error (RMSE) resulting from the cross-validation calculations. In our case study of 74 events, we had 7 incomplete radar fields, due to technical malfunction or maintenance of one of the radars. These events were not taken into account in the cross-validation. The distributions of the root mean squared error resulting from the cross-validation using the different kriging methods are plotted in box-and-whisker plots (Figure 2.13). We also calculated the RMSE of the difference between the rainfall measured by the rain gauges and the colocated radar pixel and these results (radar) are shown as well in Figure 2.13. Figure 2.13 shows that taking into account radar as secondary variable, using either KED or OCCK, leads to better results than only taking into account data from rain gauges for the medium and large extent. Also, for the medium and large extent radar performs better than rain gauge data alone (OK). For the small extent however, the rain gauge data alone perform

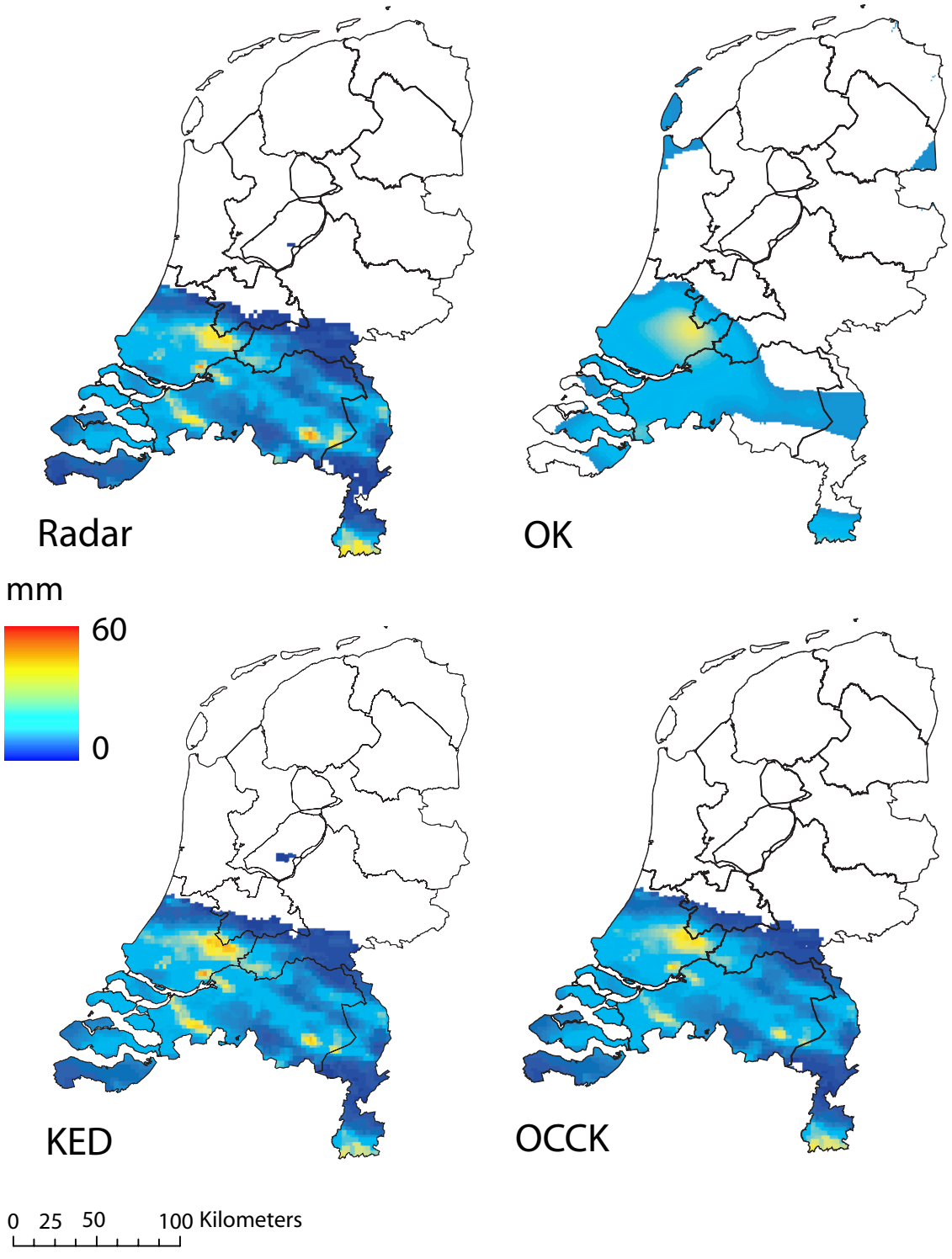

Figure 2.12 Prediction of rainfall depths for The Netherlands at 1 May 2004 according to the range corrected radar (Radar), ordinary kriging (OK), kriging with external drift (KED) and ordinary colocated cokriging (OCCK).

better and the added value of taking into account radar is not so clear. This is not surprising as we have a dense network of rain gauges at the small extent. The use of a pooled variogram model for all events instead of individual variogram models for each separate event makes little difference. For the small extent the pooled variogram model performs less than the individual variogram models whereas for the medium and large extent it is the other way around.

Figure 2.14 shows the ratio between the RMSE as calculated with OK and KED (ratio.RMSE.ok.ked, shown as +) as well as the ratio between the RMSE as calculated with OK and OCCK (ratio.RMSE.ok.cck, shown as o) as a function of the correlation between rain gauges and radar for the small-, medium-, and large extent. If the ratio is higher than 1, it means that KED or OCCK performs better than OK. Again we see that the larger the extent, the higher the added value of the radar. Figure 2.14 also shows the positive effect of the correlation between radar and rain gauge and the ratio of RMSE, especially at the medium and large extent.

We also looked at the z-score of the cross-validation exercise, which is the residual divided by kriging standard error. The z-score should have zero mean and unit variance. If the mean z-score deviates from zero this means we have a biased prediction, and if the variance is higher than 1 we underestimate the kriging variance. For each event we calculated the mean z-score using the 3 different kriging methods. The results are shown in a box-and-whisker plot (Figure 2.15). It can be seen that for almost all events and kriging methods, the mean z-score is close to zero, except for OCCK. This is probably due to our assumption that the expected value of the rain gauge data and radar data are the same. Figure 2.16 shows in a box-and-whisker plot the variance of the z-score that we calculated for each event using the 3 kriging methods. It is most striking that the pooled variogram used for both OK and OCCK leads to lower z-score variances and thus better estimation of the prediction error variance.

2.5 Discussion

In this section we deal with some remaining uncertainties and possible improvements of the methods presented in this chapter.

This chapter deals with daily rainfall. For hydrological applications it would be interesting to also be able to generate high spatial resolution rainfall fields with a higher time resolution, e.g. 3 hours. In that case the main problem we would have to cope with is the reduction of the amount of rain gauge measurements, as the largest operational rain gauge network in The Netherlands consists of volunteers who only report the daily rainfall depth. Consequently the present range correction of the weather radar cannot be performed on a higher time resolution, as this method uses the volunteer network as well. With a low density rain gauge network our method to correct for zero rainfall is also not suitable because an individual rain gauge reporting zero rainfall would have too much influence. Besides the decrease in rain gauge stations we would also have to deal with the following problems: (i) the correlation between rainfall measured by the rain gauges and radar is known to decrease at

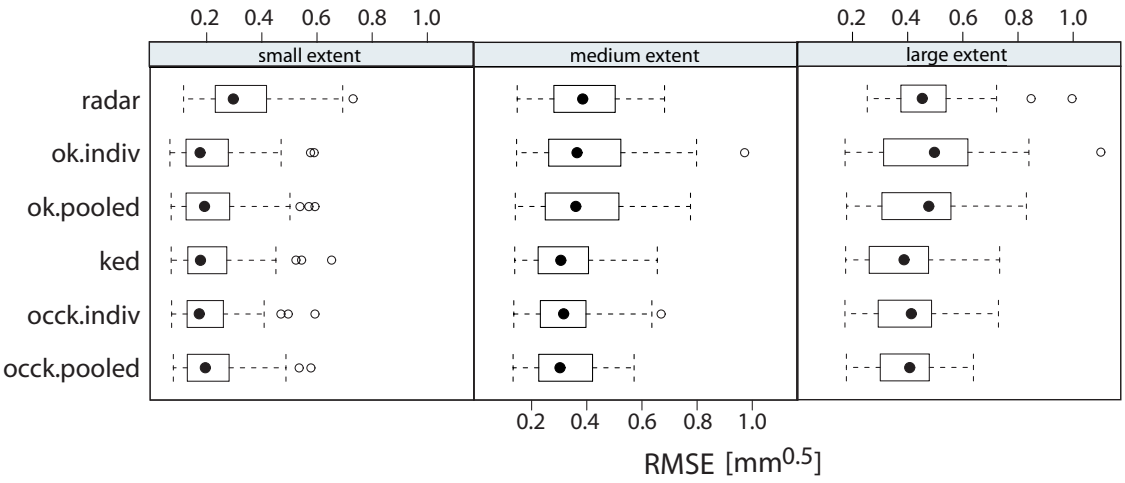

Figure 2.13 Box-and-whisker plots of the root mean squared error (RMSE) of the square-root transformed residuals from the comparison between operational radar and rain gauges (radar) [$mm^{0.5}$] as well as the root mean squared error (RMSE) of the square-root transformed residuals from the cross validation using three kriging methods [$mm^{0.5}$] (ordinary kriging OK; ordinary colocated cokriging OCCK and kriging with external drift KED). For both ordinary kriging (OK) and ordinary colocated cokriging (OCCK) we used the individual variograms (indiv) as well as the pooled variograms (pooled).

small time scales, especially when (e.g. in convective rainfall) there is a large space - time variability of rainfall; (ii) re-estimation of the variogram models as it is known that for rainfall averaged over larger spatial scales and integrated over longer periods the correlation distance is typically larger; (iii) re-consideration of the square-root transformation of rainfall data to make its distribution closer to Gaussian. Possibly for shorter periods a logarithmic transformation would be more suitable. For shorter time steps, the spatial continuity of radar measurements becomes a major advantage compared to rain gauge networks. This however does not preclude the thorough radar data processing (e.g. correction for Vertical Profile of Reflectivity (VPR) and attenuation) required to improve as far as possible the radar data quality. Besides all the advantages of using radar data, it is important to recognize the inherent limitations of radar data quality, especially as a function of range. The average range limit to keep in mind for hydrological use of weather radar is of the order of 80 km.

Results from HYREX show that distributed hydrological models are sensitive to rain gauge location and hence to the spatial variability of rainfall over the catchment, especially during convective rainfall (Bell and Moore, 2000). In the Netherlands, convective rainfall mainly occurs during summer as a result of local ascent of warm air and is characterized by heavy rainfall with a small spatial extent and a short duration. During winter time stratiform rainfall events dominate, caused by frontal systems. They have a larger spatial extent than convective rainfall, as well as a longer lifetime. For this reason, our initial purpose was to divide the events into two rainfall types (convective and stratiform) and to pool the variograms for each rainfall type, instead of using only one pooled variogram model for each extent. To identify convective areas we applied the algorithm proposed by Steiner et al. (1995)

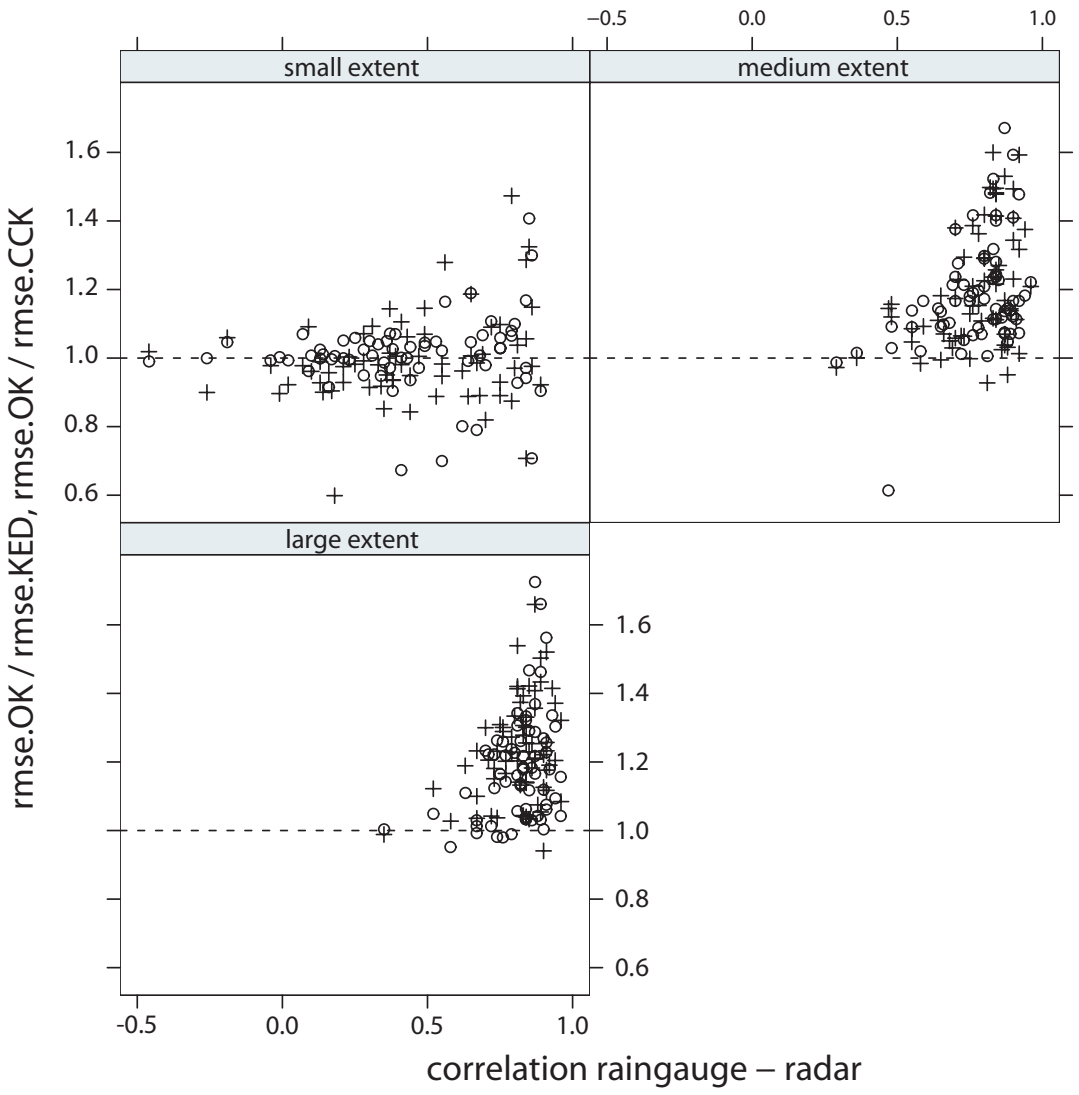

Figure 2.14 Ratio of the RMSE as calculated with ordinary kriging and kriging with external drift (RMSE.OK/RMSE.KED, shown as +) as well as the ratio of the RMSE as calculated with ordinary kriging and ordinary colocated cokriging (RMSE.OK/RMSE.CCK, shown as ∘) as function of the correlation between rain gauges and radar for the small-, medium-, and large extent. Dashed line represents the value one.

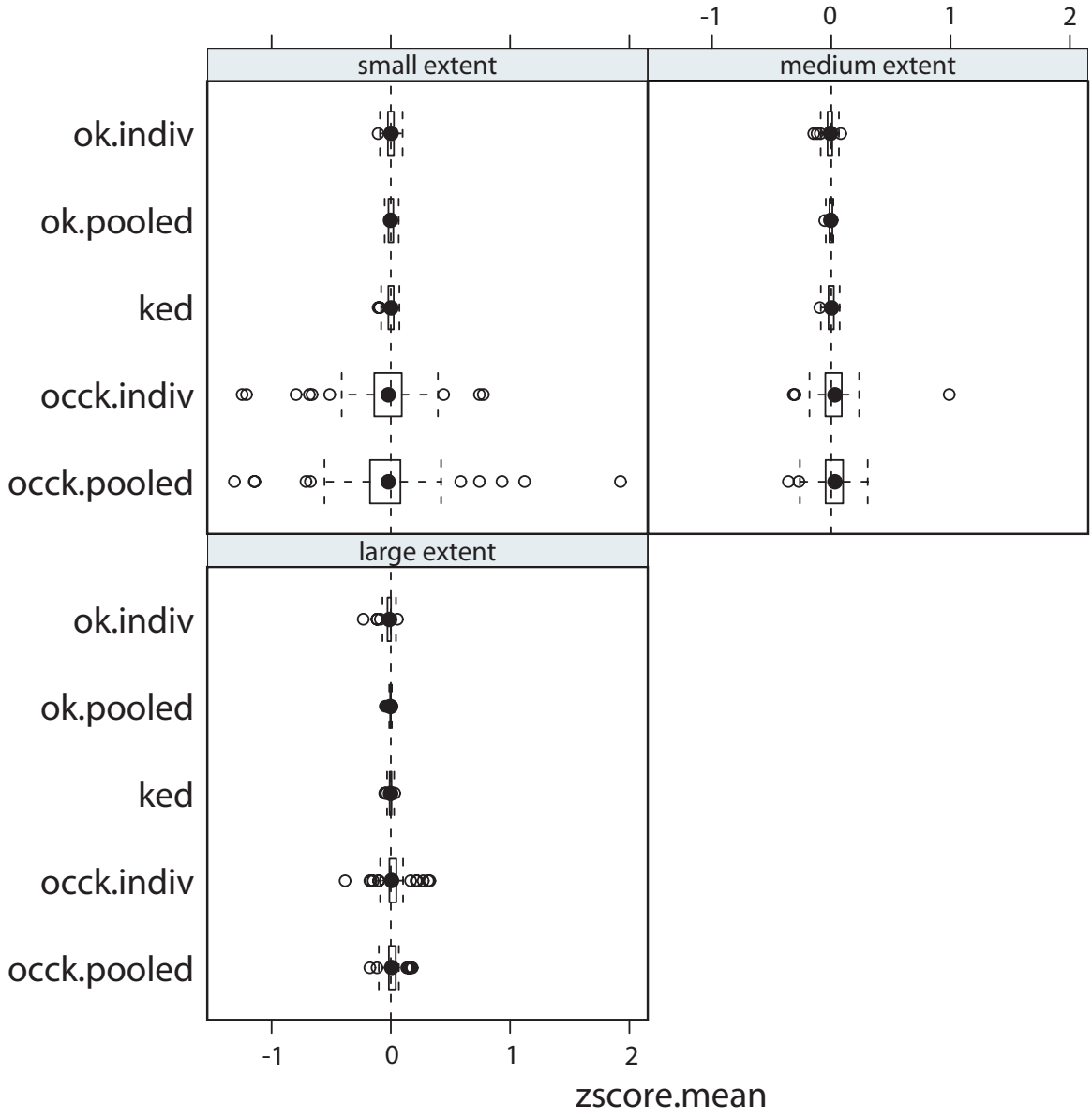

Figure 2.15 Box-and-whisker plots of the mean z-score from the cross validation using three kriging methods (ordinary kriging OK; ordinary colocated cokriging OCCK and kriging with external drift KED). Dashed line represents the value zero. For both ordinary kriging (OK) and ordinary colocated cokriging (OCCK) we used the individual variograms (indiv) as well as the pooled variograms (pooled).

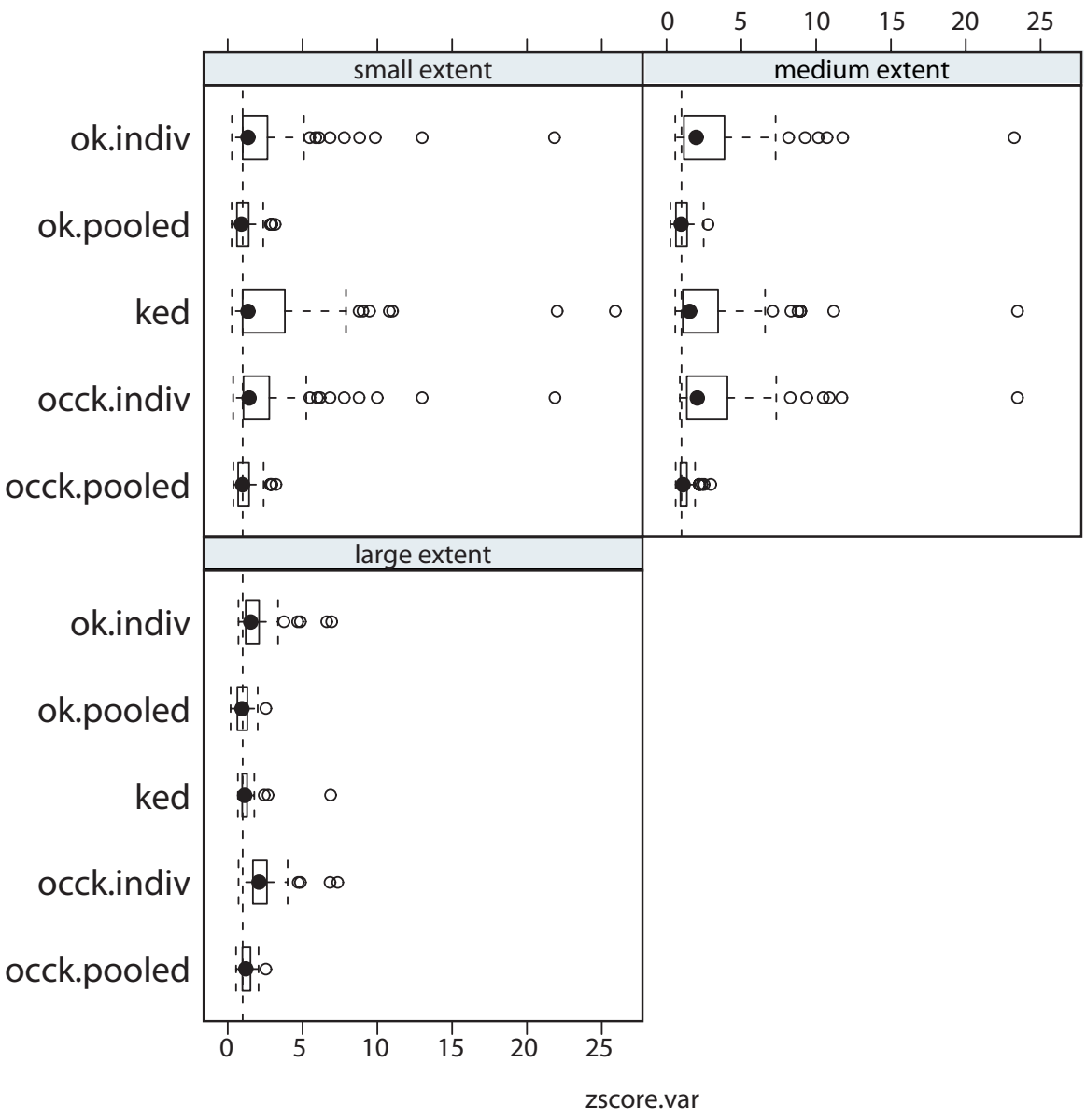

Figure 2.16 Box-and-whisker plots of the variance of the z-score from the cross validation using three kriging methods (ordinary kriging OK; ordinary colocated cokriging OCCK and kriging with external drift KED). Dashed line represents the value one. For both ordinary kriging (OK) and ordinary colocated cokriging (OCCK) we used the individual variograms (indiv) as well as the pooled variograms (pooled).

to 5-minute CAPPI radar fields using the same criteria as stated in their paper. In case the majority of the grid cells within the extent were identified at least 10 times as convective during that day, we labelled the event as convective, otherwise it was classified as stratiform. However, when we pooled the variograms per rainfall type we did not find sufficient differences between the form of the pooled variograms to justify the separated modelling. Further research is required to investigate whether a separate modelling of stratiform and convective events is required and if so, how to better distinguish between stratiform and convective events.

Although we are aware of the directional variability in rainfall fields we did not consider anisotropy in our variogram model fits, mostly because we had too little data points within our small extent. The 30 data points we had at maximum for each event at the small extent are the absolute minimum to fit an omnidirectional variogram, but provide insufficient information to estimate directional variograms. This was also the case for the medium extent. An additional reason not to use directional variograms is that estimating them and fitting suitable models, is difficult to reconcile in an automatic fashion. Moreover, using a kriging method that takes into account the secondary data of the radar, will take into account the existing anisotropy present in the radar image.

Kriging predictions were made using either the individual variogram models or the pooled variogram model. We did not take into account the quality of the variogram model fit. This can be done by using for instance markov-chain Monte Carlo techniques (Diggle et al., 1998). Probably, the effect on kriging prediction would not be large if we have enough data but it becomes relevant for sparse rain gauge networks.

We applied OCCK assuming that the Markov-type approximation (Goovaerts, 1997) holds, in order to make the automatic prediction procedure faster. It should be possible to automatically calculate and fit the cross-covariance function and implement this in the OCCK procedure. This is however beyond the scope of this chapter.

Kriging with external drift as applied in this chapter, assumes the secondary data to be free from errors. A possible improvement could be to use external drift kriging with uncertain covariates (Van de Kassteele and Stein, 2006).

Prediction techniques such as kriging tend to smooth out the local variability of rainfall, especially further away from the data locations. Kriging variances provide a measure of local uncertainty but give no insight into the joint spatial distribution of rainfall uncertainty. Because the hydrological system is non-linear, the use of smoothed rainfall fields could lead to a biased hydrological response when used as input for hydrological models. Therefore it would maybe be better to stochastically simulate rainfall fields and use an ensemble of simulated rainfall fields as input. In Appendix 2 we show how sequential simulation with colocated cokriging could be used.

2.6 Conclusions

We show that kriging with external drift and ordinary colocated cokriging successfully take into account radar as secondary information source and are more accurate than ordinary kriging (rain gauge information only), especially for larger extents with lower densities of rain gauges. The added value of radar is positively related to the correlation between the rainfall measured by the rain gauges and the colocated radar pixel. The use of a pooled variogram model instead of an individual variogram model for each event does not lead to loss of accuracy in rainfall prediction, so these pooled variogram models can be used when there is lack of data or when an automatic prediction procedure is implemented without variogram estimation.

We also show that the pooled variogram is preferred over event-based variograms in terms of correct assessment of prediction uncertainty (z-score variance of 1) for the small- and medium extent cases, where the number of data is small and event-based variograms are rather uncertain. Another conclusion is that KED and OK are more robust with respect to mean z-scores (on average zero) than OCCK. This may be due to a bias in the radar data.

Acknowledgements:
*The authors like to thank the Royal Netherlands Meteorological Institute (*KNMI*), in particular Iwan Holleman and Ton Donker, for their help and for providing us their data. J.M. Schuurmans is financially supported by TNO and R. Uijlenhoet is financially supported by The Netherlands Organization of Scientific Research (NWO) through grant 016.021.003. We acknowledge the reviewers for their valuable comments.*

3 Effect of spatial distribution of daily rainfall on interior catchment response of a distributed hydrological model

Schuurmans, J.M & M.F.P. Bierkens (2007), Effect of spatial distribution of daily rainfall on interior catchment response of a distributed hydrological model. Hydrology and Earth System Sciences, 11, pp. 677-693

Abstract

We investigate the effect of spatial variability of daily rainfall on soil moisture, groundwater level and discharge using a physically-based, fully-distributed hydrological model. This model is currently in use with the district water board and is considered to represent reality. We focus on the effect of rainfall spatial variability on day-to-day variability of the interior catchment response, as well as on its effect on the general hydrological behaviour of the catchment. The study is performed in a flat rural catchment (135 km^2) in the Netherlands, where the climate is semi-humid (average precipitation 800 mm $year^{-1}$, evapotranspiration 550 mm $year^{-1}$) and rainfall is predominantly stratiform (i.e. large scale). Both range-corrected radar data (resolution 2.5×2.5 km^2) as well as data from a dense network of 30 rain gauges are used, observed for the period March–October 2004. Eight different rainfall scenarios, either spatially distributed or spatially uniform, are used as input for the hydrological model. The main conclusions from this study are: (i) using a single rain gauge as rainfall input carries a great risk for the prediction of discharge, groundwater level and soil moisture, especially if the rain gauge is situated outside the catchment; (ii) taking into account the spatial variability of rainfall instead of using areal average rainfall as input for the model is needed to get insight into the day-to-day spatial variability of discharge, groundwater level and soil moisture content; (iii) to get insight into the general behaviour of the hydrological system it is sufficient to use correct predictions of areal average rainfall over the catchment.

3.1 introduction

Rainfall is often defined as being the key variable in hydrological systems. Considering the question how the spatial variability of rainfall influences the hydrological state, most studies have focussed on the effect on catchment discharge (e.g. Obled et al., 1994; Arnaud et al., 2002; Bell and Moore, 2000; Shah et al., 1991). Obled et al. (1994) conclude from their study (using TOPMODEL for a rural catchment of 71 km^2) that the spatial variability must be taken into account more because it improves the estimation of the basin average incoming volume, rather than because of some dynamic interactions with flow-generating processes. Arnaud et al. (2002) (using 3 different rainfall-runoff models for 4 fictitious catchments of 20–1500 km^2) however, found that rainfall variability can lead to significant different discharge, not for extreme events but for the more frequent events. This was also concluded by Shah et al. (1991): under "wet" conditions, good predictions of runoff can be obtained with a spatially averaged rainfall input but under "dry" conditions, spatial variability of rainfall has a significant influence. They suggest this is caused by the spatial distribution of soil moisture which controls the runoff production. Bell and Moore (2000) also show the importance of taking into account the spatial variability of rainfall, especially in case of convective rainfall events, which show high spatial variability. O'Connell and Todini (1996) point out the need to study the influence of space-time rainfall variability on the hydrological system in real catchments, but up to now not much attention has been given to the influence of rainfall variability on groundwater level and soil moisture content within the catchment.

A promising method to capture the variability of rainfall is meteorological radar. Real-time radar products are now readily available in many western countries in the world (e.g. Gekat et al., 2004; Krajewski and Smith, 2002; Carpenter et al., 2001). There is, however, only limited use of these products in operational hydrology. One of the reasons for this lack of use could be the uncertainty about the radar estimated rainfall field accuracy. Goodrich et al. (1995) noted that even though the spatial variability of rainfall may have significant influence on discharge, rainfall is usually assumed to be uniform in the application of hydrological models of small catchments. This is also the case in the Netherlands where often data from a single rain gauge (even outside the catchment area) are used as input for hydrological model studies.

The main objective of our study is to determine how spatial variability of daily rainfall affects soil moisture, groundwater level and discharge as calculated by a physically-based, fully-distributed hydrological model. This is done for two purposes. First, to assess the effect of rainfall spatial variability on the day-to-day variability of the interior catchment response, i.e. to obtain a good insight in the current hydrological situation of a catchment, which is of great importance to water boards (e.g. operational water management) and agriculture (e.g. irrigation, sowing). Second, to assess its effect on the general behaviour of the hydrological system (e.g. groundwater and soil moisture climatology, water balance), which is important for planning strategies. A secondary objective is to determine how well operational radar products can capture the spatial variability of the daily rainfall for the purpose of hydrological

modelling.

The study area is a rural catchment of 135 km^2 in the middle of the Netherlands. For this study area an operational fully-distributed, physically based hydrological model is available from the controlling district water board. Also, operational radar images as well as data from a dense network of rain gauges are available for the study area. Interpolated rainfall fields using data from the dense rain gauge network as well as operational radar and a combination of those two are used to describe the spatial variability of daily rainfall for the period March to October 2004. We consider daily rainfall as this is the time resolution for which the radar-estimated rainfall fields are range-corrected in the Netherlands. We anticipate that for small mountainous catchments the spatio-temporal structures of rainfall fields are important, particular at small temporal aggregation. However, daily rainfall fields are sufficient for the Netherlands, because rainfall is predominantly stratiform and discharge is groundwater flow dominated. The different daily rainfall scenarios are used in a sensitivity analysis, i.e. as input for the hydrological model while comparing the calculated maps of groundwater level and soil moisture as well as the discharge hydrographs. We hypothesize that the sensitivity of the interior catchment response calculated by the model reflects the real interior catchment response. We only performed a sensitivity study and did not perform a separate calibration for each rainfall scenario. The reason is that we wanted to investigate solely the effect of different rainfall input on the outcomes of our hydrological model, while a calibration of the model parameters for each rainfall scenario would mask the effect of different input on the hydrological variables.

The characteristics of the catchment and the hydrological model are described in Section 3.2. In this section we also provide details about available rainfall data in the Netherlands. Section 3.3 deals with the way we analyzed the data, how we interpolated the rain gauges and describes the rainfall scenarios we used. The results are given in Section 3.4, considering discharge, groundwater and soil moisture, while Section 3.5 concludes the chapter with conclusions and discussion.

3.2 Model and data

3.2.1 Study area

The Lopikerwaard catchment (135 km^2) is located in the middle of the Netherlands. Climate is semi-humid (average precipitation 800 mm $year^{-1}$, evapotranspiration 550 mm $year^{-1}$) and rainfall is predominantly stratiform (i.e. large scale). Figure 3.1a shows the exact location. The area is flat with a median surface level about -1 m N.A.P. (reference sea level, Figure 3.1b). Data about the surface level were extracted from the AHN (actual altitude database Netherlands), which is obtained by laser altimetry. The main soil type is alluvial clay deposited by rivers and peat. The main land use type is agricultural grassland (70%). There are a few small villages in the area which in total occupy about 15% of the area (Figure 3.1c). The Lopikerwaard is

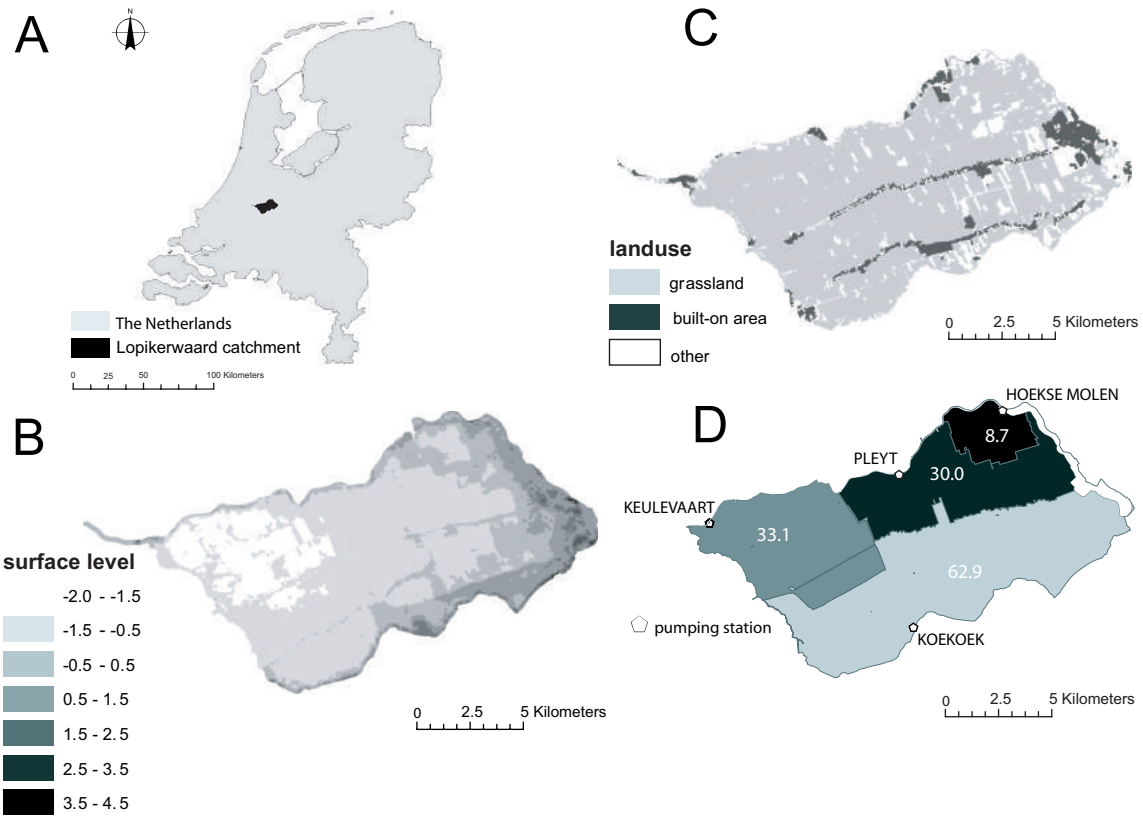

Figure 3.1 (A) Location of Lopikerwaard catchment within the Netherlands; (B) Surface level of the Lopikerwaard catchment in meters + N.A.P. (reference sea level); (C) Land use in the Lopikerwaard catchment; (D) Subcatchments within the Lopikerwaard catchment with the corresponding pumping stations, area-size of each subcatchment is given in square kilometers.

divided into four subcathments as shown in Figure 3.1d, in which the area-size of each subcatchment is given in square kilometers. In each subcatchment groundwater levels are controlled by a dense network of drainage ditches where water levels are controlled by weirs and pumps. Four pumping stations (Keulevaart, Pleyt, Hoekse Molen, Koekoek) discharge the rainfall surplus to either the river Hollandse IJssel in the north or the river Lek in the south.

3.2.2 Hydrological model

Groundwater flow and soil moisture dynamics in the Lopikerwaard were modelled using the SIMGRO model code. We refer to Querner (1997) for more detailed information of SIMGRO. SIMGRO provides for physically based finite element modelling of regional groundwater flow in relation to drainage, water supply and water level control. SIMGRO based models simulate flow of water in the saturated zone, the unsaturated zone and the surface water network in an integrated manner.

In SIMGRO, the groundwater system is hydrogeologically schematized into a number of layers, with horizontal flow (Dupuit assumption) in water-conveying layers (aquifers) and vertical flow in less permeable layers (aquitards). Hydrogeological information, such as hydraulic transmissivity, vertical flow resistance, layer thickness, storage coefficient and porosity, is required for each layer. The boundary conditions for the aquifers can be either prescribed heads (Dirichlet condition) or prescribed fluxes (Neumann condition).

The flow of water in the unsaturated zone is described by a one-dimensional storage-output model. The unsaturated zone is considered to have two reservoirs; a root zone and an unsaturated zone in between the root zone and the saturated zone. Transient flow is approximated by a series of steady states (pseudo dynamic simulation). The spatial discretization in finite elements defines the nodal subdomains. Within each nodal subdomain, the soil type and the type of land use must be defined. One nodal subdomain can have different types of land use but only one soil type. The combination of soil type and land use defines the thickness of the root zone and important characteristics of the unsaturated zone such as groundwater level dependent capillary rise, storage coefficient and field capacity. The calculated soil moisture is the amount of water in the root zone divided by the root zone thickness and is thus best comparable with volumetric soil moisture content.

The precipitation and Makkink reference evapotranspiration (Winter et al., 1995) are input variables for SIMGRO. The reference evapotranspiration is multiplied by a crop factor to obtain the potential evapotranspiration. The actual evaporation is calculated by SIMGRO as a linear function of the soil moisture state.

The Lopikerwaard model is an operational hydrological model that is used by the controlling district water board (Holleman et al., 2005). The Lopikerwaard model was schematized in SIMGRO using 17 350 nodes. The model node distance is at maximum 150–200 m. The existing drainage network was modelled using smaller node distances. The model was run for 12 years (1989–2001) and the model results were discussed with local experts from the water board (plausibility test). On the basis of this test some adjustments were made to the model. Hereafter, the model was calibrated on 3 parameters (storage coefficient, transmissivity and drainage resistance) using an automatic calibration technique (see Zaadnoordijk, 2003). This calibrated model was used for this study. We ran the model once for the period March–October 2004 (using one rain gauge within the catchment as input) and the outcomes were set as the initial conditions of the subsequent model runs.

3.2.3 Meteorological input data

Rain gauges
In the Netherlands there are two permanent rain gauge networks, which are operated by the Royal Netherlands Meteorological Institute (KNMI). The largest network consists of 330 stations and has a density of approximately 1 station per 100 km^2. This network is maintained by volunteers who report daily rainfall depth at 08:00 UTC.

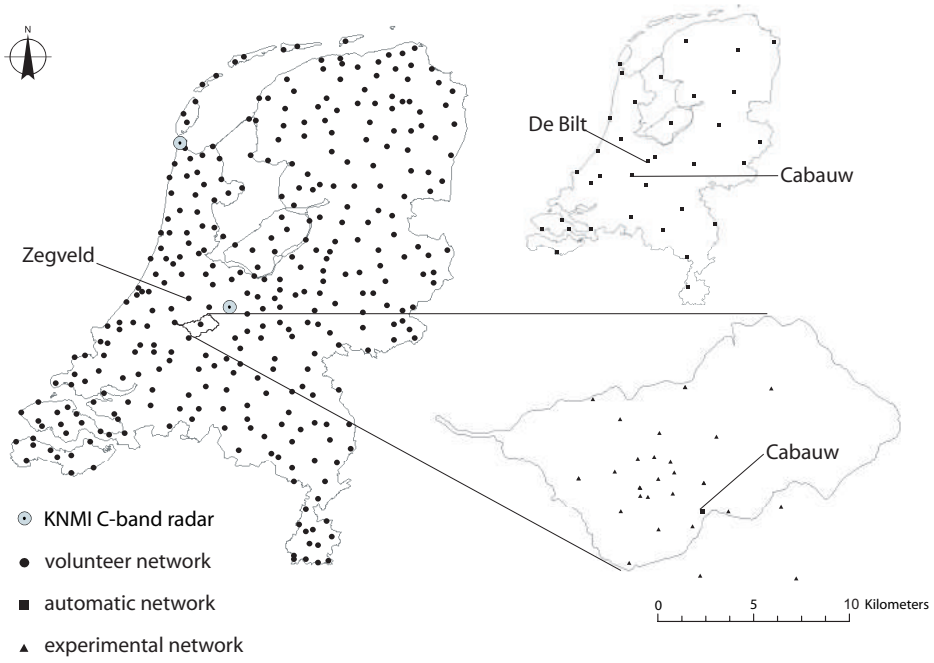

Figure 3.2 Locations of rain gauges and weather radars in the Netherlands; volunteer network with 330 rain gauges (temporal resolution of 1 day), automatic network with 35 tipping bucket rain gauges (temporal resolution of 10 min), experimental network with 30 tipping bucket rain gauges (equipped with event loggers) and 2 C-band Doppler radars.

An additional national network consists of 35 automatic rain gauges and has a density of approximately 1 station per 1000 km^2 and a temporal resolution of 10 min. Within the catchment of interest, we maintained an experimental high-density network for almost 8 months, that consisted of 30 tipping bucket rain gauges, all equipped with event loggers. The experimental network was set up to provide valuable information on the spatial structure of rainfall at short distances. For this study we mainly used our experimental network. Figure 3.2 shows the location of all the rain gauges of the three networks.

Radar

The KNMI operates two C-band Doppler radars, one at De Bilt and one at Den Helder (Figure 3.2), which both record 288 pseudo CAPPI (800 m) reflectivity fields each day (i.e. every 5 min) after removal of ground clutter (Wessels and Beekhuis, 1997). The resolution of these fields is 2.5×2.5 km^2. The measured radar reflectivity factor Z of each resolution unit is converted to surface rainfall intensity R using the Marshall-Palmer Z-R relationship, which has been found to be most suitable for stratiform

dominated rainfall events (Battan, 1973):

$$Z = 200 \times R^{1.6} \tag{3.1}$$

For both radars, the surface rainfall intensities are accumulated from 08:00 UTC until 08:00 UTC the next day, for each pixel. It is known that there is a distance-related underestimation of surface rainfall by weather radars due to spatial expansion of the radar beam and due to attenuation of the radar signal. Also overestimation due to the bright band (vertical profile of reflection) may occur. Therefore, data from the rain gauges of the volunteer network, from the same period, are used to make a range correction for each radar separately every day (Holleman, 2004). After the range correction a composite field is constructed by averaging the pixel values of the two radars up to a radius of 200 km away from each radar. Within a radius of 15 km from one radar, the information of the other radar is used. This composite radar field is an operational product of the KNMI and is used in this study.

Evapotranspiration
From the 35 stations with automatic rain gauges (Figure 3.2) also reference evapotranspiration data are available. The reference evapotranspiration is computed using the Makkink equation for grass (De Bruin, 1987), which is an empirical equation that requires only temperature and incoming short wave radiation. The data used in this study are 24 h accumulated reference evapotranspiration data over the period 00:00 UTC until 24:00 UTC, which is also an operational product of KNMI .

To adjust for the difference in accumulation period between the rainfall and evaporation data, we used evaporation data from one day earlier than the rainfall data. This can be justified by the fact that evaporation occurs mainly during daytime.

3.3 Methods

3.3.1 Introduction

We used 8 daily rainfall input scenarios for the period March to October 2004, of which 5 are spatially uniform and 3 are spatially variable rainfall fields. Details are given in Sect. 3.3.3. Using the 8 rainfall scenarios as input to the hydrological model we performed a sensitivity study on the output, i.e. the following variables:

- discharge: for all the pumping stations (Figure 3.1) we analyzed the average daily discharge resulting from the different rainfall scenarios;
- groundwater: we analyzed the development of groundwater level in time for all nodes for each rainfall scenario. From these time series we selected 1 day with highly variable rainfall to study the spatial variability of groundwater level within the catchment;
- soil moisture: for soil moisture we performed the same analysis as for groundwater.

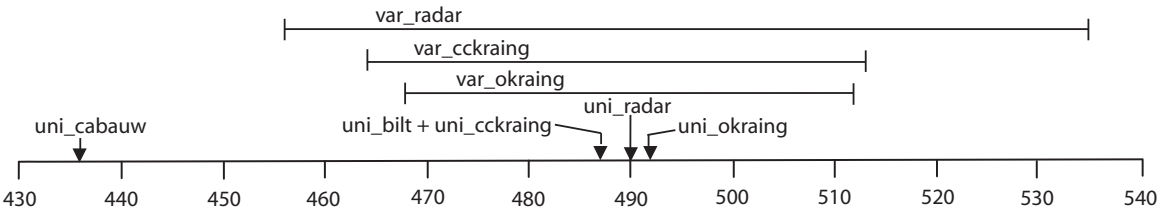

Figure 3.3 Spatial variation (range of values) of accumulated rainfall (March to October 2004) for all 8 scenarios. Spatially uniform scenarios only have one value.

3.3.2 Rainfall prediction

For rainfall prediction on each model node, we used the geostatistical interpolation technique Kriging, which is based on the concept of random functions, whereby the unknown values are regarded as a set of spatially dependent random variables. For a theoretical description readers are referred to Isaaks and Srivastava (1989), Goovaerts (1997) and Cressie (1993).

For 74 daily rainfall events with mean rainfall depth of at least 1 mm, we calculated the individual variograms of the standardized non-zero rainfall from the experimental network (Chapter 2). From these 74 individual variograms we also calculated the pooled variogram and fitted a spherical variogram model, which we used for the Kriging calculations:

$$g(h) = \begin{cases} C_0 \left(1 - \delta_k \left(h\right)\right) + C \left(\frac{3h}{2a} - \frac{h^3}{2a^3}\right) & 0 \leq h \leq a \\ C_0 + C & h > a, \end{cases} \tag{3.2}$$

in which the Kronecker delta function $\delta_k \left(h\right)$ is 1 for h=0 and 0 for $h \geq 0$. The nugget variance (C_0) is 0.172, the partial sill (C) is 1.270 and the range (a) is 10 km (see Table 2.1).

We used two different kriging techniques for the prediction of rainfall fields. Ordinary kriging was used to interpolate the measurements of the rain gauges of the experimental network. To combine both the rain gauges and the radar, we used ordinary colocated cokriging (Goovaerts, 1997). In the latter, radar is used as secondary data that influence the kriging prediction directly. Colocated cokriging accounts for the global linear correlation between rain gauges and radar. For more details on the spatial prediction methods we refer to Chapter 2.

3.3.3 Rainfall scenarios

The following scenarios of daily rainfall were used as input for the hydrological model to study its sensitivity:

(1) uni_cabauw; spatially uniform rainfall fields using only the rain gauge station Cabauw from the automatic KNMI network. This station is located within the

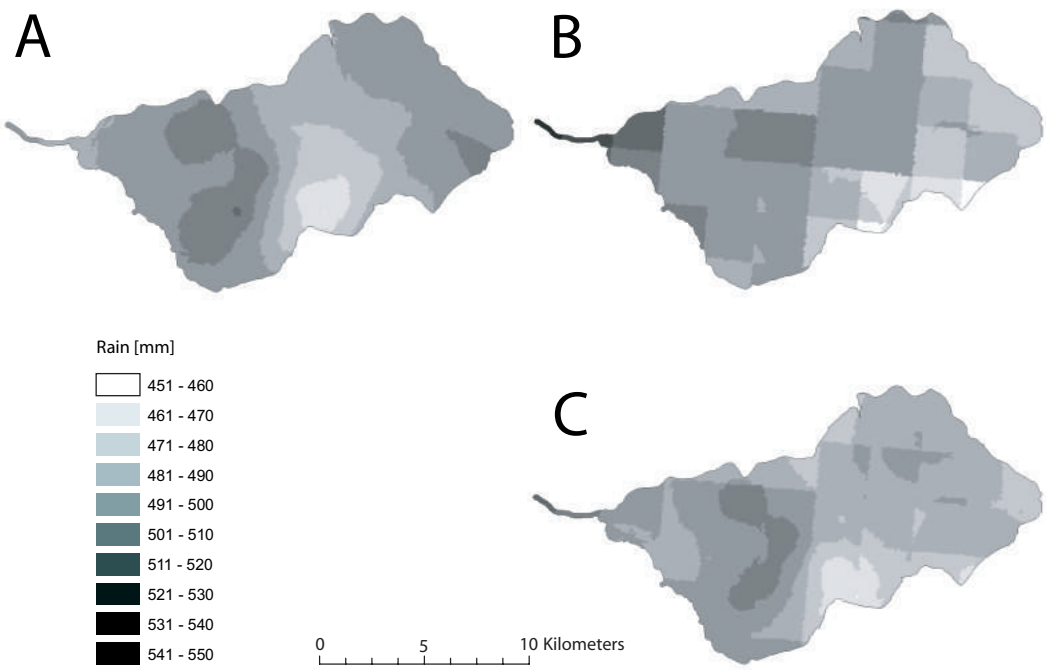

Figure 3.4 Spatial distribution of total rainfall from March to October 2004 as derived by (A) ordinary kriging (mean value 492 mm), (B) operational radar (mean value 490 mm) and (C) ordinary colocated cokriging (mean value 487 mm).

Lopikerwaard catchment and would therefore be a logical choice for hydrological studies if no other data were available.

(2) uni_bilt; spatially uniform rainfall fields using only the rain gauge station De Bilt from the automatic KNMI network. Station De Bilt is a well known rain gauge station in the Netherlands (close to KNMI headquarters) and is often used in hydrological studies without any consideration. This is mainly due to the fact that these data are easily available, free and central in the Netherlands, which in general gives the impression that it is a representative station.

(3) var_okraing; spatially variable rainfall field, using ordinary kriging to make point predictions using all the rain gauges of the experimental network.

(4) uni_okraing; same as scenario (3), but spatially uniform. Each day, the areal average of the daily spatially variable rainfall field is calculated, providing a spatially uniform rainfall field.

(5) var_radar; spatially variable rainfall field, using the operational radar data of KNMI.

(6) uni_radar; same as scenario (5), but spatially uniform.

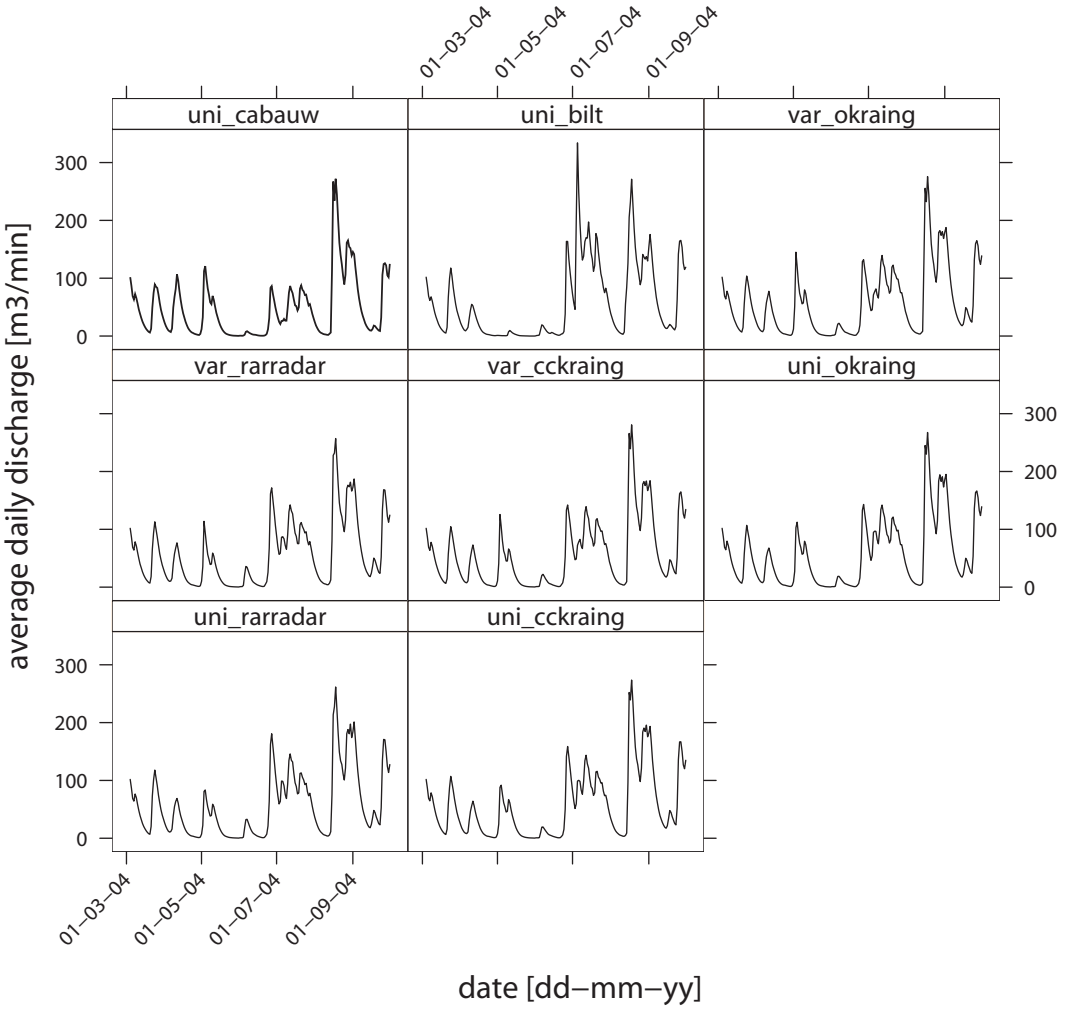

Figure 3.5 Hydrographs of pumping station Koekoek for all the rainfall scenarios.

(7) var_cckraing; spatially variable rainfall field, using ordinary colocated cokriging to make point predictions using all the rain gauge stations of the experimental network as well as the operational KNMI radar data.

(8) uni_cckraing; same as scenario (7), but spatially uniform.

For the time series running from March to October 2004 there were 22 days (10%) with missing or incomplete radar images. No radar image means no scenario 5 until 8 for these days. In that case we used scenario 3 or 4 (ordinary kriging).

Figure 3.3 shows the total rainfall amount for the period March to October 2004 for all 8 scenarios, that was calculated by summing up the daily rainfall input of each model node. In Figure 3.3 the spatially variable scenarios therefore show a range of values whereas the spatially uniform scenarios only have a single value. The total rainfall amount of station Cabauw stands out as it is about 10% less than the other uniform rainfall fields. Nevertheless, this rain gauge station is the only rain gauge

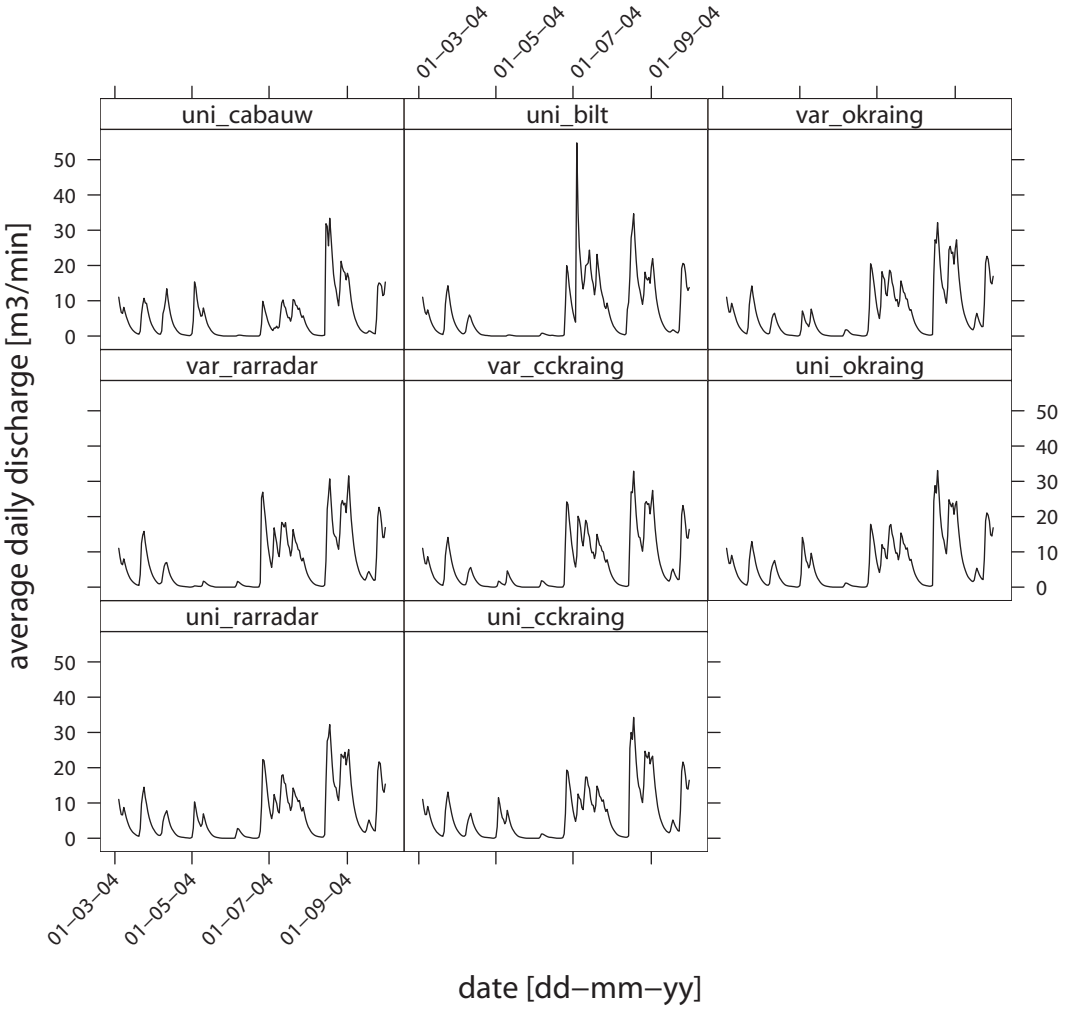

Figure 3.6 Hydrographs of pumping station Hoekse Molen for all the rainfall scenarios.

station of the automatic KNMI network located within the Lopikerwaard catchment and would have been a logical choice for hydrological studies.

Figure 3.4 shows the spatial distribution of the total rainfall from March to October 2004 as derived by ordinary kriging (scenario 3), operational radar (scenario 5) and ordinary colocated cokriging (scenario 7). We see that even over a relatively large period of 7 months, there are differences in rainfall of 50 to 100 mm over distances of about 15 km. The operational radar data show most spatial variability, followed by the rainfall fields obtained by ordinary colocated cokriging and ordinary kriging, as could also be seen in Figure 3.3. We also see in Figure 3.4 that for the three spatially variable rainfall scenarios, the smallest amount of total rainfall fell in the mid-south and the largest amount of rainfall fell in the west of the Lopikerwaard catchment.

Table 3.1: Percentage of days within March–October 2004 the discharge threshold value is exceeded. Threshold values vary per pumping station and are given underneath their names.

Scenario	Hoekse Molen $15\,m^3\ min^{-1}$	De Pleyt $65\,m^3\ min^{-1}$	Keulevaart $65\,m^3\ min^{-1}$	De Koekoek $115\,m^3\ min^{-1}$
uni_cabauw	8	9	7	10
uni_bilt	17	19	17	22
var_okraing	15	17	11	17
uni_okraing	13	15	10	16
var_rarradar	16	17	12	15
uni_rarradar	14	16	11	16
var_cckraing	15	17	11	17
uni_cckraing	12	14	11	16

3.4 Results

3.4.1 Discharge

With the hydrological model, we calculated for each rainfall scenario the average daily discharge of all the main pumping stations in the Lopikerwaard (Figure 3.1d) for the period March to October 2004. We select two pumping stations, the one belonging to the largest subcatchment (Koekoek) and the one belonging to the smallest subcatchment (Hoekse Molen), to show the hydrographs that result from the different rainfall scenarios. Figures 3.5 and 3.6 show the hydrographs for all rainfall scenarios of respectively pumping station Koekoek and Hoekse Molen. The hydrographs clearly show that for both pumping stations the rainfall scenario uni_bilt deviates most from the other scenarios. This holds true for all 4 pumping stations. Two major differences in the hydrographs are caused by a rainfall event in the beginning of May that was registered in the Lopikerwaard but not in De Bilt and a rainfall event in the beginning of July that was registered in De Bilt but was less prominent in the Lopikerwaard.

For all 4 pumping stations we analyzed the hydrographs and calculated the mean and standard deviation of the average daily discharge. The results are given in Figure 3.7. Most prominent are the results from the two rainfall scenarios that used only a single rain gauge, uni_cabauw and uni_bilt. Using only rainfall data from station Cabauw leads for all pumping stations to lower discharges and lower variation in discharge. Using only rainfall data from station De Bilt gives about the same mean, but yields a higher variation in discharge for all pumping stations. Between the spatially variable and spatially uniform rainfall scenarios we see little difference in the discharge statistics.

We also looked at the occurrence of high discharge. For each pumping station we defined a threshold value for the discharge, that more or less equals the sum of the mean and standard deviation of the discharge. Table 3.1 shows the percentage of days

within the period March–October 2004 (212 days) that discharge threshold values were exceeded, with the threshold values given underneath the pumping stations. From this table we see again that for all subcatchments the rainfall scenario based on only data from station Cabauw (uni_cabauw) leads to a lower amount of discharge peaks, while using data from only station De Bilt leads to a higher amount of discharge peaks in comparison to the other rainfall scenarios.

Although we cannot find structural differences in the time series statistics of discharge between spatially variable and spatially uniformed rainfall scenarios, there are certainly differences in discharge on specific days. These differences are caused by the spatial distribution of rainfall.

3.4.2 Groundwater

For one randomly selected node, number 15552 located in the northwest, we show the development of groundwater level in time for all rainfall scenarios (Figure 3.8). As we saw in the hydrographs, the development of groundwater level in time using rainfall scenario uni_bilt differs most from the other rainfall scenarios. Again, the main differences are found around May and July. Using data only from station De Bilt results in lower groundwater levels in May and higher groundwater levels in July in comparison to the other scenarios.

We analyzed the development of groundwater level in time for all nodes. Figure 3.9 shows the spatial distribution of the mean temporal groundwater level and Figure 3.10 shows the spatial distribution of the standard deviation of the temporal groundwater level. Note that the maps clearly show the imprint of the drainage network as a result of the artificially maintained water levels. To show the small differences between the spatially uniform and spatially variable scenarios, the spatial distribution of the difference (variable minus uniform scenarios) is shown as well. For all scenarios the spatial pattern of mean temporal groundwater level is more or less the same, although uni_cabauw and uni_bilt both show slightly lower groundwater levels in the eastern part of the Lopikerwaard. Using spatially variable instead of spatially uniform rainfall scenarios leads to slightly (2 cm) higher mean groundwater levels in the west and east and slightly (2 cm) lower groundwater levels in the middle part of the Lopikerwaard if we use information from the rain gauges. Using information from the radar leads to slightly (2 cm) lower groundwater levels in the west and slightly higher (2–4 cm) groundwater levels in the eastern part of the Lopikerwaard. The spatial pattern of the standard deviation of the temporal groundwater level of uni_bilt differs most from the other scenarios, showing an overestimation of the temporal variation of groundwater level. Uni_cabauw leads to slightly lower standard deviations. Using spatially-distributed rainfall scenarios instead of spatially uniform scenarios leads to higher standard deviations in the north and lower standard deviation in the south.

To get an impression of the effect of the different rainfall scenarios on day-to-day spatial variability, we selected one day with highly spatially variable rainfall. Figure 3.11 shows the rainfall within the Lopikerwaard for all rainfall scenarios at 1

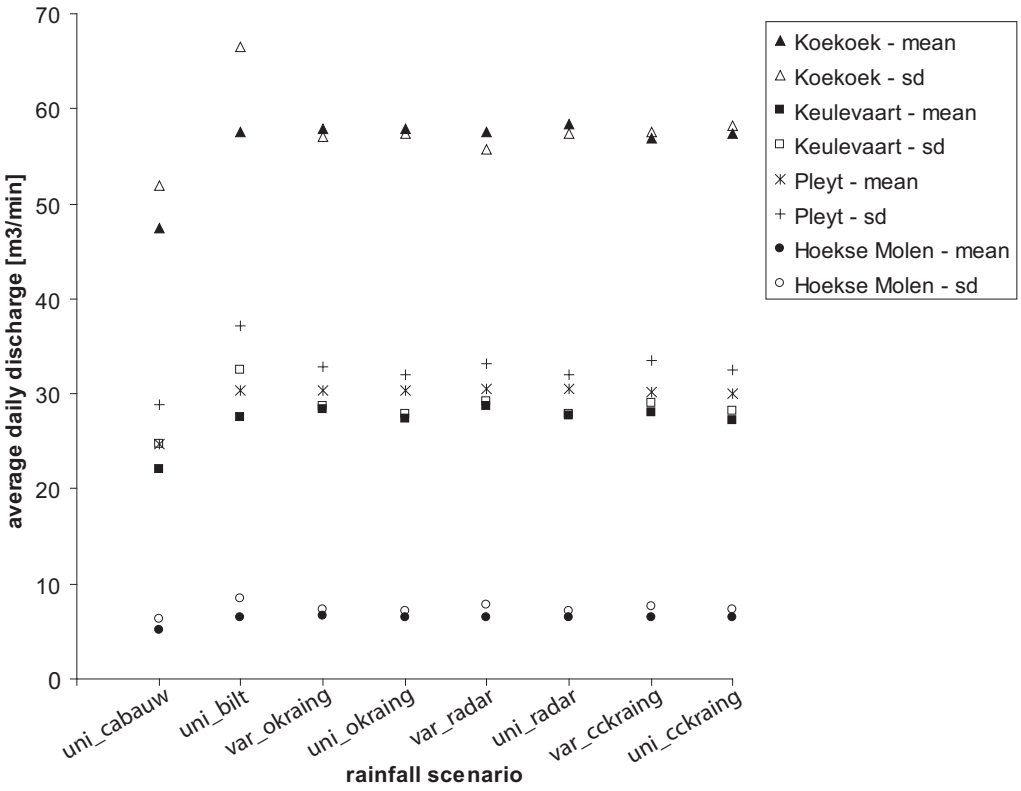

Figure 3.7 Mean and standard deviation of the average daily discharge for all 4 pumping stations in the Lopikerwaard for the period March–October 2004.

May 2004. Figure 3.12 shows its effect on the groundwater level (m from ground level) throughout the Lopikerwaard for all the rainfall scenarios. Again, rainfall scenario uni_bilt differs most from the other rainfall scenarios. At 1 May 2004 we see that the groundwater level within the Lopikerwaard using rainfall scenario uni_bilt is much lower than if we use rainfall information from the catchment itself, even if we use only one rain gauge (uni_cabauw). The spatially variable rainfall scenarios all show a different spatial pattern of groundwater level than the corresponding spatially uniform rainfall scenarios. Using spatially variable rainfall scenarios leads at 1 May 2004 to deeper groundwater levels in the north-eastern part of the Lopikerwaard.

3.4.3 Soil moisture

Again, we use node number 15552 to show the development of the soil moisture content in time for all scenarios (Figure 3.13). Similar to the hydrographs and groundwater the development of soil moisture content in time using scenario uni_bilt differs most from the other scenarios. Again, the main differences occur around May and July. Using data only from station De Bilt results in lower soil moisture contents in May and higher soil moisture contents in the beginning of July in comparison to the other

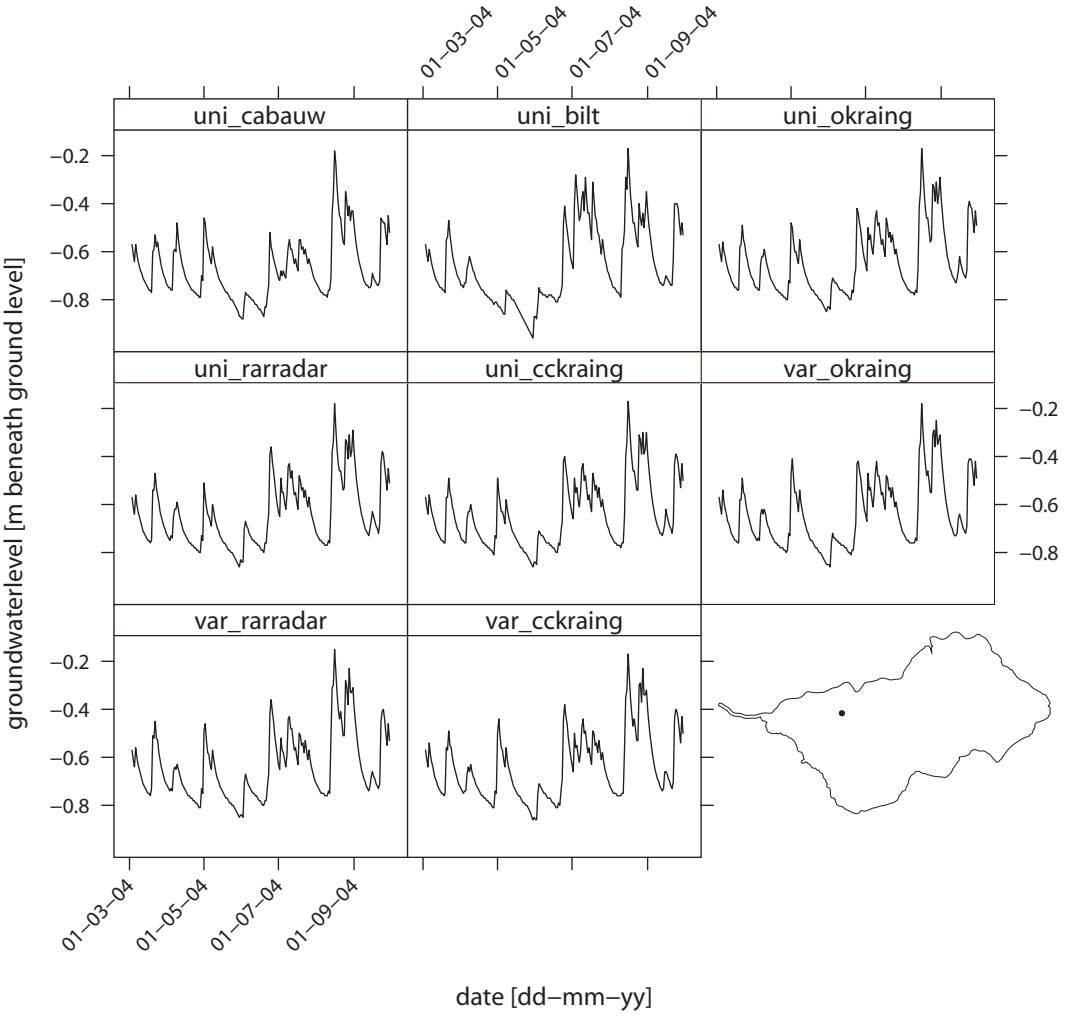

Figure 3.8 Development of groundwater level [m from ground level] in time of node number 15552 for all rainfall scenarios. The location of node number 15552 is given in lower right corner.

rainfall scenarios. The spatially variable rainfall scenarios yield at specific days higher peaks than the corresponding spatially uniform rainfall scenarios.

Also for soil moisture we analyzed its development in time for all nodes. The results are similar to that of groundwater and not shown here. The spatial pattern of the mean temporal soil moisture content is for all the rainfall scenarios more or less the same. The temporal variance in soil moisture content is overestimated when using rainfall information from station De Bilt in comparison to the other rainfall scenarios. For the other scenarios, the spatial pattern of temporal variation of soil moisture content is more or less the same.

To get insight in the day-to-day variability of soil moisture, Figure 3.14 shows the effect of the 1 May rainfall event (Figure 3.11) on the soil moisture content within the Lopikerwaard. The soil within the Lopikerwaard using rainfall scenario uni_bilt is much drier than if we use rainfall information from the catchment itself, even if we use

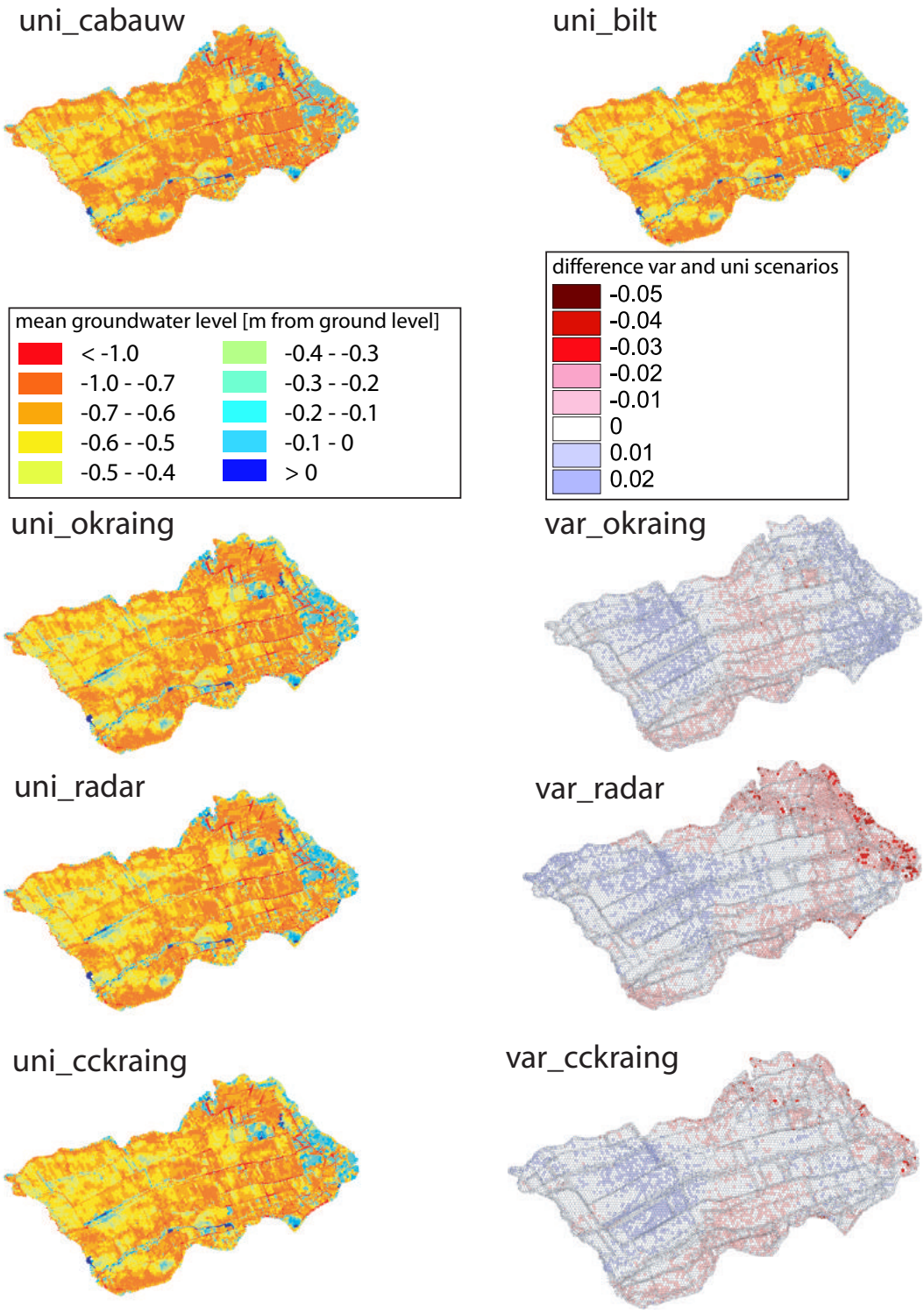

Figure 3.9 Spatial pattern of mean groundwater level [m from ground level] during March–October 2004 for all rainfall scenarios. For the spatially variable scenarios the spatial pattern of the differences (variable minus uniform) to the corresponding spatially uniform scenarios are shown.

only one rain gauge (uni_cabauw). The spatially variable rainfall scenarios all show a different spatial pattern of soil moisture than the corresponding spatially uniform rainfall scenarios. Using spatially variable rainfall scenarios leads at 1 May 2004 to higher soil moisture content in the western part and lower soil moisture content in the north-eastern part of the Lopikerwaard. This corresponds with the spatial pattern of rainfall (Figure 3.11). For all scenarios, the lowest soil moisture contents correspond with the urban areas of the Lopikerwaard (Figure 3.1b).

3.5 Conclusions and discussion

In this study we show that at specific days the spatial variability of daily rainfall has a major effect on discharge and spatial distribution of groundwater level and soil moisture content of the catchment. However, for the general behaviour of the hydrological system the use of uniform areal average rainfall suffices. Above all, this study shows that there is a great risk in using a single rain gauge, especially when located outside the catchment, for the prediction of discharge, spatial distribution of soil moisture and spatial distribution of groundwater level. For the general hydrological behaviour, this study corroborates the conclusion stated by Obled et al. (1994) that the spatial distribution of rainfall must be taken into account more because it improves the basin-average incoming volume rather than because of some dynamic interactions with flow-generating processes. However, for particular days, incorporating spatially variable information on rainfall is of great importance for the spatial distribution of interior catchment response.

Operational radar products proved to be a good method to capture the spatial variability of daily rainfall. The total amount of rainfall for the period March–October 2004 as estimated by the operational radar corresponds to the total amount found by the kriged rainfall fields based on 30 rain gauges within the catchment. The spatial variation (range of values) of the total rainfall was found to be higher for radar than for the kriged rain gauges. This is, among other factors influencing radar-estimated rainfall accuracy, maybe also caused by the fact that the dense network of rain gauges was not equally distributed over the catchment. However, based on the results of spatial prediction of soil moisture content and groundwater level at 1 May 2004 (Figs. 3.14 and 3.12) we can conclude that the same pattern is produced using either one of the spatially-distributed rainfall scenarios. Also considering the hydrographs and the discharge statistics, we can conclude that using radar-estimated rainfall input leads to similar (or slightly more varying) discharges as using a dense network of rain gauges. This shows that standard range-corrected radar products are sufficiently informative about the spatial variability of rainfall to be used in hydrological applications.

This study uses a hydrological model to study the sensitivity of spatially variable rainfall on interior catchment response. This can of course only be done if the model reflects the true catchment response. As often mentioned for this kind of studies, the results are dependent on the spatio-temporal variation of rainfall and the characteristics of the catchment, or in this case the characteristics of the hydrological model. It

is known that there is a space-time correlation in rainfall variability. Krajewski et al. (1991) found that basin response shows higher sensitivity with respect to the temporal resolution than to spatial resolution of the rainfall data. This study shows that even for daily rainfall it is important to take account of the spatial rainfall variability, if one aims to predict the internal hydrological state of the catchment.

The spatial variability of rainfall as well as the sensitivity of the hydrological model to this spatial variability is often neglected in hydrological studies. Failing to consider spatial variability of rainfall adequately will lead to errors in the values of the model parameters (e.g. storage capacity, drainage resistance) which will be wrongly adjusted to compensate for errors in the rainfall input data. Wrong conclusions about the hydrological reaction of a specific area due to e.g. climate change can be one of the consequences. This study clearly shows the danger of using rainfall information from a single rain gauge, which is still common practice in hydrological engineering, because of cost considerations or because of reluctance of using operational radar data (e.g. because its predictive quality is often discussed). With this study we show the potential and necessity of using the operational radar products in hydrological studies.

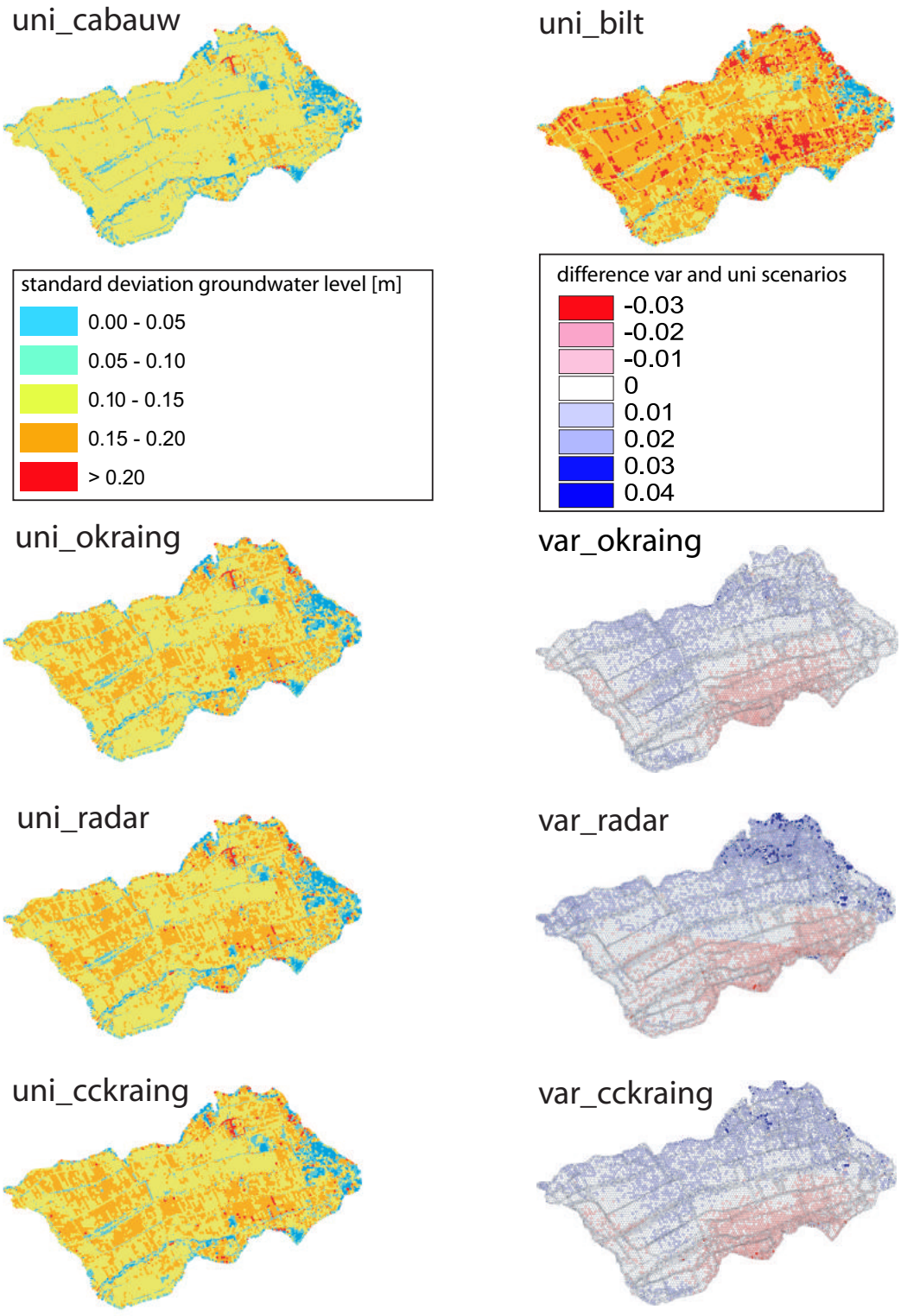

Figure 3.10 Spatial pattern of temporal standard deviation of groundwater level [m] during March–October 2004 for all rainfall scenarios. For the spatially variable scenarios the spatial pattern of the differences (variable minus uniform) to the corresponding spatially uniform scenarios are shown.

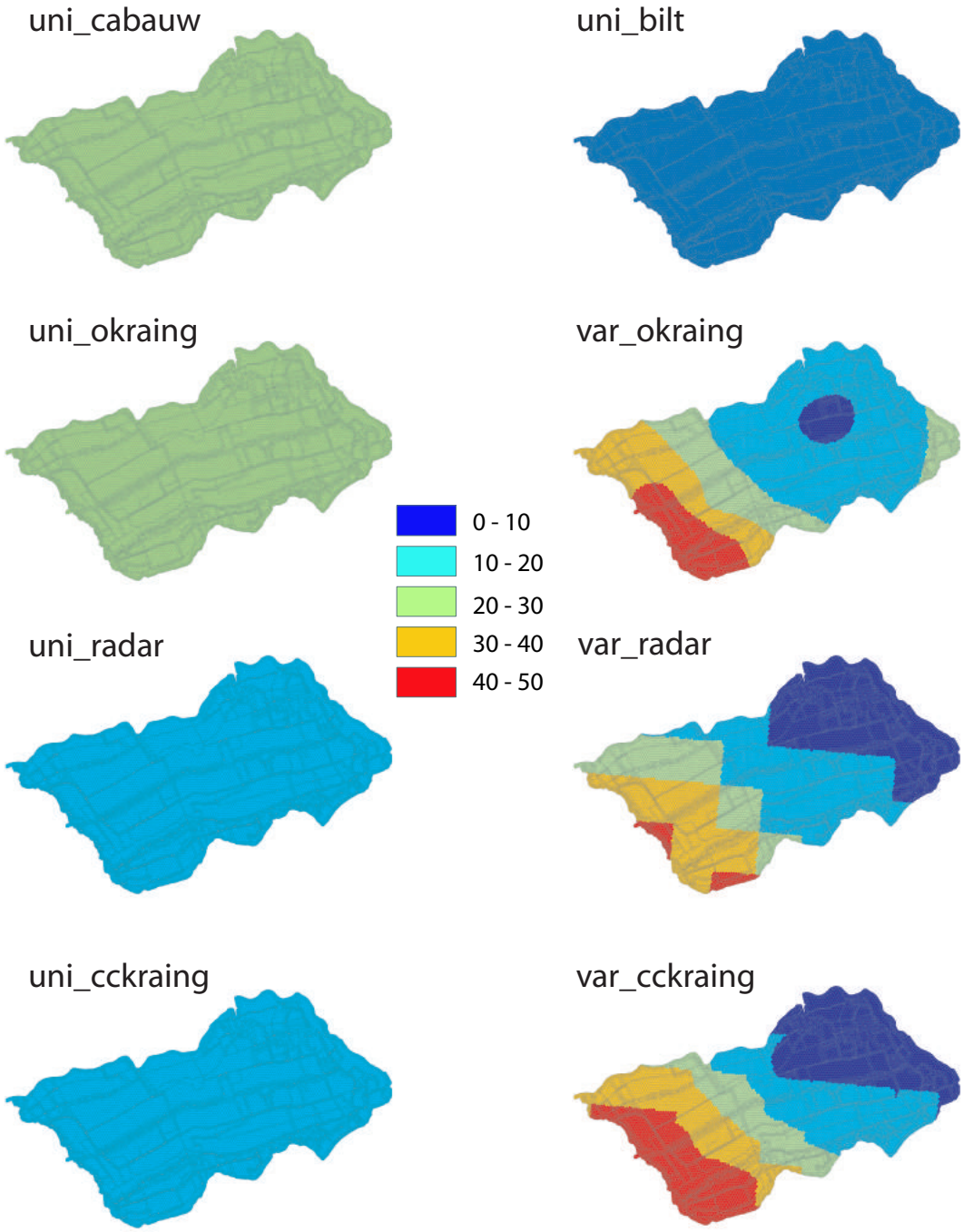

Figure 3.11 Spatial pattern of rainfall in mm on 1 May 2004 for the different rainfall scenarios in the Lopikerwaard.

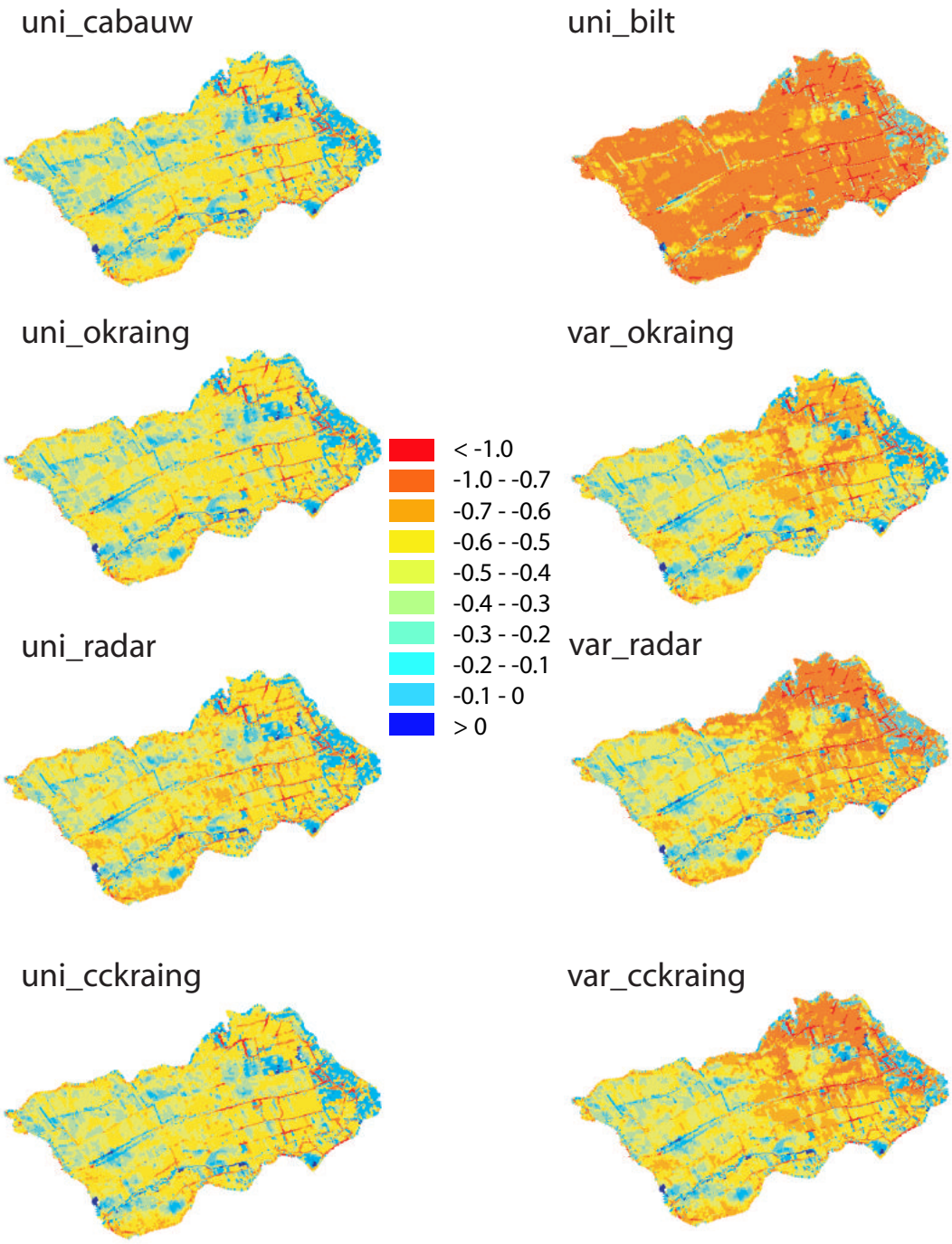

Figure 3.12 Spatial variation of groundwater level [m from ground level] on 1 May 2004 for the different rainfall scenarios.

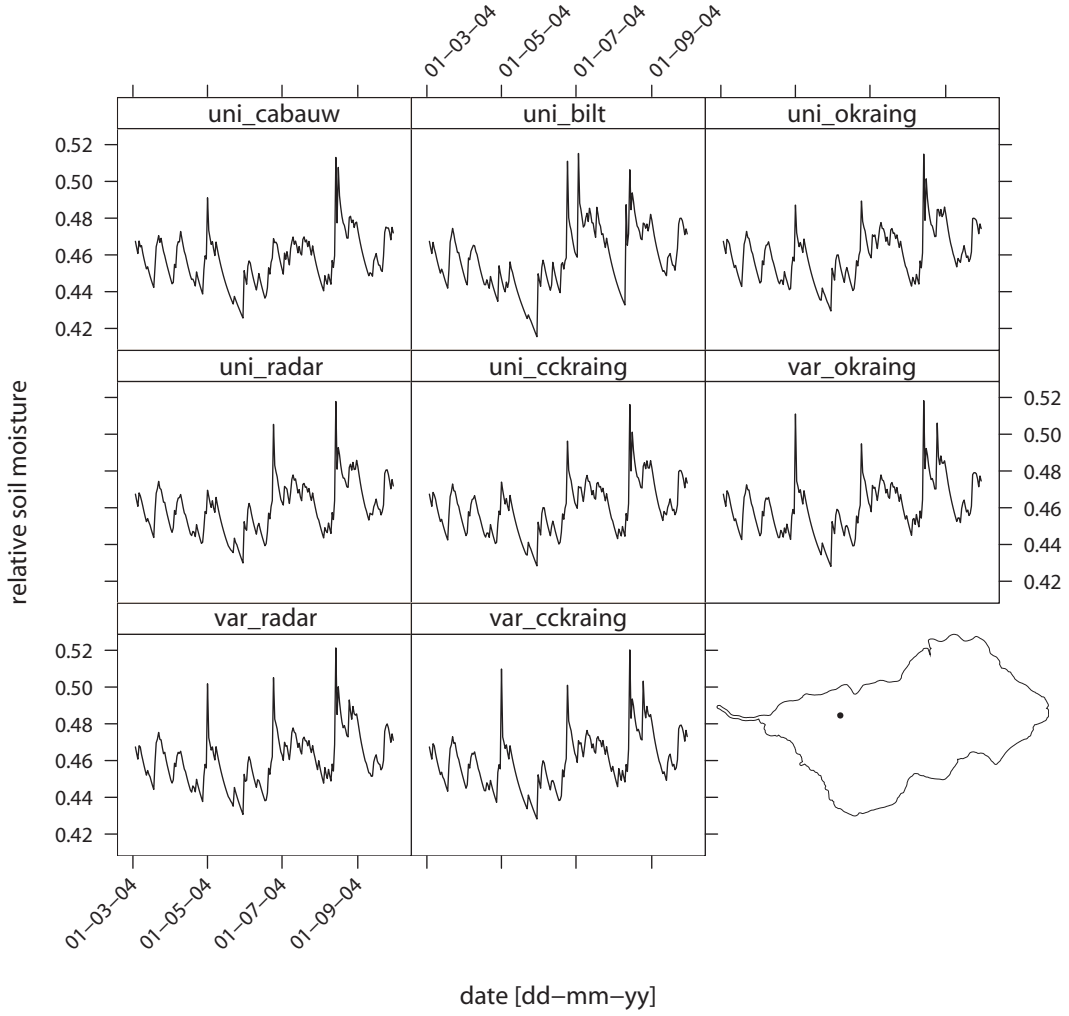

Figure 3.13 Development of soil moisture content in time of node number 15552 for all rainfall scenarios. The location of node 15552 is given in lower right corner.

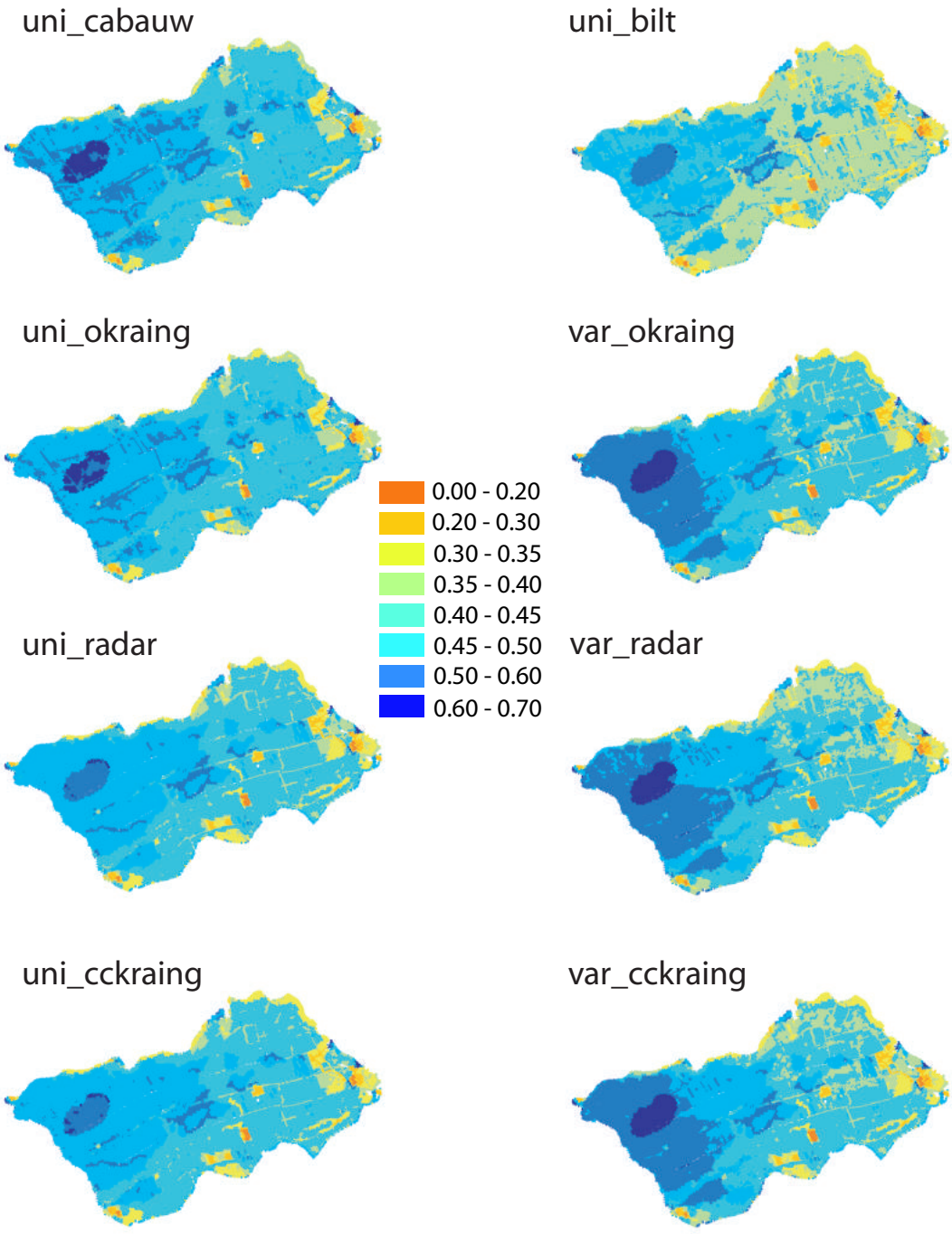

Figure 3.14 Spatial pattern of soil moisture content [–] on 1 May 2004 for the different rainfall scenarios in the Lopikerwaard.

4 Remotely sensed latent heat fluxes for improving modelled soil moisture predictions: a case study

Schuurmans, J.M, F.C. van Geer & M.F.P. Bierkens (2008), Remotely sensed latent heat fluxes for improving modelled soil moisture predictions: a case study. Submitted to Remote Sens. Environ.

Abstract

This chapter investigates whether the use of remotely sensed latent heat fluxes improves the accuracy of spatially-distributed soil moisture predictions by a hydrological model. By using real data we aim to show the potentials and limitations in practice. We use (i) satellite data of both ASTER and MODIS for the same two days in the summer of 2006 that, in association with the Surface Energy Balance Algorithm for Land (SEBAL), provides us the spatial distribution of daily ET_{act} and (ii) an operational physically based distributed (25 m x 25 m) hydrological model of a small catchment (70 km^2) in The Netherlands that simulates the water flow in both the unsaturated and saturated zone. Firstly, model outcomes of ET_{act} are compared to the processed satellite data. Secondly, we perform data assimilation that updates the modelled soil moisture. We show that remotely sensed ET_{act} is useful in hydrological modelling for two reasons. Firstly, in the procedure of model calibration: comparison of modelled and remotely sensed ET_{act} together with the outcomes of our data assimilation procedure points out potential model errors (both conceptual and flux-related). Secondly, assimilation of remotely sensed ET_{act} results in a realistic spatial adjustment of soil moisture. As both ASTER and MODIS images were available for the same days, this study provides also an excellent opportunity to compare the worth of these two satellite sources. It is shown that, although ASTER provides much better insight in the spatial distribution of ET_{act} due to its higher spatial resolution than MODIS, they appeared in this study just as useful.

4.1 Introduction

Insight into the spatial distribution of soil moisture within a catchment is of great importance for e.g. farmers and water boards. Accurate prediction of spatially-distributed soil moisture is helpful for optimizing irrigation gifts, hydrological drought forecasting and the assessment of catchment wetness for flood control. Physically based spatially-distributed hydrological models have the potential to provide this insight. As more spatially-distributed information about land surface characteristics becomes available and computer capacity increases, the distributed hydrological models are also developed at higher spatial resolutions (Bergström and Graham, 1998). Potentially these high resolution models can give us insight into the hydrological processes in more detail. However, the possibilities to calibrate those models or to validate the accuracy of the model predictions is often limited by the number of (distributed) measurement data. In most cases only observations of groundwater are available at a few points, while in-situ measurements of soil moisture are rare. Discharge data, if available, give only integrated hydrological information of an area. A data source that does provide spatially-distributed soil moisture data, or soil moisture related data, are satellites. This chapter focusses on satellites that are equipped with thermal bands. Models that are based on the surface energy balance like for instance SEBS (Su, 2002) and SEBAL (Bastiaanssen et al., 2005) can convert thermal band satellite images into images of actual evapotranspiration. These products can be used for model verification or model calibration, as was demonstrated by Immerzeel and Droogers (2008).

The purpose of this study is to answer the question: "Can remotely sensed latent heat fluxes (i.e. actual evapotranspiration, ET_{act}) improve the accuracy of the prediction of spatially-distributed soil moisture as made by a distributed hydrological model?". We will answer this question by using a *real case* study, by which we aim to show the potentials and limitations of our approach for hydrological model validation in practice. Outcomes of an operational physically based distributed (25 m x 25 m) hydrological model of a small catchment (70 km^2) in The Netherlands are compared with satellite (both ASTER and MODIS) based ET_{act} for the same two days in summer 2006. The Surface Energy Balance for Land (SEBAL) is used in this study to process the satellite data. We use an operational physically based distributed (25 m x 25 m) hydrological model that simulates the water flow in both the unsaturated and saturated zone, from now on referred to as METASWAP. It is not the scope of this study to calibrate this model. In order to improve the model predictions of soil moisture we assimilate ET_{act} into our model, using a statistical correction method that weighs the error of both hydrological model based and satellite based ET_{act}. In an earlier study we already assimilated ET_{act} into a spatially-distributed hydrological model (Schuurmans et al., 2003). Although promising, the results of this former study remained unverified, as was pointed out by Pipunic et al. (2008). In this study we use soil moisture measurements from 5 locations within the catchment, as well as validation data of SEBAL from The Netherlands, in order to get insight into the error of both hydrological model based and satellite based ET_{act} rather then using different (unknown) weighing factors as we did in our previous study. As both an ASTER and

MODIS image were available for the two days (8 June and 17 July), this study also provides an excellent opportunity to compare the worth of these two satellite sources.

The remainder of this chapter is organized as follows. Section 4.2 gives a description of the catchment and the data that are used in this study. Section 4.3 deals with the methods; first the, for this study, most important principles of our hydrological model (METASWAP) are given as well as some validation results considering soil moisture and groundwater level. The method section continues with a brief description of the SEBAL algorithm and finally the data assimilation procedure and its parameterization are described. Results from the comparison between METASWAP and SEBAL based ET_{act} as well as the outcomes of our data assimilation method are shown in Section 4.4, which are discussed in Section 4.5. In Section 4.6 we state the main conclusions of this study and give some recommendations to improve the hydrological model used.

4.2 Study area and data

4.2.1 Study area

Our study area is called the "Langbroekerwetering" and lies in the central part of The Netherlands (Figure 4.1A). The Langbroekerwetering (~ 70 km^2) is located along the rim of the Holocene Rhine-Meuse delta (low elevation, peat and clay of the last 4000 years: Berendsen and Stouthamer, 2000), which onlaps coversands and sandur outwash deposits in front of a Saalian ice-pushed ridge (high elevation, 150.000 years old: Busschers et al., 2007). Figure 4.1B shows the elevation together with the location of the rain gauges and the soil moisture measurements, land use and soil types of the Langbroekerwetering. For a description of the soil types we refer to Table 4.1. At the higher elevations with coarse sand forest dominates the area, while in the lower area grassland dominates. Within the area some small villages (built-up area) are located. The landuse map is derived from the Dutch national land-cover database LGN (Oort et al., 2007; De Wit and Clevers, 2004).

Table 4.1: Description of soil types within study area (Wösten et al., 1988) as well as the indexed error zone (see Section 4.3.3).

soil unit	description	error zone
7	drift sand	5
8	podzol in loam poor fine sand	3
9	podzol in loamy fine sand	3
12	enkeerd in loamy fine sand	4
14	podzol in coarse sand	5
16	light clay	2
17	clay with heavy clay layers	1
18	clay on peat	1
19	clay on sand	2

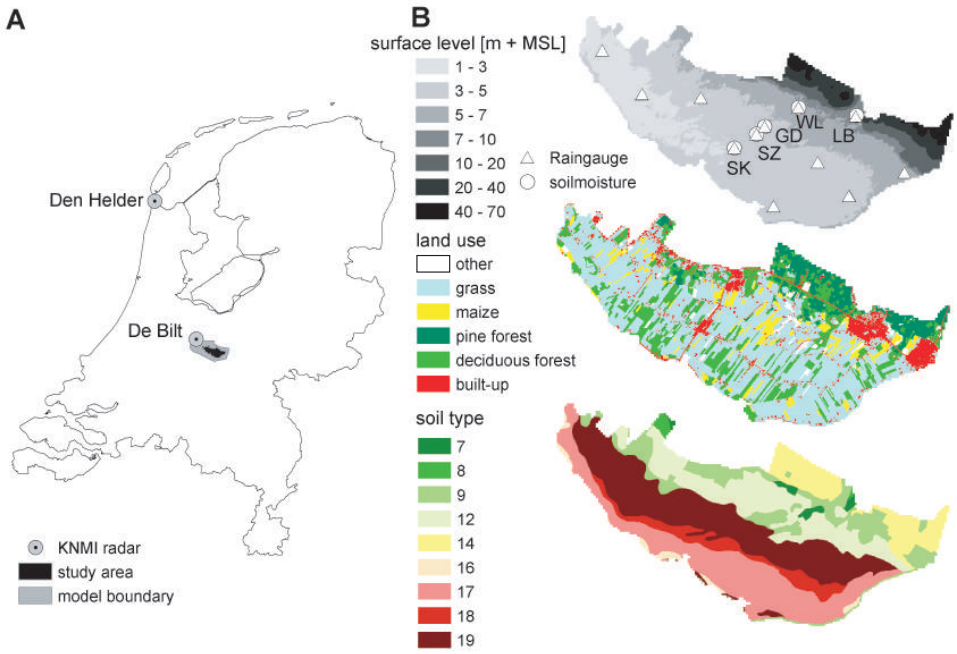

Figure 4.1 A: Location of study area within the Netherlands and the location of the two rainfall radars. B: surface level [m + mean sea level] with rain gauge and soil moisture measurement locations, land use and soil types (see Table 4.1) of study area.

4.2.2 Data

Rainfall
The daily rainfall fields that are used as input for our hydrological model are a combination of meteorological radar (Figure 4.1A) and rain gauges within and closely around the model area. The interpolation method used is a geostatistical method that combines radar estimates with rain gauge observations. The method makes use of colocated cokriging and is explained in more detail in Chapter 2. Figure 4.2A shows the spatial distribution of the total rainfall during March–November 2006 within the study area. There is up to 200 mm difference over 8 months within 15 km, which is even more than what we found in 2004 in another equally sized catchment (50–100 mm over 7 months, see Chapter 3). Figure 4.2B shows the time series of the spatial mean rainfall within the study area and the reference evapotranspiration.

Evapotranspiration
Our hydrological model uses Makkink (De Bruin, 1987; Makkink, 1957; Winter et al., 1995) reference evapotranspiration (ET_{ref}) as input. The variables needed to calculate ET_{ref} (Equation 4.1) were measured in De Bilt (Figure 4.1A) by the Royal Netherlands Meteorological Institute (KNMI). The KNMI delivered daily values of ET_{ref}, which we assumed to be spatially uniform over the model area. Further details about the evapotranspiration simulation in our hydrological model can be found in Sub-

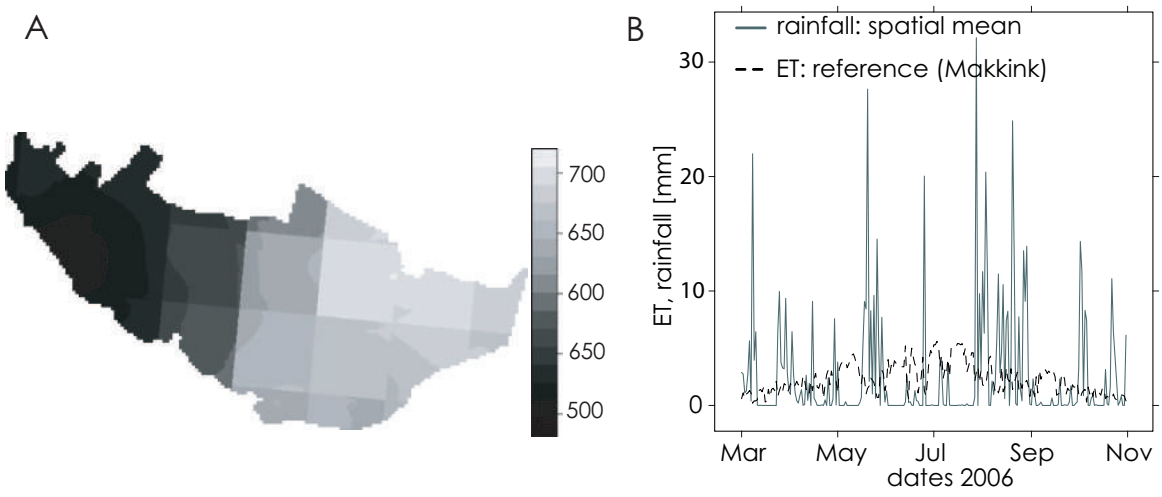

Figure 4.2 Spatial distribution of total rainfall [mm] March–November 2006 (A) and time series of the spatial mean of rainfall within the study area and the reference evapotranspiration (B).

section 4.3.1. To investigate whether remotely sensed daily ET_{act} can improve our hydrological model, we use both ASTER (Advanced Spaceborne Thermal Emission and Reflection radiometer) and MODIS (MODerate resolution Imaging Spectroradiometer) satellite measurements of summer 2006 in association with the Surface Energy Balance Algorithm for Land (SEBAL). This provided us with images of ET_{act} that have a spatial resolution of 15 m x 15 m for ASTER and 250 m x 250 m for MODIS. Both satellite sources were available at 8 June and 17 July 2006. More details about SEBAL can be found in Subsection 4.3.2.

Soil moisture

At 5 locations within the study area we measured soil moisture (Figure 4.1B: SK, SZ, GD, WL and LB). The soil moisture locations were selected such that they lie within different soil types. At each location we measured soil moisture at 5 depths: 5, 10, 15, 30 and 50 cm below surface. Measurements were done using 20 cm ECH$_2$O probes (EC-20), which use the capacitance technique (an electromagnetic technique comparable to time domain reflectometry (TDR)) to derive the dielectric permittivity of a medium (Bogena et al., 2007). The sensors were placed vertically to avoid water stagnation. All measurements were done in duplo with $\sim$ 1 m horizontal distance between the sensors. The output of our ECH$_2$O sensors, volumetric moisture content (VMC [cm^3 cm^{-3}]), was measured with a temporal resolution of 5 min. For each location we performed a calibration with observed VMC (Appendix 3). According to the manufacturer the accuracy is $\sim$ 2% with soil specific calibration. The application of electromagnetic sensors to conductive media, such as saline soils, certain clay soil and organic soils is hindered due to significant attenuation effects of the desired signal (Bogena et al., 2007). Czarnomski et al. (2005) concluded that the EC-20 performed nearly as well as a TDR probe in a field experiment. In Section 4.3.1 we show the soil moisture measurements together with the modelled soil moisture.

Groundwater
There are several observation wells within the study area that are measured twice a month. The measured hydraulic heads are compared to the modelled groundwater levels. A map with the results per observation well are given in Section 4.3.1.

4.3 Methods

4.3.1 Hydrological model

This section starts with a short description of the model code of METASWAP, focussing on the land-plant-atmosphere interaction that is important for the later assimilation of ET_{act} in METASWAP. After that, validation results of the model concerning soil moisture and groundwater level are given.

MetaSWAP code
The model used in this study is a coupled groundwater (saturated zone) and unsaturated zone model, referred to as METASWAP from now on. The groundwater model is based on the MODFLOW model code (McDonald and Harbaugh, 1983). The unsaturated zone model, is a quasi steady-state model that uses a sequence of steady-state water content profiles for dynamic simulation (Van Walsum and Groenendijk, 2008). The steady-state water content profiles were obtained by running a steady-state version of the SWAP model (Van Dam, 2000) off-line. The model area is divided into SVAT-units (Soil Vegetation Atmosphere Transfer), which are smaller or equal to the size of the MODFLOW cell. One MODFLOW cell can be coupled to several SVAT-units. The SVAT-units form parallel vertical columns, which are divided into a root zone and a subsoil layer. METASWAP distinguishes 21 different soil types. For each soil type the model has predefined sub-layers with corresponding soil physical parameters (Van Genuchten parameters) to be able to convert pressure head to soil moisture content. Only vertical flow according to Richards' equation is taken into account. All lateral exchanges are assumed to take place in the saturated zone. The thickness of the root zone is user specified (Table 4.2).
In our model, the size of the MODFLOW cells is 100 m x 100 m. The SVAT-units have a resolution of 25 m x 25 m inside the study area and 100 m x 100 m outside the study area, within the model boundaries (Figure 4.1A). The groundwater model is schematized into 7 layers. For more specifications of the groundwater model we refer to Appendix 4.
A flux that is of importance for soil moisture, and which is influenced also by the soil moisture conditions is evapotranspiration. Our model uses Makkink (De Bruin, 1987; Makkink, 1957; Winter et al., 1995) reference evapotranspiration (ET_{ref} [mm day^{-1}]) as input (spatially uniform), which is an empirical equation that only takes into account the incoming short wave radiation and air temperature (Equation 4.1).

The measured ET_{ref} in this study comes from De Bilt.

$$\lambda \rho ET_{ref} = 0.65 \cdot \frac{s}{(s+\gamma)} \cdot K^{\downarrow}, \tag{4.1}$$

in which λ is the latent heat of vaporization (2.27 E+06 J kg^{-1}), ρ is the density of water [kg m^{-3}], s is the gradient of the vapor pressure curve [mbar K^{-1}], γ is the psychometric constant (0.66 mbar K^{-1} at sea level) and $K^{\downarrow}$ [W m^{-2}] the incoming short wave radiation. The potential evapotranspiration (ET_{pot} [mm day^{-1}]) is calculated by multiplying ET_{ref} with a crop factor (cf [-]: Equation 4.2), which is related to the land use type and can vary throughout the season (Feddes, 1987).

$$ET_{pot} = cf \cdot ET_{ref} \tag{4.2}$$

The actual evapotranspiration (ET_{act} [mm day^{-1}]) is equal or a fraction of ET_{pot} depending on the soil moisture conditions and the land use type (Equation 4.3).

$$ET_{act} = FR \cdot ET_{pot}, \tag{4.3}$$

in which FR is the called the Feddes reduction factor from now on. Figure 4.3 shows the so called Feddes-reduction curve (Feddes et al., 1978), which gives the relation between FR and the soil moisture pressure head. The values of the critical pressure heads (h_1 until h_4) can be defined for each land use type, see Table 4.2. It must be noted that the choice of these values is one of the uncertainty sources in the model. Between h_1 and h_2 the evapotranspiration is reduced due to oxygen deficiency in the root zone (too wet soils), but this is neglected in our model, except for maize (see Table 4.2). Between h_2 and h_3 (the latter is called the reduction point) evapotranspiration is not hampered by soil moisture conditions. Whether h_3 equals h_{3l}, h_{3h} or an linear interpolation in between these two values, depends on the potential transpiration rate (default h_{3l} if $ET_{pot} = 1$ mm day^{-1}; h_{3h} if $ET_{pot} = 5$ mm day^{-1}). Between h_3 and h_4 (latter is called wilting point) the evaporation is reduced due to soil moisture deficit. The root zone is divided into 10 equal sized sub-layers, assuming a constant root density, and the reduction function is applied to each sub layer. The final modelled ET_{act} is the mean of those 10 sub layers. The model takes also interception evaporation into account. It is possible to define an interception capacity for each land use type. In this study only for forest an interception capacity is defined. The interception capacity for pine forest is 1.0 mm m^{-2} throughout the season and 0.3-1.0 mm m^{-2} for deciduous forest depending on the season.

Parameterization and validation

In the following validation results of METASWAP are given. First for the unsaturated zone (soil moisture) and then for the saturated zone (groundwater level).

Figure 4.4 shows for all soil moisture measurement locations the measured (both left and right side) and modelled volumetric moisture content at the 5 different depths. According to the measurements at location SK the upper layers (5 & 15 cm) are modelled too wet; 30 & 50 cm are modelled well and 70 cm is again too wet. However, we experienced during fieldwork that these data should be used carefully. Besides the

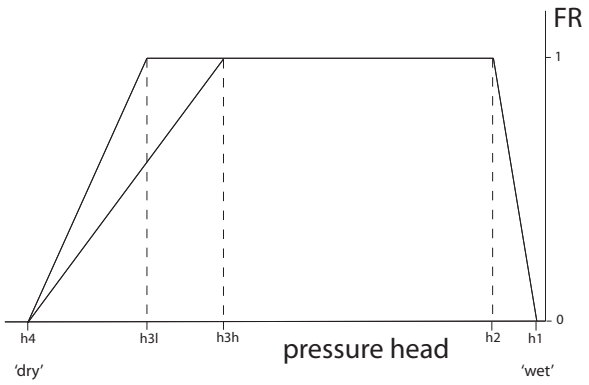

Figure 4.3 Feddes reduction factor (FR) as function of pressure head: between h_1 and h_2 there is reduction of potential evaporation because of oxygen deficit of root. Between h_2 and h_3 ET_{act} equals ET_{pot}. Between h_3 (h_{3l} and h_{3h} correspond to resp. $ET_{pot} = 1$ mm day^{-1} and $ET_{pot} = 5$ mm day^{-1}) and h_4 there is evapotranspiration reduction due to water deficit. After (Feddes et al., 1978)

Table 4.2: Root zone thickness (rz [m]), crop factors (cf [-]) and predefined pressure heads [m] (Taylor and Ashcroft, 1972) of Feddes curve (Figure 4.3) for the land use types within the study area and their areal percentage. Only land use types with an areal percentage higher than 2 % are taken into account.

land use	% area	rz	cf	h_1	h_2	h_{3h}	h_{3l}	h_4
grass	54	0.3	1.0	0	0	-2	-8	-80
maize	6	0.6	0 - 1.3	-0.15	-0.3	-3.25	-6	-80
built-up	8	0.3	0.05	0	0	-3.2	-8	-80
pine forest	8	1.0	1.0	0	0	-3.2	-8	-80
deciduous forest	20	1.0	1.0	0	0	-3.2	-8	-80

fact that the measurements are done in heavy clay, which can lead to significant attenuation effects (Bogena et al., 2007), we observed clay cracks that were formed in these soils during severe drought. For location SZ, the model is wetter than the measurements at all depths. The dynamics of the measurements are however modelled well for the depths 5 & 15 cm. In the deeper layers the measurements show much less dynamics than the model shows. For location GD the model represents the measurements quite well during the wet periods. However during drying out of the soil the model remains too wet. At location WL the model is too wet, except for the period in July where the modelled soil moisture at 5 and 15 cm is modelled dryer than was measured. In the forest, at location LB, the model is too dry for the upper layers. At 50 and 70 cm the model is slightly too wet, except for the dry period. It must be mentioned that especially the upper layer of LB contains a lot of organic material, which can decrease the accuracy of measurement considerably (Bogena et al., 2007).

For a description of the groundwater part of the model and its parameterization we refer to Appendix 4. Our model has constant head boundaries, which are the output of a larger model (from which this model was cut) after it was run for 5 years (2001 - 2006). The results of this 5-year model run are compared with measurements

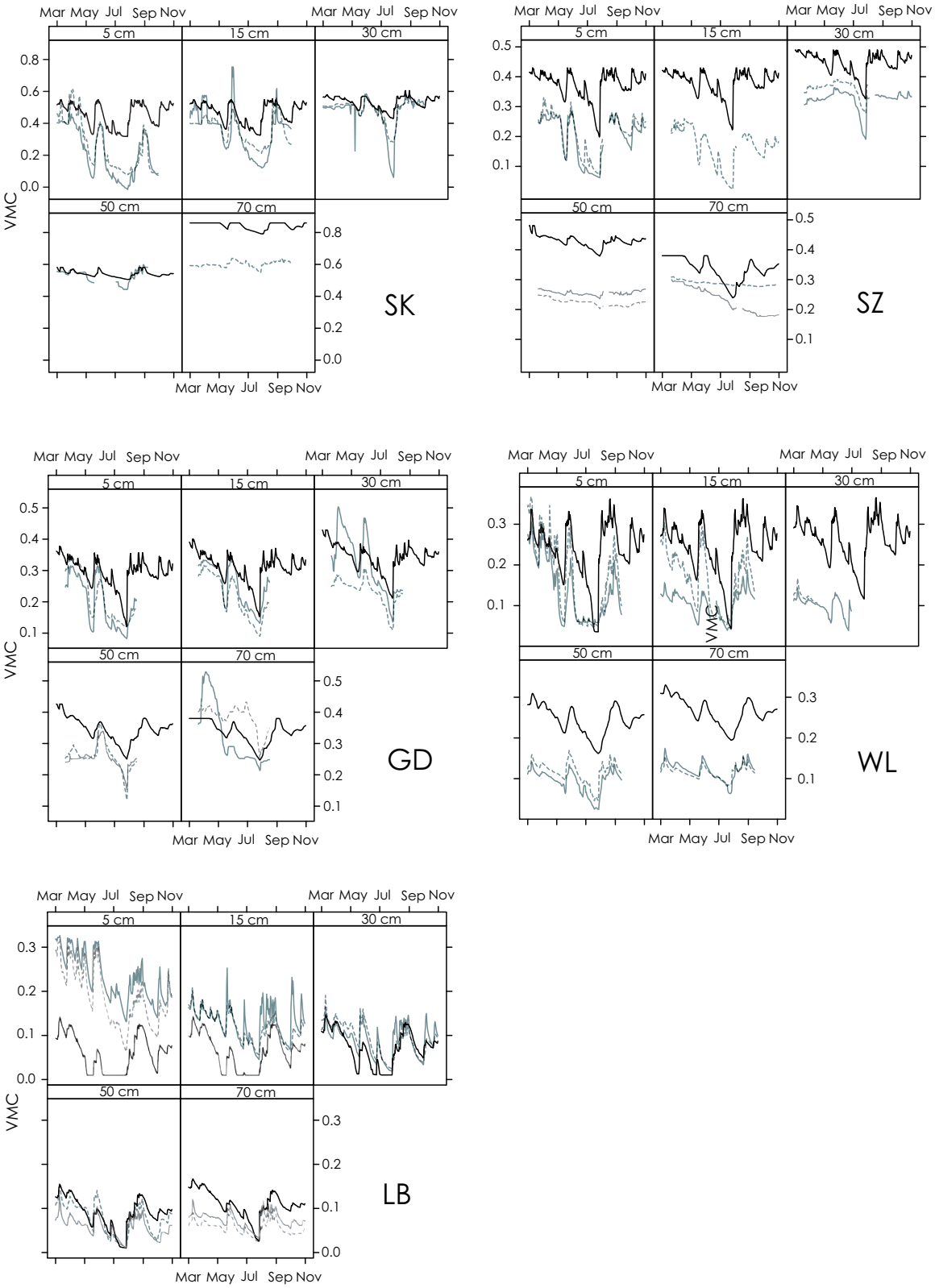

Figure 4.4 Time series of volumetric soil moisture content [cm^3 cm^{-3}] per measurement location and per depth according to model (black solid line) and measurements (left side:grey solid line, right side: grey dotted line)

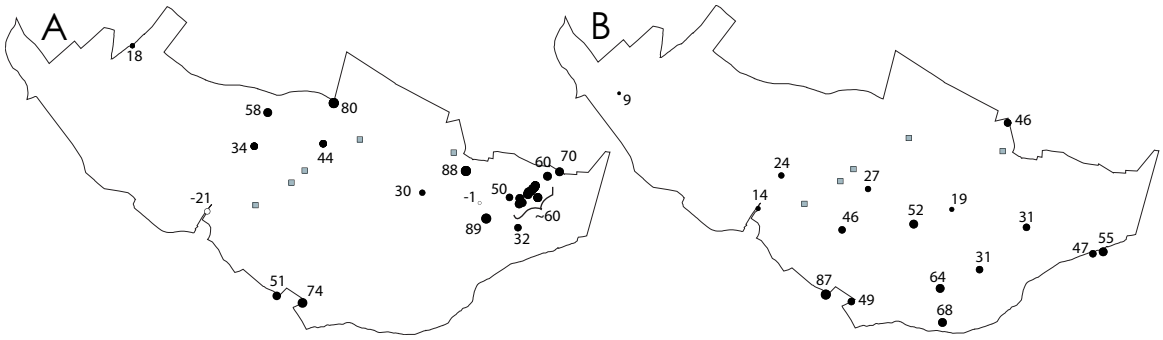

Figure 4.5 Bubble plot of bias in phreatic (A) and confined (B) groundwater during 2001 - 2006 [cm]. Positive values (model too wet) are represented by black dots, negative values (model too dry) are represented by white dots. Locations of the soil moisture measurements are indicated with grey squares.

from observation wells within the study area, of which most are measured twice a month. Figure 4.5 shows bubble plots of the bias (mean difference between model and measurement) in cm for respectively the phreatic and confined groundwater level. Positive bias values, meaning the model is too wet, are indicated as black dots, negative bias values (model too dry) are indicated as white dots. Figure 4.5 shows that the majority of the dots is black, indicating that the modelled groundwater level is too high.

4.3.2 SEBAL

In the following SEBAL is only briefly explained, for a complete description we refer to Appendix 5. The Surface Energy Balance Algorithm for Land (SEBAL) is based on the surface-energy balance (Equation 4.4).

$$R_n = G_0 + H + \lambda\rho E, \tag{4.4}$$

in which R_n [W m^{-2}] is the net radiation; G_0 [W m^{-2}] is the soil heat flux; H [W m^{-2}] is the sensible heat flux and λE [W m^{-2}] is the latent heat flux that is associated with actual evapotranspiration (ET_{act}) by the latent heat of vaporization (λ) and ρ is the density of water [kg m^{-3}].

The instantaneous energy balance, at time of satellite overpass, can be partly (R_n and G_0) solved with satellite data and ground based meteorological data. Having $R_{n,i}$ (subscript i stands for instantaneous) and $G_{0,i}$ the remaining problem is the division between the (instantaneous) sensible (H_i) and the (instantaneous) latent heat flux (λE_i), which can be expressed by the (instantaneous) evaporative fraction (Λ_i [-])

$$\Lambda_i = \frac{\lambda E_i}{R_{n,i} - G_{0,i}} = \frac{\lambda E_i}{\lambda E_i + H_i} = \frac{R_{n,i} - G_{0,i} - H_i}{R_{n,i} - G_{0,i}} \tag{4.5}$$

If H_i is solved for each satellite pixel, λE_i is the residue of the energy balance. SEBAL computes H_i using a so-called "self calibration" procedure. The coldest pixel is selected in the satellite image, where it is assumed that H_i=0 (and $\lambda E_i = R_{n,i}$-$G_{0,i}$), and the warmest pixel is selected where it is assumed that $H_i = R_{n,i}$-$G_{0,i}$ (and λE_i=0).

The temperature difference between the land surface and the atmosphere at reference level (ΔT) that is needed to match the value of H at a given aerodynamic resistance is calculated. For the cold pixel ΔT=0, for the warm pixel ΔT is solved iteratively using equations that are based on the Monin-Obukhov Similarity Theory. After that a linear relationship is fitted for the ΔT–T_s relationship (T_s is surface temperature based on satellite image), which is thus image specific.

With the ΔT-T_s relationship, together with the wind velocity u_{z2} that is based on the interpolation method Meteolook (Voogt, 2007), the sensible heat flux H_i can be calculated for each pixel of the satellite image. λE_i follows from solving the energy balance, Equation 4.4. This means that the instantaneous evaporative fraction (Λ_i) is known for every satellite pixel. SEBAL assumes that the daily evaporation fraction is the same as the instantaneous evaporation fraction. This means that if the daily net radiation ($R_{n,24}$) and daily soil heat flux ($G_{0,24}$) are known, the daily latent heat flux λE and thus the daily evaporation E is known for each satellite pixel.

The roughness length that is needed for SEBAL, comes from the Royal Netherlands Meteorological Institute (KNMI). This map is based on the Dutch national land-cover database LGN (Oort et al., 2007; De Wit and Clevers, 2004), as is the land use map in our hydrological model. The roughness map is slightly modified with an orographic correction and a small time correction for agricultural land use, using NDVI.

4.3.3 Data assimilation

This section describes the data assimilation method we used. Firstly, the different steps of the assimilation procedure are described. Thereafter details about the parameterization of these steps for this case study are given.

Data assimilation method

Step 1: new ET_{act}
Each day a satellite image is available we have information about ET_{act} [mm day^{-1}] from both METASWAP and SEBAL (resp. $ET_{act,m}$ and $ET_{act,s}$). For $ET_{act,m}$ we also include the interception evaporation (in the model this is calculated independently from ET_{act}). If we know the standard error of the METASWAP and SEBAL based ET_{act} (resp. $SE_{ET_{act,m}}$ and $SE_{ET_{act,s}}$), we can make the following statistical correction of

ET_{act} per model node that gives us a new, updated value of ET_{act} ($ET_{act,new}$):

$$ET_{act,new} = ET_{act,m} + \frac{SE^2_{ET_{act,m}}}{SE^2_{ET_{act,m}} + SE^2_{ET_{act,s}}} \cdot (\widetilde{ET_{act,s}} - ET_{act,m}) \tag{4.6}$$

The values of $ET_{act,s}$ should be in the range of $ET_{act,m}$ in order to be of value in the next step, where we are interested in the updated evapotranspiration reduction. However, we found that $ET_{act,s}$ is overall higher than $ET_{act,m}$. Therefore, we scale $ET_{act,s}$, assuming that the spatial variability of evapotranspiration reduction shown by SEBAL ($\frac{ET_{act,s}}{ET_{pot,s}}$) is correct, but that $ET_{act,s}$ is biased due to a bias in $ET_{pot,s}$. In Equation 4.6 $\widetilde{ET_{act,s}}$ is the bias corrected (i.e. scaled) $ET_{act,s}$ given in Equation 4.7, in which $\overline{ET_{pot,m}}$ and $\overline{ET_{pot,s}}$ are the spatial mean ET_{pot} according to respectively METASWAP and SEBAL within the total model area.

$$\widetilde{ET_{act,s}} = \frac{ET_{act,s}}{ET_{pot,s}} \cdot (ET_{pot,s} + \overline{ET_{pot,m}} - \overline{ET_{pot,s}}) \tag{4.7}$$

The statistical correction (Equation 4.6) weighs $ET_{act,m}$ and $ET_{act,s}$ based on their confidence: if $SE_{ET_{act,m}}$ is high, the updated value $ET_{act,new}$ will tend to $ET_{act,s}$ and vice versa. In Equation 4.6 we state that (i) $ET_{act,m}$ is unbiased and (ii) that the error in $ET_{act,m}$ is temporally variable but its variance is constant in time.

Step 2: new pressure head for root zone
With $ET_{act,new}$ we can derive a new Feddes reduction factor, FR_{new} [-] (see also Equation 4.3):

$$FR_{new} = \frac{ET_{act,new}}{ET_{pot,m}}, \tag{4.8}$$

in which $ET_{pot,m}$ [mm day^{-1}] is the ET_{pot} according to the model. With FR_{new}, in combination with the SVAT-unit specific parameters of the Feddes curve (Figure 4.3 and Table 4.2), we can determine a new pressure head for the root zone of each SVAT-unit ($h_{rz,new}$).

Step 3: new pressure head for zone 2
Besides a new initial pressure head of the root zone, METASWAP also needs a new initial pressure head for the zone between root zone and phreatic groundwater level (zone 2), called $h_{z2,new}$.

Step 4: new groundwater levels
METASWAP also needs new initial groundwater levels.

Parametrization

Step 1: new ET_{act}

Table 4.5 shows the values that were needed to make the bias correction of $ET_{act,s}$ (Equation 4.7). At maximum 0.5 % (ASTER image on 8 June) of the satellite pixels retrieved a negative corrected ET_{act} ($\widetilde{ET_{act,s}}$), which was set to zero. To determine $SE_{ET_{act,m}}$ we calculated ET_{act} according to METASWAP for the situation that we have the *measured* instead of the *modelled* VMC. We can determine $SE_{ET_{act,m}}$ at five locations, as we have five soil moisture measurement locations. At each location the VMC was measured in duplo at five different depths (5, 15, 30, 50, 70 cm). For each depth we took the mean of the duplo measurements. Because the model uses pressure heads instead of VMC, we used the Van Genuchten equation (Equation 4.9), which is an analytical function to calculate VMC from the pressure head (Van Genuchten, 1980). We rewrote this equation to Equation 4.10 with which we retrieved at each location a time series of the pressure head for the five different depths.

$$\Theta(h) = \begin{cases} \Theta_r + \frac{\Theta_s - \Theta_r}{(1+|\alpha h|^n)^m} & h \leq 0 \\ \Theta_s & h > 0 \end{cases} \tag{4.9}$$

In Equation 4.9 $\Theta(h)$ is VMC [cm^3 cm^{-3}] at pressure head h [cm]; Θ_r and Θ_s are respectively the residual and saturated soil moisture content [cm^3 cm^{-3}]; α (> 0) [cm^{-1}] is related to the inverse of the air-entry pressure; n (> 1) [-] is a measure of the pore-size distribution; and $m = 1 - n^{-1}$ [-]. By taking the inverse of Equation 4.9, we get:

$$h = \begin{cases} -(\Theta_r + [\langle(\frac{\Theta_s - \Theta_r}{\Theta(h) - \Theta_r})^{m^{-1}} - 1\rangle^{n^{-1}} \cdot \frac{1}{\alpha}] & \Theta(h) \leq \Theta_s \\ h = 0 & \Theta(h) > \Theta_s \end{cases} \tag{4.10}$$

METASWAP distinguishes 21 different soil types. For each of these soil types the model has predefined sub layers and corresponding soil physical Van Genuchten parameters, which are needed in Equations 4.9 and 4.10. In Table 4.3 these parameters are given for the 10 different soil types in our study area. With Table 4.2, that relates the pressure heads with FR, a time series of FR could be determined for each depth. Using Equation 4.3, we can derive a time series of ET_{act} at each depth. To define a value for ET_{act} of the entire root zone ($ET_{act,rz}$), we used a weighted average of the depths, depending on the root zone thickness (Equation 4.11). At the measurement locations, we only have two different root zone depths: 30 cm (SK, SZ, GD, WL) and 100 cm (LB).

$$ET_{act,rz} = \begin{cases} \frac{1}{6} \cdot ET_{act,5cm} + \frac{2}{6} \cdot ET_{act,15cm} + \frac{3}{6} \cdot ET_{act,30cm} & rz = 30cm \\ \frac{1}{20} \cdot ET_{act,5cm} + \frac{2}{20} \cdot ET_{act,15cm} + \frac{3}{20} \cdot ET_{act,30cm} & \\ +\frac{4}{20} \cdot ET_{act,50cm} + \frac{10}{20} \cdot ET_{act,70cm} & rz = 100cm \end{cases} \tag{4.11}$$

With $ET_{act,rz}$ we can determine the error in $ET_{act,m}$ ($ET_{act,m} - ET_{act,rz}$) for each soil moisture measurement location (Figure 4.6) and calculate $SE_{ET_{act,m}}$. The error in $ET_{act,m}$ as derived here is a conservative estimation of the model error because the

possible measurement error of the soil moisture probes are counted as model error. We state that the derived $SE_{ET_{act,m}}$ at each location is representative for a part of the model area (error zone), as we have only five measurement locations but want to apply the statistical correction method to all SVAT-units. Table 4.1 shows to which error zone the different soil types in the study area are classified, which is based on the soil physical parameters. Table 4.4 shows the values of $SE_{ET_{act,m}}$, as well as the error zones for which the five measurement locations are representative.

$SE_{ET_{act,s}}$ is assumed to be spatially uniform because SEBAL is good in detecting the relative spatial variation of ET_{act} within an area. Because we had no measurements of ET_{act} within the study area it was not possible to calculate the $SE_{ET_{act,s}}$ ourselves. However, data are available (source: www.waterwatch.nl) of a validation study in The Netherlands where in 1995 weekly ET_{act} measurements of SEBAL are compared to eddy-correlation measurements (306 measurements). This study shows a value for $SE_{ET_{act,s}}$ of 1.5 - 1.9 mm week^{-1}. Assuming this error is random, and choosing the upper bound, we get $SE_{ET_{act,s}} = \frac{1.9}{\sqrt{7}} = 0.72$ mm day^{-1}.

Step 2: new pressure head for root zone
To apply step 2 of the data assimilation method, the following problems must be overcome, which are mainly caused by the rigid shape of the Feddes curve:

- in our hydrological model FR is seldom higher than 1 because the model cannot evaporate more than the potential evapotranspiration (it can happen when additional interception evaporation occurs). Because we now use $ET_{act,new}$, which is a combination of $ET_{act,m}$ and $\widetilde{ET_{act,s}}$, FR_{new} can be higher than 1;
- if $FR_{new} \geqslant 1$, which pressure head between h_2 and h_3 of the Feddes curve should be chosen?,
- in case FR before update (FR_m) was equal to 1 and $FR_{new} < 1$, the soil moisture content can drop considerably, hypothetically from h_2 to somewhere between h_3 and h_4.

To overcome the above listed problems we defined four updating scenarios for soil moisture:

- scen 1: $FR_m = 1$ and $FR_{new} >= 1$: no update of soil moisture. h_{rz} is not updated because there was and is no evapotranspiration reduction;
- scen 2: $FR_m < 1$ and $FR_{new} >= 1$: soil becomes wetter. In contrast to our previous study (Schuurmans et al., 2003) we do not take the reduction point (h_3) but make a linear interpolation between h_2 and h_3 of the Feddes curve, based on the value of FR_{new}.We set a minimum and maximum value for FR, (FR_{min} resp. FR_{max}). If $FR_{new} \geq FR_{max}$ then $h_{rz,new} = h_2$, if $FR_{new} = FR_{min}$ then $h_{rz,new} = h_3$ (reduction point);

- scen 3: $FR_m = 1$ and $FR_{new} < 1$: soil becomes dryer but only in case a buffer threshold is crossed. In this scenario a buffer is implemented, in order to make the assimilation method more robust. The wetter the SVAT-unit is before update, the more FR_{new} may differ from 1 before a new pressure head is defined;
- scen 4: $FR_m < 1$ and $FR_{new} < 1$: soil becomes either dryer or wetter. In this scenario an update of h_{rz} takes place somewhere between h_3 and h_4 of the Feddes curve.

For scenario 2 FR_{min} was set to 1, FR_{max} was set to 15. The choice of the value FR_{max} is based on the comparison that was made between METASWAP and SEBAL based ET_{act}. We want to avoid that the soil moisture of METASWAP becomes suddenly very high so we chose a value that was rare. For scenario 3 we implemented a buffer, which is given in Equation 4.12, in which f determines the robustness of the filter.

$$FR_{new} \geq \frac{f(\Theta_{h_3} - \Theta_{h_{rz}})}{1 - \Theta_{h_{rz}}} + 1 \Rightarrow FR_{new} = 1 \tag{4.12}$$

Figure 4.7 shows an example of the critical threshold of FR_{new} (above which it is set to one) as function of $\Theta_{h_{rz}}$ (just before update) for 5 different values of f (Θ_{h_3} = 0.40; Θ_{sat} = 0.55). The closer $\Theta_{h_{rz}}$ is to Θ_{sat}, the more FR_{new} may differ from 1 before an update of the root zone pressure head occurs. In this study we chose $f = 0.3$.

Step 3: new pressure head for zone 2
With the analytical Van Genuchten-Mualem equation (Mualem, 1976), which gives the relation between hydraulic conductivity and pressure head, we can calculate the hydraulic conductivity $K_{h_{rz,new}}$ that corresponds with $h_{rz,new}$(Equation 4.13).

$$K_\theta = \begin{cases} K_{sat} \cdot Se^L \cdot \langle 1 - (1 - Se^{\frac{1}{m}})^m \rangle^2 & h \leq 0 \\ K_{sat} & h > 0, \end{cases} \tag{4.13}$$

in which K_{sat} is the hydraulic conductivity at saturation [cm d^{-1}], L [-] is an empirical pore-connectivity parameter, and Se [-] is the effective saturation given by:

$$Se = \frac{\theta_{(h)} - \theta_r}{\theta_s - \theta_r} = \frac{1}{(1 + |\alpha h|^n)^m} \quad h \leq 0 \tag{4.14}$$

At phreatic groundwater level $K = K_{sat}$. For zone 2 we derive $K_{h_{z2,new}}$ by taking the geometric mean:

$$K_{h_{z2,new}} = \sqrt{K_{h_{rz,new}} \cdot K_{sat}} \tag{4.15}$$

$K_{h_{z2,new}}$ is transformed to a corresponding pressure head ($h_{z2,new}$) by using a pre-defined lookup-table with pressure heads and hydraulic conductivities. If the phreatic groundwater level is within the root zone, $h_{z2,new} = h_{rz,new}$.

Step 4: new groundwater levels
For the initial groundwater levels we used the groundwater levels before update as initial field.

Table 4.3: Soil physical (Van Genuchten) parameters of the soils (depth bottom [m]) in the study area: Θ_s is the saturated water content [cm^3 cm^{-3}], Θ_r is the residual water content [cm^3 cm^{-3}], K_{sat} is the saturated hydraulic conductivity [cm d^{-1}], α (> 0) is related to the inverse of the air-entry pressure [cm], n (> 1) is a measure of the pore-size distribution [-] and L is an empirical pore-connectivity parameter [-].

soil	sublayer	depth bottom	Θ_s	Θ_r	K_{sat}	α	n	L
7	1	100	0.36	0.01	13.21	0.0224	2.167	0
8	1	0.3	0.43	0.01	17.46	0.0249	1.507	-0.14
8	2	100	0.36	0.01	3.3	0.0224	2.167	0
9	1	0.5	0.43	0.02	9.65	0.0227	1.548	-0.983
9	2	100	0.38	0.02	3.89	0.0214	2.075	0.039
12	1	0.9	0.43	0.02	9.65	0.0227	1.548	-0.983
12	2	100	0.38	0.02	3.89	0.0214	2.075	0.039
14	1	0.15	0.43	0.01	17.46	0.0249	1.507	-0.14
14	2	100	0.32	0.01	43.55	0.0597	2.059	0.343
16	1	0.25	0.42	0.01	1.17	0.0118	1.224	-4.795
16	2	100	0.49	0	2.22	0.0107	1.28	-2.123
17	1	0.25	0.55	0	15.46	0.0532	1.081	-8.823
17	2	100	0.57	0	13.28	0.0171	1.11	-4.645
18	1	0.25	0.55	0	15.46	0.0532	1.081	-8.823
18	2	0.6	0.57	0	3.32	0.0171	1.11	-4.645
18	3	100	0.86	0	2.75	0.0127	1.274	-1.832
19	1	0.25	0.43	0	2.25	0.0096	1.284	-2.733
19	2	0.6	0.49	0	2.22	0.0107	1.28	-2.123
19	3	100	0.38	0.02	3.89	0.0214	2.075	0.039

Table 4.4: Standard error of the model based ET_{act} ($SE_{ET_{act,m}}$) [mm day^{-1}] per measurement location, which are assumed to be representative for a part of the study area, indicated as the error zone (see Table 4.1)

	SK	SZ	GD	WL	LB
error zone	1	2	3	4	5
$SE_{ET_{act,m}}$	0.69	0.78	0.94e-02	0.41	0.69

4.4 Results

This section starts with a comparison between the METASWAP and SEBAL based ET_{act} ($ET_{act,m}$ resp. $ET_{act,s}$). After that the results of spatially updated soil moisture due to our data assimilation method are given.

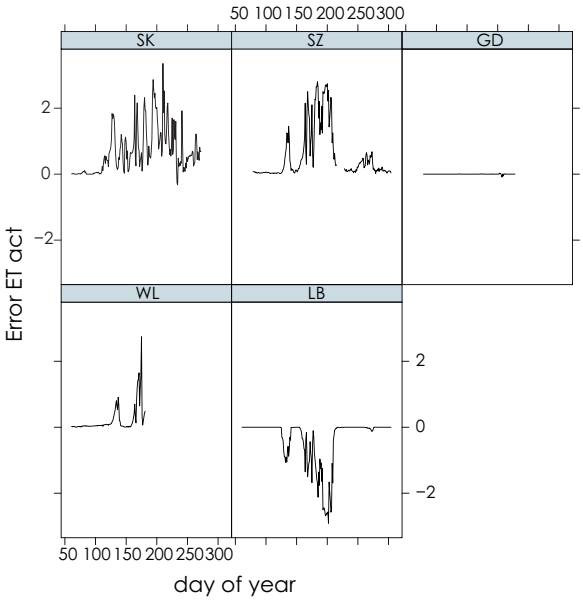

Figure 4.6 Time series of error in ET_{act} ($ET_{act,m} - ET_{act,rz}$) [mm day^{-1}] for each soil moisture measurement location.

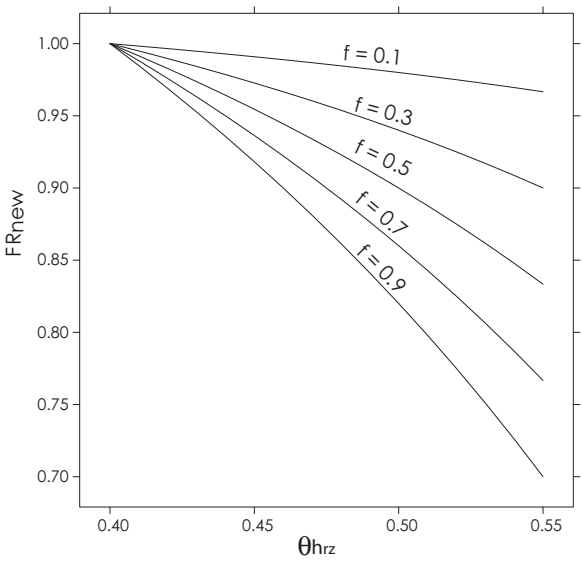

Figure 4.7 Example of the critical threshold of FR_{new}(above which it is set to one) as function of $\Theta_{h_{rz}}$ (just before update) for 5 different values of f (Equation 4.12: $\Theta_{h_3} = 0.40$; $\Theta_{sat} = 0.55$).

4.4.1 ET_{act} comparison

Figure 4.8 shows the spatial distribution of ET_{act}, ET_{pot}, $\widetilde{ET_{act,s}}$ (Equation 4.7) and FR for 8 June 2006 according to SEBAL (ASTER and MODIS) and METASWAP. Figure 4.9 shows the same but then for 17 July 2006. Values for ET_{ref} as well as the spatial mean values of the other variables in Figures 4.8 and 4.9 are given in Table 4.5.

For 8 June $ET_{act,s}$ is overall higher than $ET_{act,m}$ due to an overall higher ET_{pot}. After a bias correction of 2.5 and 2.74 mm for respectively ASTER and MODIS the ET_{act} values compare well. This day both SEBAL and METASWAP show little to none evapotranspiration reduction, except for METASWAP in the northeastern part of the study area (FR images in Figure 4.8). The spatial variation of $ET_{pot,m}$ is due to the difference in crop factors. For the major part of the study area (at least 82 %, Table 4.2) $ET_{pot,m}$ is equal to ET_{ref}, because the crop factor is 1.0. The built-up areas are clearly distinguishable, which is caused by the fact that built-up areas have a very low "crop factor" (0.05). The ASTER image reveals more spatial variation than the MODIS image, which is due to its higher spatial resolution (15 m x 15 m for ASTER and 250 m x 250 m for MODIS). In both the ASTER and MODIS image, areas with forest and built-up areas are recognizable as areas with a relatively high and respectively low ET_{pot} value.

For 17 July we applied a bias correction of 1.96 and 2.09 mm for respectively ASTER and MODIS in order to make the ET_{act} values of SEBAL and METASWAP comparable. This day both SEBAL and METASWAP show evapotranspiration reduction within the area, but their spatial distribution differs. METASWAP shows a high spatial variability in ET_{act}. In the northeast, the area at the high elevation with coarse sand and forest, ET_{act} is very low, even zero at some places. In the middle part there is hardly any evapotranspiration reduction, and in the southeastern part there is again evapotranspiration reduction. The ET_{pot} within METASWAP shows hardly any spatial variation, because the major part has the same crop factor, except for areas with maize, which have a crop factor of 1.3 that time of year according to METASWAP and the built-up areas with a "crop factor" of 0.05. In contrast to METASWAP, where there are clearly 3 regions, SEBAL shows more an overall evapotranspiration reduction. Both in the ASTER and MODIS images, built-up areas are recognizable as areas with a relatively low ET_{act}.

4.4.2 soil moisture update

Table 4.6 shows for each satellite image, the percentage of METASWAP nodes for each update scenario (Section 4.3.3). Scenario 3 is split into 3a and 3b: 3a no update of soil moisture because of buffer, 3b update in spite of buffer. Figure 4.10 shows a spatial plot of the update scenarios for the ASTER and MODIS images of 8 June and 17 July 2006. Although ASTER shows much more spatial variability in ET_{act}, due to its

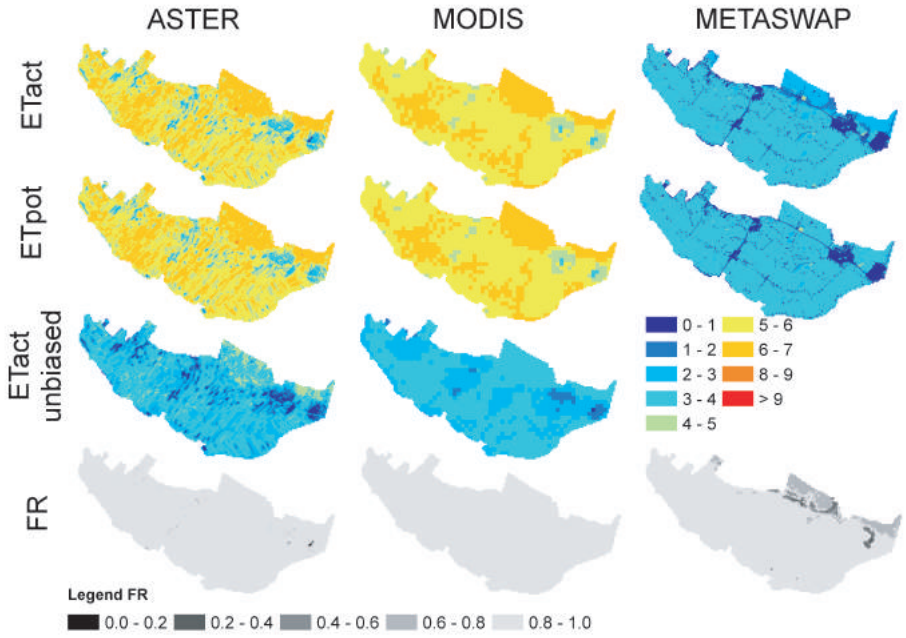

Figure 4.8 Spatial plot of ET_{act} and ET_{pot} [mm day^{-1}] as derived by SEBAL from ASTER and MODIS images and by METASWAP as well as the bias corrected ET_{act} SEBAL images for 8 June 2006.

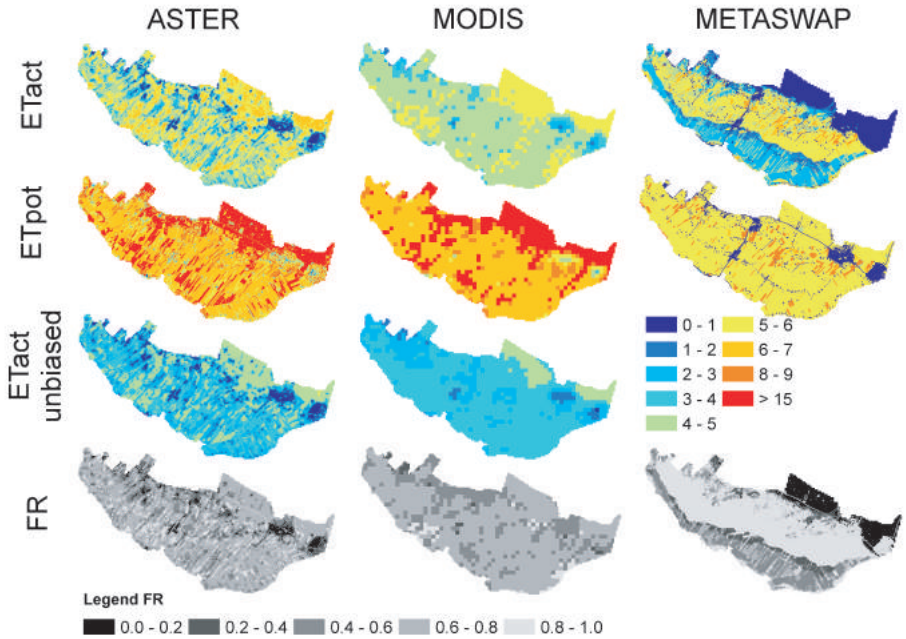

Figure 4.9 Same as Figure 4.8 but for 17 July 2006.

Table 4.5: Comparison between ET [mm day^{-1}] as derived by SEBAL (ASTER AND MODIS) and METASWAP: ET_{ref} according to Makkink, spatial mean of respectively $\widetilde{ET_{pot}}$ and ET_{act} ($\overline{ET_{pot}}$ and $\overline{ET_{act}}$) and the spatial mean ET_{act} after bias correction ($\overline{\widetilde{ET_{act}}}$: Equation 4.7).

	8 June			**17 July**		
variable	ASTER	MODIS	METASWAP	ASTER	MODIS	METASWAP
$\overline{ET_{ref}}$	–	–	3.38	–	–	5.40
$\overline{ET_{pot}}$	5.53	5.77	3.03	6.96	7.09	5.00
$\overline{ET_{act}}$	5.51	5.77	2.94	4.43	4.58	3.33
$\overline{\widetilde{ET_{act}}}$	3.05	3.05	–	3.22	3.25	–

higher spatial resolution than MODIS, in the spatial pattern of the update scenarios there is hardly any difference between ASTER and MODIS.

On 8 June, both with ASTER and MODIS, about half of the study area ($\sim 40-50\%$) has no update of the root zone pressure head (scen 1) because both $ET_{act,m}$ and $ET_{act,new}$ are equal or higher than ET_{pot}. The other half of the lower part of the study area becomes, despite the buffer, dryer after update (scen 3b) because $ET_{act,new}$ indicates evapotranspiration reduction. About 10% of the study area, at the high elevations with coarse sand and forest, the root zone pressure head is updated within the segment of evapotranspiration reduction (scen 4: pressure head update between h_3 and h_4, Figure 4.3), because both $ET_{act,m}$ and $ET_{act,new}$ indicate evapotranspiration reduction.

17 July shows a completely different picture: in the major part of the study area ($\sim$ 80%) the root zone pressure head is updated within the segment of evapotranspiration reduction (between h_3 and h_4, Figure 4.3), because both $ET_{act,m}$ and $ET_{act,new}$ indicate evapotranspiration reduction. About 10 % of the study area has no soil moisture update (scen 1) because $ET_{act,m}$ and $ET_{act,new}$ show no evapotranspiration reduction. These are clearly the built-up areas, that have a very low ET_{pot} because of the very low "crop factor". Another 10 % of the study area becomes, despite the buffer, dryer after update (scen 3b) because $ET_{act,new}$ indicates evapotranspiration reduction.

Table 4.6: Percentage METASWAP nodes for each soil moisture update scenario for each day a satellite image was available. Scenario 3 is divided in 3a (no soil moisture update due to buffer) and 3b (update of soil moisture in spite of buffer).

source	scen 1	scen 2	scen 3a	scen 3b	scen 4
ASTER 8 June 2006	54	2	0	33	11
ASTER 17 July 2006	11	0	0	13	76
MODIS 8 June 2006	40	0	0	47	13
MODIS 17 July 2006	12	0	0	12	76

Figure 4.11 shows the spatial difference of the root zone storage between the unperturbed and updated METASWAP run using either ASTER or MODIS images of 8 June 2006 and 17 July 2006. The difference is plotted 1 day after update, 10 days after update and at the end of the modelling period (1 Nov 2006). Negative values

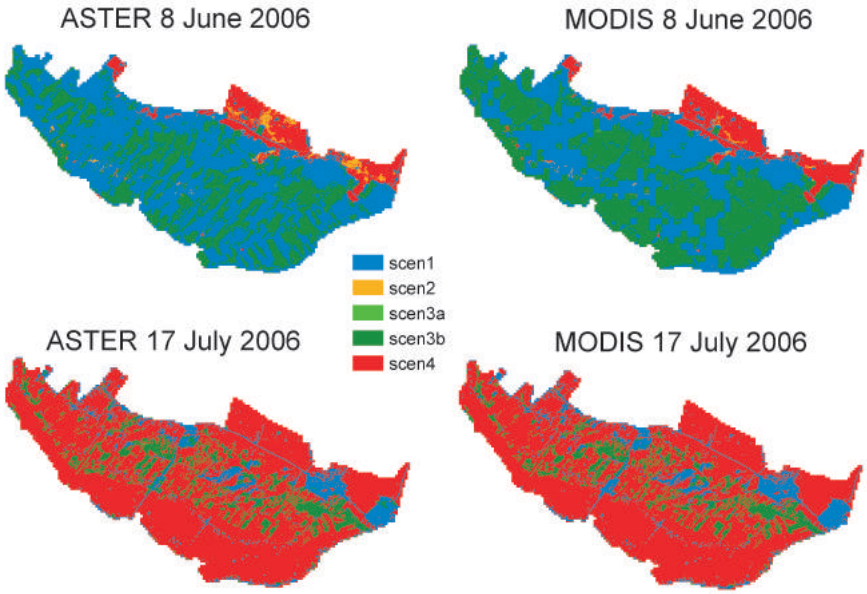

Figure 4.10 Spatial plot of update scenarios of our data assimilation method (DA) using both ASTER and MODIS images of 8 June and 17 July 2006. Scenario 1 and 3a (no update soil moisture) are indexed as blue respectively light green areas, scenario 2 (soil becomes wetter with DA) is orange, scenario 3b (soil becomes dryer with DA) is dark green and scenario 4 (either wetter or dryer but within the evapotranspiration reduction) is red.

(indicated with blue in the figure) mean that the root zone storage in the updated model run is higher than in the unperturbed run, so METASWAP becomes wetter after update. The opposite is true for the positive difference values, which are indicated with red in the figure.

For 8 June the overall modelled soil moisture in the lower area decreased after implementation of our data assimilation method, especially within the soil units 19 & 12. Considering the time series of measured and modelled soil moisture at the 5 measurement locations (Figure 4.4) this seems to be realistic. However, the 5 measurement locations are point measurements and it is hard to identify their representativeness over the whole study area. In the higher region of the study area the modelled soil moisture is slightly increased in the areas that are indicated as scenario 2 (Figure 4.10). However, Figure 4.8 shows that for the entire northeastern part (indicated with scenario 4 in Figure 4.10) the evapotranspiration calculated by METASWAP is higher than the evapotranspiration calculated by SEBAL. The reason that despite this, the soil moisture is not increased is due to the fact that $ET_{act,new}$ is a linear combination of both $ET_{act,m}$ and $\widetilde{ET_{act,s}}$. Because $ET_{act,m}$ is extremely low in this period, $ET_{act,new}$ is also low, which means the increase in root zone storage is only marginal.

17 July is an interesting day with evapotranspiration reduction for both METASWAP and SEBAL, but with a different spatial distribution. This day three different regions

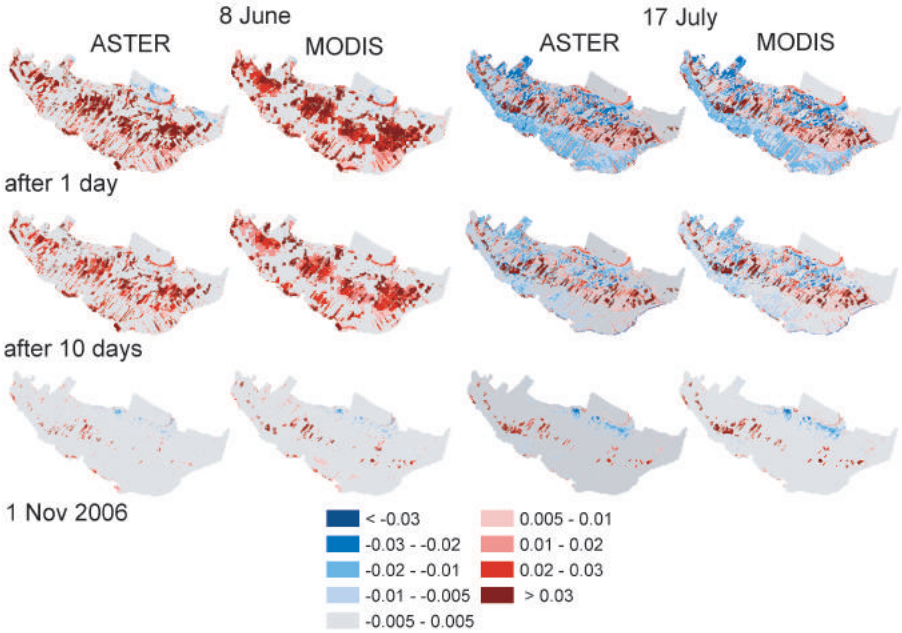

Figure 4.11 Spatial difference of the root zone storage [m] between unperturbed and updated model run using either ASTER or MODIS images of 8 June 2006 and 17 July 2006 after 1 day, 10 days and at the end of modelling period (1 Nov 2006). Negative values (blue) mean METASWAP becomes wetter after update, positive values (red) mean METASWAP becomes dryer after update.

in the spatial pattern of the differences between $\widetilde{ET_{act,s}}$ and $ET_{act,m}$ can be distinguished:

- region 1: the northeastern part where $\widetilde{ET_{act,s}} > ET_{act,m}$;
- region 2: the middle part where $ET_{act,m} > \widetilde{ET_{act,s}}$;
- region 3: the southwest part where $\widetilde{ET_{act,s}} > ET_{act,m}$.

In region 1 both SEBAL and METASWAP show evapotranspiration reduction but the amount of reduction shown by METASWAP is extremely high. Still, there is hardly any increase of the soil moisture content, which is due to the reason explained above (low $ET_{act,new}$ value).

In region 2 soil moisture is reduced, which seems plausible considering the modelled and measured soil moisture (Figure 4.4).

In region 3 the modelled soil moisture is increased. Both SEBAL and METASWAP show evapotranspiration reduction but the SEBAL based reduction is lower. This is the most difficult area for which to decide whether this is plausible or not. The soil moisture measurement location SK is situated at the border of soil unit 19. This is an area with heavy clay that showed severe clay cracks during this period that in reality

could reduce the evapotranspiration of grass (that roots mainly in the upper part). Besides, the soil moisture measurements of the upper layer should be handled with care.

4.5 Discussion

Differences between $ET_{act,s}$ and $ET_{act,m}$ are caused by either an error in $ET_{act,s}$ or and error in $ET_{act,m}$. An error in ET_{act} for its part can be caused by either an error in ET_{pot} or in the evapotranspiration reduction factor (FR). METASWAP and SEBAL use a completely different method to determine the evapotranspiration. METASWAP is based on Makkink which is much less physically based than SEBAL. Makkink only takes into account the atmospheric demand, not the aerodynamic part. It is therefore explicable that Makkink underestimates ET_{pot} and thus ET_{act}. Winter et al. (1995) concluded that Makkink resulted in monthly evaporation that agreed reasonable with the energy budget, but that it showed high variance in daily values and is therefore less useful for daily estimates. This could cause the overall difference between $ET_{pot,s}$ and $ET_{pot,m}$ of $\sim$ 2 mm day $^{-1}$ that we found for 8 June and 17 July, both for ASTER and MODIS.

In areas with forest METASWAP shows for both days severe evapotranspiration reduction in contrast to SEBAL. It could be discussed whether SEBAL maybe overestimates ET_{act} in areas with forest. However, increasing the crop factor in METASWAP is no solution for solving the evapotranspiration reduction in the northeastern part of the study area. We found that increasing the crop factor of forest only led to a faster dry out of the soil and thus lower ET_{act} values in an earlier stage. This prevented us from increasing the crop factor of forest.

We hypothesize that the big difference between $\widetilde{ET_{act,s}}$ and $ET_{act,m}$ in the northeast region of the study area (forest dominated, groundwater level is $\backsim$ 60 m below surface) is caused by a conceptual error in METASWAP. Evapotranspiration in forests is a complex process, mainly because of changes in root water uptake under stress. This has been the subject of many studies. The essence is that trees have special ways of water conservation allowing them to keep evapotranspiration going during dry spells. Trees, but also some small plants like dandelion, radish and carrot, use water in a much more complex way than is implemented in this model, the so-called "hydraulic redistribution" or "hydraulic lift" (Warren, 2007; Lee et al., 2005; Dawson, 1996; Caldwell et al., 1998). This was also concluded in Feddes et al. (2001). Deep rooted plants take in water from deeper moist soil layers (e.g. groundwater table) and exude that water during the night into the drier upper soil layers. Tap roots (a straight tapering root that grows vertically down) can also transfer rainwater from the surface to reservoirs deep underground and redistribute water upwards after the rains. Lee et al. (2005) found in Brazil that trees could store 10% of the annual precipitation as deep as 13 meters. In some cases taproots can reach down more than 100 times the height of the plant above ground.

Despite the big difference between $ET_{act,m}$ and $\widetilde{ET_{act,s}}$ in the northeastern part of the study area, the soil moisture content of the root zone becomes hardly any higher after data assimilation. It should therefore be questioned (i) whether ET_{act} is a good variable to update the soil moisture content of the root zone if in reality the evaporation process of forests is much more complex and (ii) a different, non-linear assimilation method should be applied.

4.6 Conclusions and recommendations

4.6.1 Conclusions

The results of this study show that with the satellite based ET_{act} images we can indicate areas with structural errors in our hydrological model. Together with the observation wells and soil moisture measurements, we are able to identify the possible causes of error, being either flux related or model-concept related. In this case study, despite the lower spatial resolution of the MODIS images, they appeared just as useful as the ASTER images.

We showed that assimilation of ET_{act} resulted in a spatial pattern of soil moisture adjustment that we consider to be realistic, apart from the area with forest and deep groundwater level. However, due to a lack of other spatially-distributed validation data it is hard to prove this. Although we installed soil moisture sensors at five different locations this appeared not to be enough to validate the accuracy of the spatially-distributed soil moisture update. In the future it would therefore be necessary to collect more spatially-distributed information to verify the improvements in hydrological models made by assimilation of ET_{act} data derived from satellites.

Only during periods with evapotranspiration reduction, there is a linkage between soil moisture and ET_{act}, which makes it useful to use satellite based ET_{act} in order to improve the accuracy of soil moisture as calculated by our hydrological model. Besides, the temporal resolution of satellite based ET_{act} is not guaranteed to be the same as the return period of the (polar orbiting) satellite because of cloud conditions. This makes a regular online adjustment of modelled soil moisture content not feasible.

Data assimilation updates state variables of the hydrological model but does not solve the underlying cause of error in the hydrological model that leads to the difference between modelled and remotely sensed ET_{act}. Data assimilation should therefore not be considered as a replacement for model calibration.

4.6.2 Recommendations

Based on the results of this study we make some recommendations regarding how the hydrological model that was used in this study could be improved.

Considering the fact that in The Netherlands almost 70% of the annual rainfall

($\backsim$ 800 mm year^{-1}) evaporates, this is a flux that is important to estimate accurately. As we stated in the beginning of the discussion section, it is explicable that Makkink underestimates ET_{act} because it only takes into account the atmospheric demand, not the dynamic part of the evapotranspiration process. In 1990 the Food and Agriculture Organization of the United Nations (FAO) reviewed several methods to calculate crop evapotranspiration. A panel of experts recommended the adoption of the Penman-Monteith (P-M) combination method as a new standard for reference evapotranspiration (Allen et al., 1998). Penman-Monteith (P-M) is a physically based equation for evapotranspiration and takes into account the atmospheric demand as well as the difference in crop canopy and aerodynamic resistance. The practical drawback of the implementation P-M because of its considerably larger number of variables than Makkink has become less problematic since now methods such as MeteoLook (Voogt, 2007) have been developed, which makes a number of the P-M variables available at each point in space. Hopefully, with implementation of P-M into METASWAP, the values of METASWAP and SEBAL based ET_{act} will lie in the same range of values.

Due to the rigid shape of the Feddes curve problems occur in the implementation of our data assimilation method (Section 4.3.3, step 2). A solution could be to make the relationship between soil moisture (or pressure head) and actual evapotranspiration S-curved, like is often done with the Jarvis method (Jarvis, 1976). The Jarvis method can then be implemented in P-M surface resistance to account for the effect of soil moisture availability on ET_{act}.

Finally, we believe that the current land-plant-atmosphere interaction concept of METASWAP, that reduces the potential evapotranspiration by the soil moisture availability in a root zone with constant depth, is not applicable to forest areas because of reasons mentioned in the discussion. A different model concept should be tested and implemented, as was also recognized by Feddes et al. (2001).

Acknowledgements:
The authors wish to thank Wouter Meijninger and Wim Bastiaanssen (WaterWatch) for applying Sebal to the satellite images and for their advice. Also we are grateful to the Water Board Hoogheemraadschap Stichtse Rijnlanden (HDSR) for financial support with the remote sensing analyses and logistic support with the hydrological model. Paul van Walsum and Ab Veldhuizen (Alterra) are thanked for their support with METASWAP, Judith Snepvangers (TNO/Deltares) with her help with MODFLOW and the Royal Netherlands Meteorological Institute (KNMI) for their rainfall and evapotranspiration data. Inger de Groot and Chris Roosendaal from Utrecht University are thanked for their help with installing and collecting field data as well as calibration of the soil moisture equipment. J.M. Schuurmans is financially supported by Deltares.

5 Ability to forecast regional soil moisture with a distributed hydrological model using ECMWF rainfall forecasts

Schuurmans, J.M & M.F.P. Bierkens (2008), Ability to forecast regional soil moisture with a distributed hydrological model using ECMWF rainfall forecasts. Accepted for publication in Journal of Hydrometeorology

Abstract

This study mimics an online forecast system to provide 9 day ahead forecasts of regional soil moisture. It uses modified ensemble rainfall forecasts from the numerical weather prediction model of the European Centre for Medium-Range Weather Forecasts (ECMWF), which are provided by the Royal Netherlands Meteorological Institute (KNMI). Both the individual ensembles as well as the mean of the ensembles are used as input for a hydrological model of a 70 km^2 study area during March–November 2006. The outcomes are compared to the model run with high resolution rainfall fields (based on 14 rain gauges within the study area and meteorological radar) as input. It is shown that the total spatial mean rainfall is forecasted very well for all lead times. The measured rainfall (spatial mean) shows a distribution with peaks at 0–1 mm day^{-1} and > 10 mm day^{-1}. These peaks are underestimated by the ensemble mean of the forecasts and this underestimation increases with lead time. This is not the case when ensemble members are used. Besides, the modelled uncertainty in rainfall by ECMWF underestimates the true uncertainty for all lead times and the number of rainfall events (thresholds 0.1, 0.5 and 1.0 mm) is overestimated. Absolute temporal mean bias values in root zone storage (i.e. soil moisture) larger than 1 mm start to show for lead times over 3 days. The lower- and upper bounds of bias at a lead time of 9 days are respectively $\sim$ -4 mm to 7 mm (negative values meaning the forecasted soil moisture is underestimated). The bias in root zone storage shows a spatial pattern that represents the spatial pattern of total rainfall: areas with less rainfall than spatial average show a negative bias and vice versa. Local differences within this spatial pattern are due to land use and soil type. Our results suggest that ensemble forecasts of soil moisture using ensemble rainfall forecasts from ECMWF are

of practical use for water management, even at regional scales.

5.1 Introduction

Insight into the spatial distribution of soil moisture within a catchment is of great importance for e.g. farmers and water boards. Accurate short- to medium-range prediction of spatially-distributed soil moisture is helpful for optimizing irrigation gifts, hydrological drought forecasting and the assessment of catchment wetness for flood control. Because rainfall is one of the most important input variables in hydrological models, the accuracy of the soil moisture prediction highly depends on the accuracy of the rainfall forecast.
Recent studies successfully used ensemble rainfall predictions from numerical weather prediction models (NWPs) in hydrological models (e.g. De Roo et al., 2003; Gouweleeuw et al., 2005; Olsson and Lindström, 2008; Pappenberger et al., 2005; Roulin and Vannitsem, 2005; Roulin, 2007). However, these studies all focus on the prediction of discharge.
In this study we use rainfall forecasts from the Ensemble Prediction System (EPS) of the European Centre for Medium-Range Weather Forecasts (ECMWF) as input for a spatially-distributed hydrological model focusing on soil moisture, instead of discharge. The ECMWF EPS system produces 6 hourly rainfall output in the form of an operational run, a control run and 50 ensembles. The operational run is the full model run at high resolution. The control run has the same input conditions as the operational run but for calculation time reduction the model resolution is lower. The 50 ensembles are produced by perturbing the initial state of the control run. All ensemble members are equally likely to occur (Persson, 2001). The scope of this study is to verify the ability to forecast the spatial distribution of soil moisture using EPS rainfall forecasts.
Our hydrological model simulates the water flow in both the unsaturated and saturated zone of a 70 km^2 catchment in The Netherlands. Within this catchment rainfall is measured using meteorological radar and 14 rain gauges. ECMWF forecasts, provided by the Royal Netherlands Meteorological Institute (KNMI), are compared with measured rainfall from radar and rain gauges. Ensemble hydrological model runs are performed using each ensemble member of the rainfall forecast as input. Also the ensemble mean is used as input for our hydrological model. Output from both forecasting systems are compared with output from the hydrological model forced with the observed rainfall data.
The remainder of this chapter is organized as follows. Section 5.2 starts with a description of the ensemble soil moisture prediction system. The study area is described in Subsection 5.2.2. Details about the hydrological model are given in Subsection 5.2.3. Subsection 5.2.4 describes the rainfall data used, both measured rainfall as well as the rainfall forecasts. Section 5.3 gives the results, both for the rainfall accuracy (Subsection 5.3.1) and for the soil moisture accuracy (Subsection 5.3.2). Section 5.4 lists the main conclusions of this study and points out the opportunities for further research.

5.2 Method and data

5.2.1 Ensemble soil moisture prediction system

Six hourly ECMWF EPS rainfall forecasts during the period March-November 2006 are provided by the Royal Netherlands Meteorological Institute (KNMI). We accumulated these forecasts to daily forecasts with a time span of 06 UTC – 06 UTC, resulting in 9 daily rainfall forecasts (lead times 1 to 9 days). These daily forecasts (both the individual ensemble members and the ensemble mean) are compared with measured rainfall that has a time span of 08 UTC - 08 UTC (rainfall fields estimated with both radar and rain gauges). The error caused by the 2 hours difference in time span is investigated (Section 5.2.4)
We use two different soil moisture forecast systems:

1. each ensemble member of the rainfall forecast is used as input for the hydrological model. This gives each day 50 realizations of soil moisture for lead time 1 day (lt1) up to 9 days (lt9);

2. the ensemble mean of the rainfall forecast is used as input for the hydrological model. This gives each day one realization of soil moisture for lead time 1 day (lt1) up to 9 days (lt9).

The reason why we use these two different soil moisture forecast systems is because the unsaturated zone of our hydrological model is a non-linear system. The computational costs of system 2 are significantly lower than those of system 1. Therefore it is interesting to investigate the difference between the mean of the soil moisture ensemble members calculated with system i and the soil moisture calculated with system ii. However, if we want to show the reliability (i.e. consistency) of predicted soil moisture or want to make probabilistic forecasts we need to run system 1.

The model is also run with measured (spatially variable) rainfall as input, which we will call the "true run" from now on. Results of forecasted soil moisture are compared to the true run per lead time. For each forecast run the initial values from the true run were set for the unsaturated and saturated zone. The input for reference evapotranspiration was set at their observed values. In reality this should also be set at the forecasted values. However, we are interested in the effect of rainfall forecast and these results should be considered as the upper bound of skill of the system.

5.2.2 Study area

Our study area is called the "Langbroekerwetering" and lies in the central part of The Netherlands (Figure 5.1A). The Langbroekerwetering (~ 70 km^2) is located along the rim of the Holocene Rhine-Meuse delta (low elevation, peat and clay of the last 4000 years: Berendsen and Stouthamer, 2000), which onlaps coversands and sandur outwash deposits in front of a Saalian ice-pushed ridge (high elevation, 150.000 years

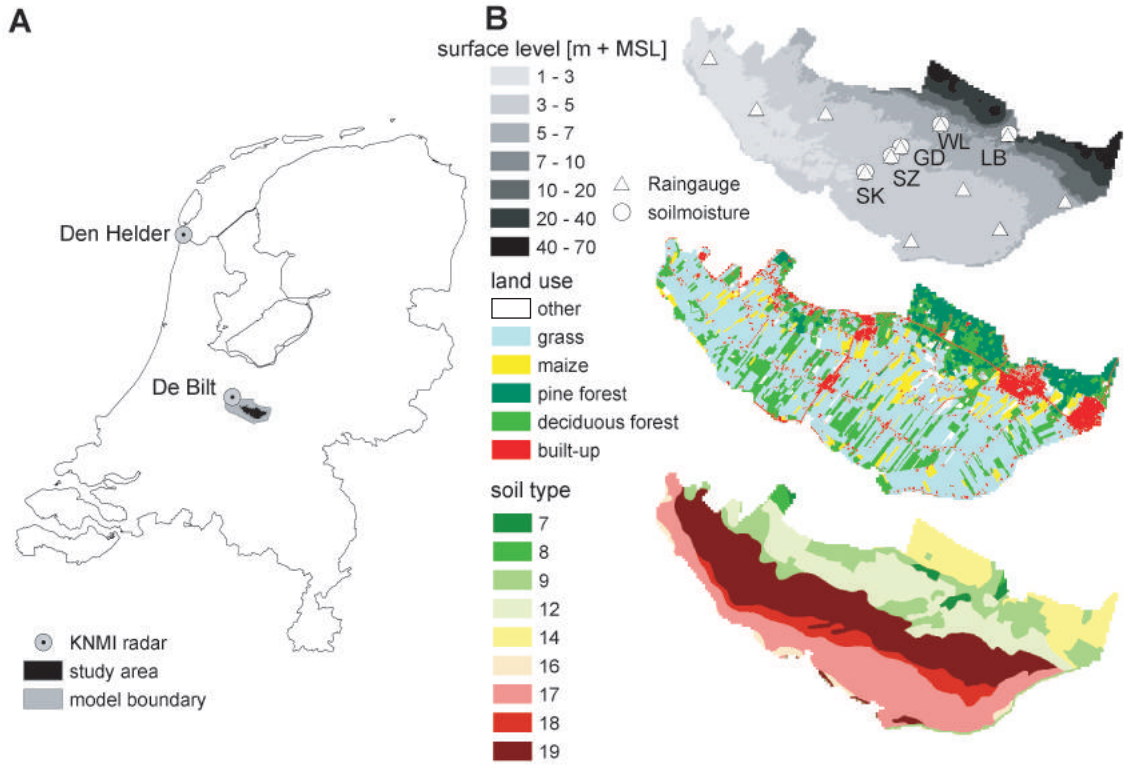

Figure 5.1 A: Location of study area within the Netherlands and the location of the two rainfall radars. B: surface level [m + mean sea level] with rain gauge and soil moisture measurement locations, land use and soil types (see Table 5.1) of study area.

old: Busschers et al., 2007). Figure 5.1B shows the elevation together with the location of the rain gauges and the soil moisture measurements, land use and soil types of the Langbroekerwetering. For a description of the soil types we refer to Table 5.1. At the higher elevations with coarse sand forest dominates the area, while in the lower area grassland dominates. Within the area some small villages (built-up area) are located. The landuse map is derived from the Dutch national land-cover database LGN (Oort et al., 2007; De Wit and Clevers, 2004).

5.2.3 Hydrological model

The model used in this study is a coupled groundwater (saturated zone) and unsaturated zone model, refered to as METASWAP from now on. The groundwater model is based on the MODFLOW model code (McDonald and Harbaugh, 1983). The unsaturated zone model is a quasi steady-state model that uses a sequence of steady-state water content profiles for dynamic simulation (Van Walsum and Groenendijk, 2008). The steady-state water content profiles were obtained by running a steady-state version of the SWAP model (Van Dam, 2000) off-line. The model area is divided in SVAT-units (Soil Vegetation Atmosphere Transfer), which are smaller or equal to the

Table 5.1: Description of soil types within study area (Wösten et al., 1988).

soil unit	description
7	drift sand
8	podzol in loam poor fine sand
9	podzol in loamy fine sand
12	enkeerd in loamy fine sand
14	podzol in coarse sand
16	light clay
17	clay with heavy layers
18	clay on peat
19	clay on sand

size of the MODFLOW cell. One MODFLOW cell can be coupled to several SVAT-units. The SVAT-units form parallel vertical columns, which are divided into a root zone and a subsoil layer. METASWAP distinguishes 21 different soil types. For each soil type the model has predefined sub-layers with corresponding soil physical parameters (Van Genuchten parameters) to be able to convert pressure head to soil moisture content. Only vertical flow according to Richards' equation is taken into account. All lateral exchanges are assumed to take place in the saturated zone. The thickness of the root zone is user specified. In this study we use a thickness of 0.3 m for grassland and built-up area, 0.6 m for maize and 1.0 m for forest.
In our model, the size of the MODFLOW cells is 100 m x 100 m. The SVAT-units have a resolution of 25 m x 25 m inside the study area and 100 m x 100 m outside the study area, within the model boundaries (Figure 5.1A). The groundwater model is schematized into 7 layers. For more specifications of the groundwater model we refer to Appendix 4.
A flux that is of importance for soil moisture, and which is influenced also by the soil moisture conditions is evapotranspiration. Our model uses Makkink (De Bruin, 1987; Makkink, 1957; Winter et al., 1995) reference evapotranspiration (ET_{ref}) as input (spatially uniform). The measured ET_{ref} in this study comes from De Bilt. The potential evapotranspiration (ET_{pot}) is calculated by multiplying ET_{ref} with a crop factor that is related to the land use type and can vary throughout the season (in our model 1.0 throughout the season for grassland and forest; 0–1.3 for maize and 0.05 for built-up area). The actual evapotranspiration (ET_{act}) is equal or a fraction of (ET_{pot}) depending on soil moisture conditions and land use type. In forest areas also interception evaporation occurs. The interception capacity for pine forest is set to 1.0 mm m^{-2} throughout the season and 0.3–1.0 mm m^{-2} for deciduous forest depending on the season.

5.2.4 rainfall data

The measured rainfall is a combination of meteorological radar and rain gauges within and closely around the model area. The interpolation method used is a geostatistical method that combines radar estimates with rain gauge observations. The

method makes use of colocated cokriging and is explained in more detail in Chapter 2. Figure 5.2A shows the spatial distribution of the rainfall accumulated during March–November 2006 within the study area. There is up to 200 mm difference over this 8 month period within 15 km, which is even more than that found in 2004 in another equally sized catchment (50–100 mm over 7 month: Chapter 3). Figure 5.2B shows the time series of the spatial mean rainfall within the study area and the reference evapotranspiration.

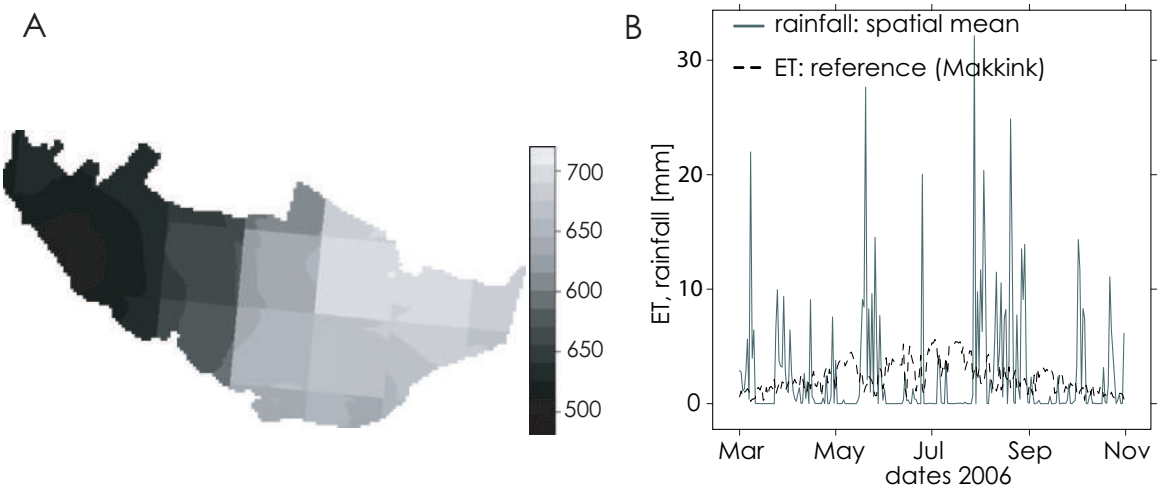

Figure 5.2 Spatial distribution of accumulated rainfall [mm] March–November 2006 (A) and time series of the spatial mean of rainfall within the study area and the reference evapotranspiration (B).

The ECMWF EPS rainfall forecasts within the Netherlands were interpolated by the KNMI to a regular 0.5 degrees x 0.5 degrees grid. For this study we used the forecasts at 0 UTC with a time step of 6 hours nearest to De Bilt (Figure 5.1) and accumulated these to daily rainfall. As mentioned in Section 5.2.1, the time span of the forecasts is 06 UTC–06 UTC, while the time span of the measured rainfall is 08 UTC–08 UTC. We investigated the error caused by the difference in time span using the automatic rain gauge at De Bilt that recorded hourly data. Figure 5.3 shows per day the amount of rainfall that should be added to the time span of the 06 UTC–06 UTC to get the same amount during 08 UTC–08 UTC (solid line). The measured rainfall (08 UTC–08 UTC) is also shown (dashed line). In 10 % of the days the difference was not zero, and the maximum was 6.5 mm. This difference is ignored in this study.

5.3 Results and Discussion

5.3.1 ECMWF rainfall accuracy

Figure 5.4 shows the cumulative rainfall distribution of the measured (spatial mean) and forecasted (ensemble mean) rainfall per lead time. Table 5.2 shows the total rain-

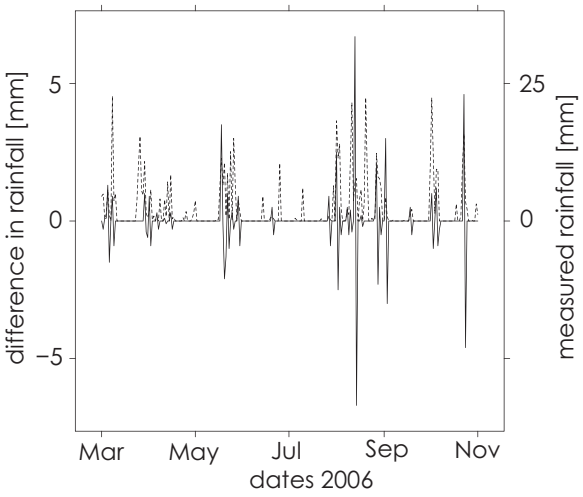

Figure 5.3 Difference in rainfall depth [mm] due to the difference in time span between the forecasts and the measured rainfall (solid line) as well as the measured daily (08 - 08 UTC) rainfall (dashed line). Data come from rain gauge station De Bilt (hourly data).

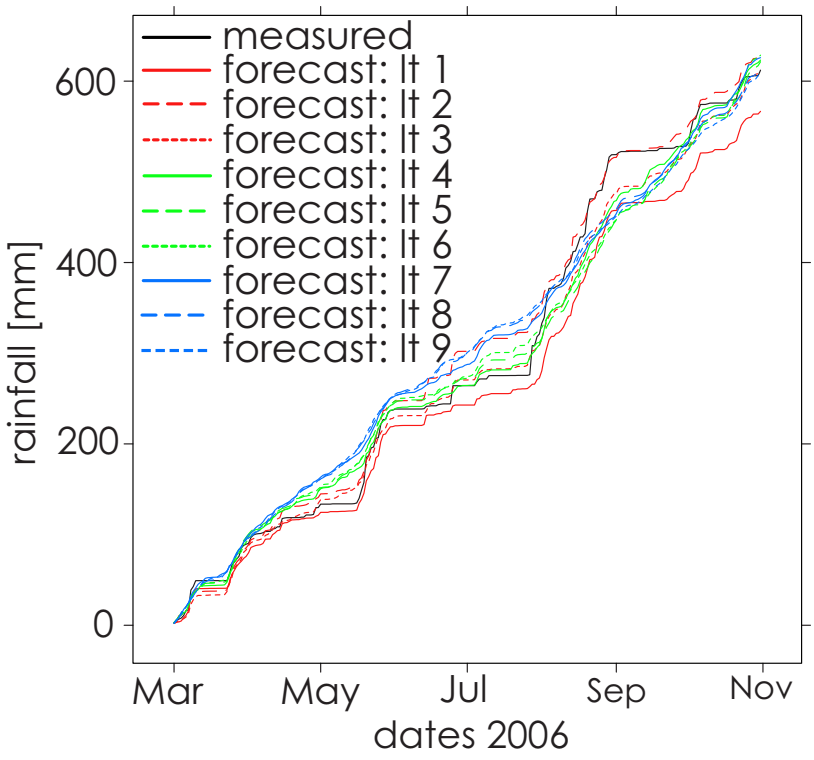

Figure 5.4 Cumulative rainfall distribution of the measured (spatial mean) and the forecasted (ensemble mean) rainfall per lead time.

fall amount during the study period of measured and forecasted rainfall. The total amount of rainfall during the study period is forecasted within 3% of the measured rainfall, except for lt1 (7% less than measured rainfall).

Table 5.2: Total rainfall during March–November 2006 according to measurements (spatial mean) and forecasts (ensemble mean) for lead time 1–9 days.

measured	lt1	lt2	lt3	lt4	lt5	lt6	lt7	lt8	lt9
612	567	629	612	623	621	629	626	611	609

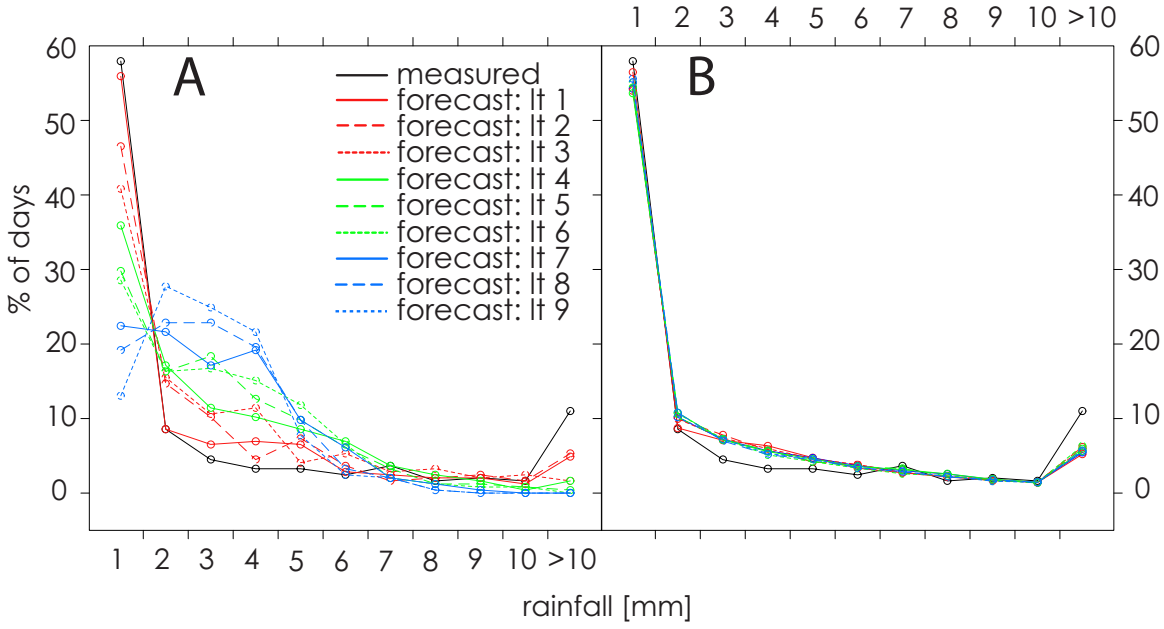

Figure 5.5 Percentage of days as function of rainfall amount for the measured (spatial mean) and forecasted rainfall per lead time. Figure A is based on ensemble mean, Figure B is based on ensemble members.

The distribution of measured and forecasted daily rainfall over different ranges is shown in Figure 5.5. Figure 5.5 A is based on the ensemble mean, Figure 5.5 B is based on the ensemble members. Most of the days ($\sim$ 60%) the spatial mean measured rainfall within the study area was between 0–1 mm day^{-1}, followed by $>$ 10 mm day^{-1} ($\sim$ 10%). Figure 5.5 A shows that for the forecasted rainfall based on ensemble mean, the percentage of days with 0–1 mm day^{-1} gradually decreases with increasing lead time. This phenomena also occurs for events with $>$ 10 mm day^{-1}. However, when using the ensemble members, the forecasted rainfall follows more or less the distribution of measured rainfall for all lead times. This suggests that it is better to use the ensemble members, as the ensemble mean is apparently to smooth a representation of rainfall variability. This smoothing effect increases with lead time which is due to the larger spread between ensemble members, making the ensemble mean closer to climatological mean.

Figure 5.6 shows a medley of statistics for forecasted rainfall; i.e. bias, root mean squared error (RMSE), mean absolute error (MAE) and correlation (r^2) between measured (spatial mean) and forecasted rainfall are plotted per lead time. Also the ensemble spread (temporal mean standard deviation of ensemble members), which is a

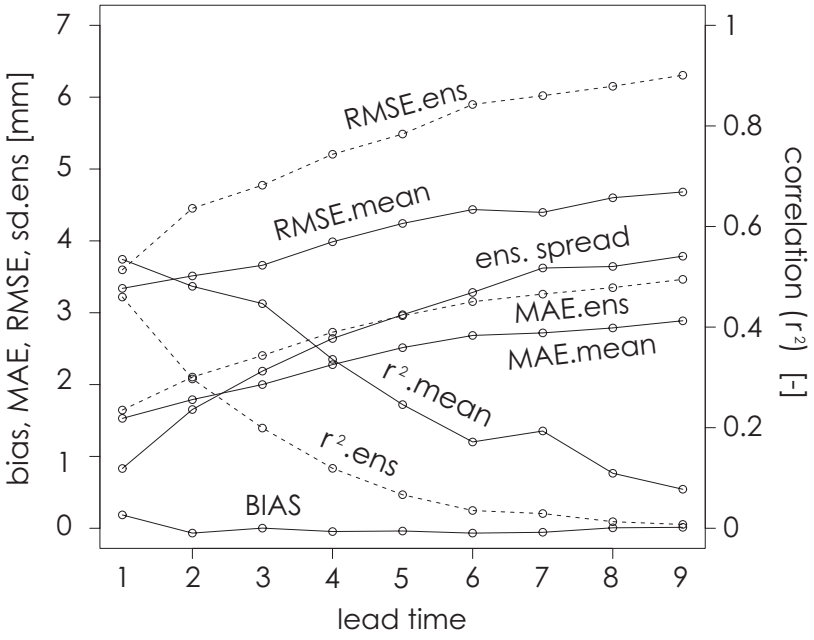

Figure 5.6 Rainfall forecast statistics per lead time; bias, root mean squared error (RMSE), mean absolute error (MAE) and correlation (r^2) between ensemble mean rainfall forecasts and spatial mean measured rainfall. Also the ensemble spread (temporal mean) is shown. RMSE, MAE and r^2 are calculated using both the ensemble mean (.mean) and the individual ensemble members (.ens).

measure for the rainfall forecast reliability, is shown per lead time. For completeness, we also included RMSE, MAE and r^2 calculated from the ensemble members. The RMSE and MAE of the ensemble mean increase with lead time and the correlation decreases. The bias however remains more or less constant around zero with lead time, which means that under- and overestimation of rainfall are compensated as could also be seen from Figure 5.4.

As expected the RMSE and MAE of the ensemble members is higher than the RMSE and MAE of the mean, while r^2 is lower. In fact, if observations and ensemble members are assumed to be realizations of the same underlying stochastic process, and the bias is zero, RMSE of the ensembles members should in theory be $\sqrt{2}$ ($\sim$1.4) as large as that of RMSE of the ensemble mean. The ensemble spread increases, and thus the rainfall forecast reliability decreases, with lead time. However, comparing the ensemble spread with the RMSE of the ensemble mean and noticing the bias is close to zero, we must conclude that the modelled uncertainty underestimates the true uncertainty of the forecast for all lead times. A possible explanation is that the ensemble forecasts only consider the uncertainty of initial conditions, while also model errors (e.g. rainfall parameterization, scale discrepancy between atmosphere model and catchment) yield additional errors.

We used Table 5.3 to calculate the categorical measures of skill, which indicate how well rainfall events are predicted (Johnson and Olsen, 1998). Figure 5.7 shows the bias ratio, probability of detection (POD), critical success index (CSI) and false alarm rate

Table 5.3: Categories of rainfall prediction used to calculate categorical measures of skill. A threshold of 0.1 mm day^{-}1 is used to indicate a rainfall event

	Predicted: no rain	Predicted: rain
Observed: no rain	Z	F
Observed: rain	M	H

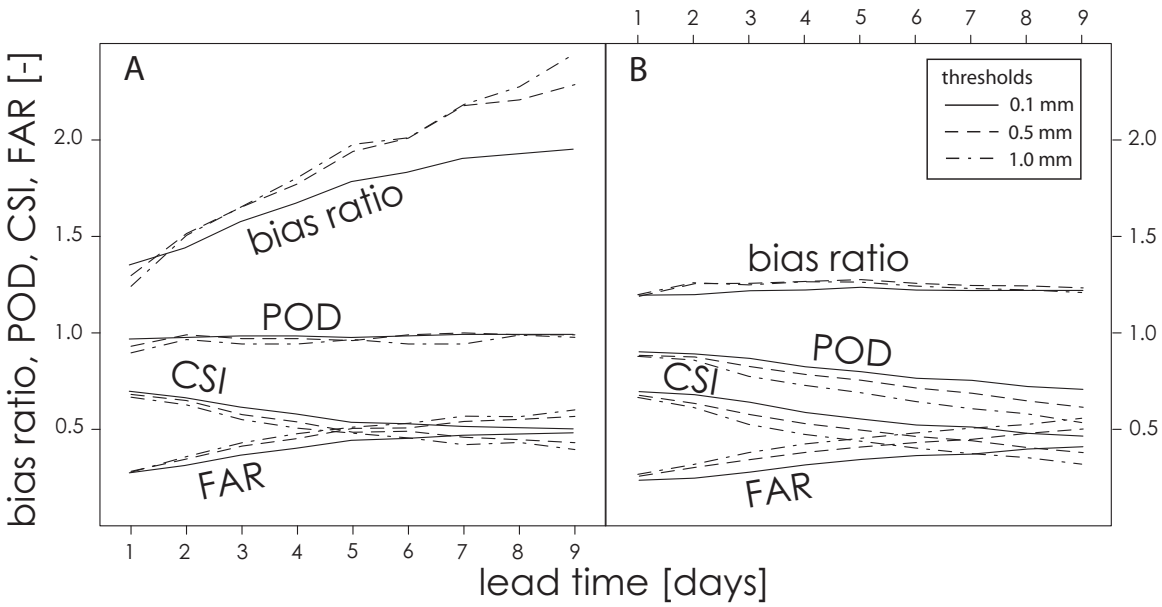

Figure 5.7 Categorical measures of skill for detecting rainfall using three different thresholds (0.1, 0.5 and 1.0 mm): bias ratio, probability of detection (POD), false alarm rate (FAR) and critical success index (CSI). All skill measures are calculated using both the ensemble mean (A) and all the individual ensemble members of the rainfall forecast (B).

(FAR). Bias ratio is the ratio between predicted and observed rainfall events ($= \frac{F+H}{M+H}$). POD ($= \frac{H}{M+H}$) gives the fraction of rainfall events that are successfully forecasted. CSI ($= \frac{H}{H+M+F}$) is the number of hits divided by hits, misses and false alarms. FAR ($= \frac{F}{F+H}$) indicates how often rainfall events are predicted but not observed. In a forecast without bias, the bias ratio equals 1 (POD + FAR = 1). In a perfect forecast POD=1, CSI=1 and FAR=0. The measures of skill were calculated for both the ensemble mean as well as for all the individual ensemble members. For the observed rainfall we use the spatial mean rainfall. Three different thresholds are taken (0.1, 0.5 and 1.0 mm day^{-1}) to indicate a rainfall event. The motivation for the choice of these thresholds is the detection limit of conventional tipping bucket rain gauges (0.1 mm day^{-1}) and the interception capacity of forest in our model (1.0 mm m^{-2} throughout the season for pine forest and 0.3-1.0 mm m^{-2} for deciduous forest). Figure 5.7A shows a strong increase of bias ratio with lead time for the ensemble mean, especially for the higher threshold. For the individual ensemble members, the bias ratio is more or less constant ($\sim$ 1.3) with lead time for all the thresholds. Also for POD and FAR we see a difference between the ensemble mean and the individual ensemble members. As could be expected the ensemble mean leads to an increase of number of forecasted rain

events, which means that bias ratio, POD and FAR are higher for the ensemble mean than for the individual ensemble members. The POD based on the ensemble mean is more or less constant($\sim$ 1) with lead time for all the thresholds. However, based on the individual ensemble members POD decreases with lead time, especially for higher thresholds. CSI decreases with lead time (especially for higher thresholds) but shows hardly any difference between ensemble mean and ensemble members. FAR increases with lead time, especially for higher thresholds. The differentiation of bias ratio, POD and FAR between ensemble mean and individual ensemble members with increasing lead time can be explained by the increase of ensemble spread with increasing lead time as was shown in Figure 5.6.

5.3.2 Soil moisture accuracy

As mentioned in Section 5.2.1 we use two different soil moisture forecast systems:

1. each ensemble member of the rainfall forecast is used as input for the hydrological model;
2. the ensemble mean of the rainfall forecast is used as input for the hydrological model.

We compare, per lead time, the difference between the forecasted storage in the root zone and the storage in the root zone according to the true run. Figure 5.8 shows the bias (temporal mean during the study period) in case the true run is compared to the mean of the forecasted soil moisture ensembles (system 1). Positive bias values mean that the forecast underestimates the root zone storage of the true run. Figure 5.9 shows the same, but this time the true run is compared with the storage in root zone from the run with the ensemble mean of the rainfall forecast as input (system 2). For both systems, the bias increases with lead time. Absolute bias values higher than 1 mm begin to show around lt3. The lower- and upper bounds of bias at lt9 are respectively $\sim$ -4 mm to 7 mm. For both systems we see a spatial pattern in the bias that becomes more pronounced with increasing lead time. The spatial pattern of the bias in root zone storage strongly resembles the spatial pattern of total rainfall (Figure 5.2A). The area with less rainfall than the spatial average (i.e. the western part of the study area) shows a negative bias, whereas the area with more rainfall than the spatial average (i.e. the eastern part) shows a positive bias. This can be explained by the fact that the true run is forced with spatially variable rainfall, while the rainfall forecasts are spatially uniform. In the western part more rain falls according to the forecasts, which leads to higher values in root zone storage and thus to negative bias (and vice versa for the eastern part). Superimposed on this overall spatial pattern in bias, local differences occur, which can be attributed to differences in land use and soil type. If we compare Figures 5.8 and 5.9 with the pattern of land use in Figure 5.1B we see that forest exhibits locally higher values of bias in root zone storage, i.e. underestimation of forecasted soil moisture. We think that the reason for this underestimation of forecasted soil moisture in areas with forest lies in the fact that

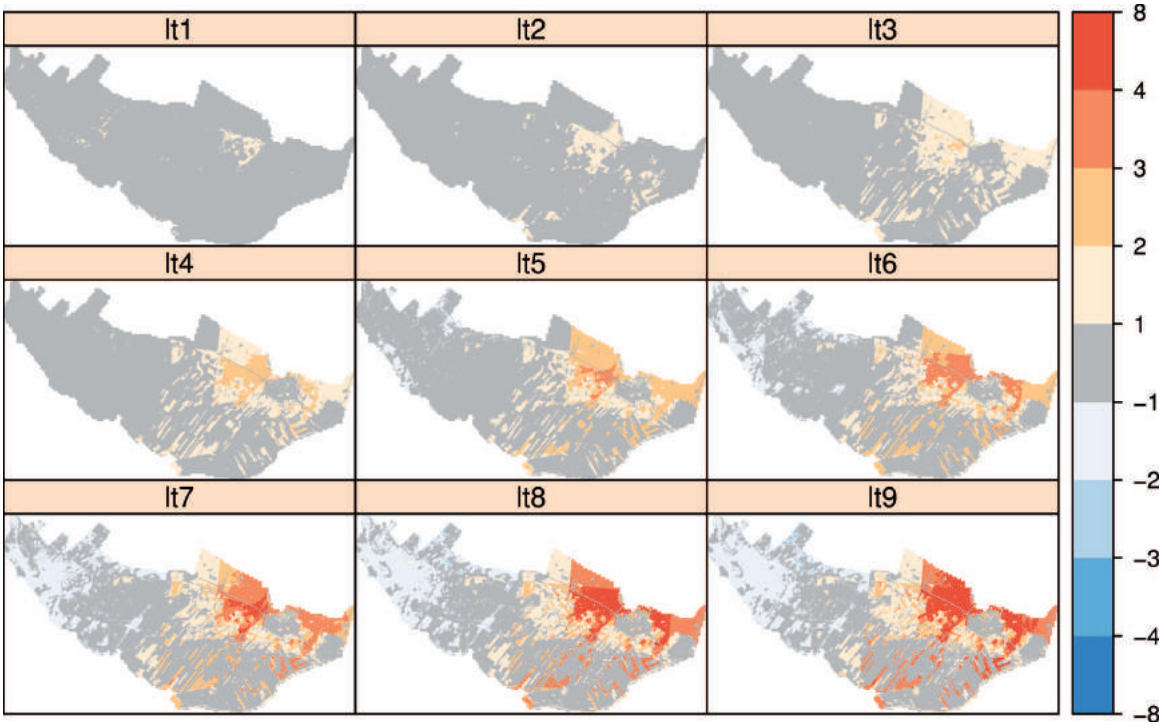

Figure 5.8 Temporal mean bias in root zone storage [mm] during March–November for soil moisture forecast system 1; true run compared to the ensemble mean of forecasted soil moisture. Positive bias values mean that the forecast underestimates the root zone storage of the true run.

in these areas the interception (evaporation) is overestimated. As shown in Section 5.3.1 the total rainfall is almost the same for each lead time but the events with high rainfall intensity are underestimated, while the number of rain events (thresholds 0.1, 0.5 and 1.0 mm day^{-1}) are overestimated (FAR $>$ 1; Figure 5.7). In reality however, increased occurrence of rain could go together with reduced evapotranspiration (due to more clouds and thus reduced solar radiation). This effect is not taken into account as we use observed evapotranspiration in our soil moisture forecast system. built-up areas show no bias within a region of positive bias (northeast). This is not surprising as in built-up areas there is hardly any relationship between rainfall and soil moisture as rainfall does not infiltrate (either because of drainage or low infiltration capacity). We also see some differences in bias in root zone storage in areas with the same land use but with different soil types which suggests that soil type plays a role as well.

Table 5.4 gives the spatial mean values of the temporal mean bias, RMSE and MAE of root zone storage for both forecast systems for each lead time. Figure 5.10 shows in box-and-whisker plot the spatial distribution of the temporal mean bias in root zone storage for both soil moisture forecast systems (system 1 in white, system 2 in grey) per lead time. From this table and figure it can be concluded that it makes not much difference whether one uses soil moisture forecast system 1 or 2, although system 1 gives slightly better results than system 2. However, with system 1 it is possible to make probabilistic forecasts and to show per SVAT-unit the uncertainty

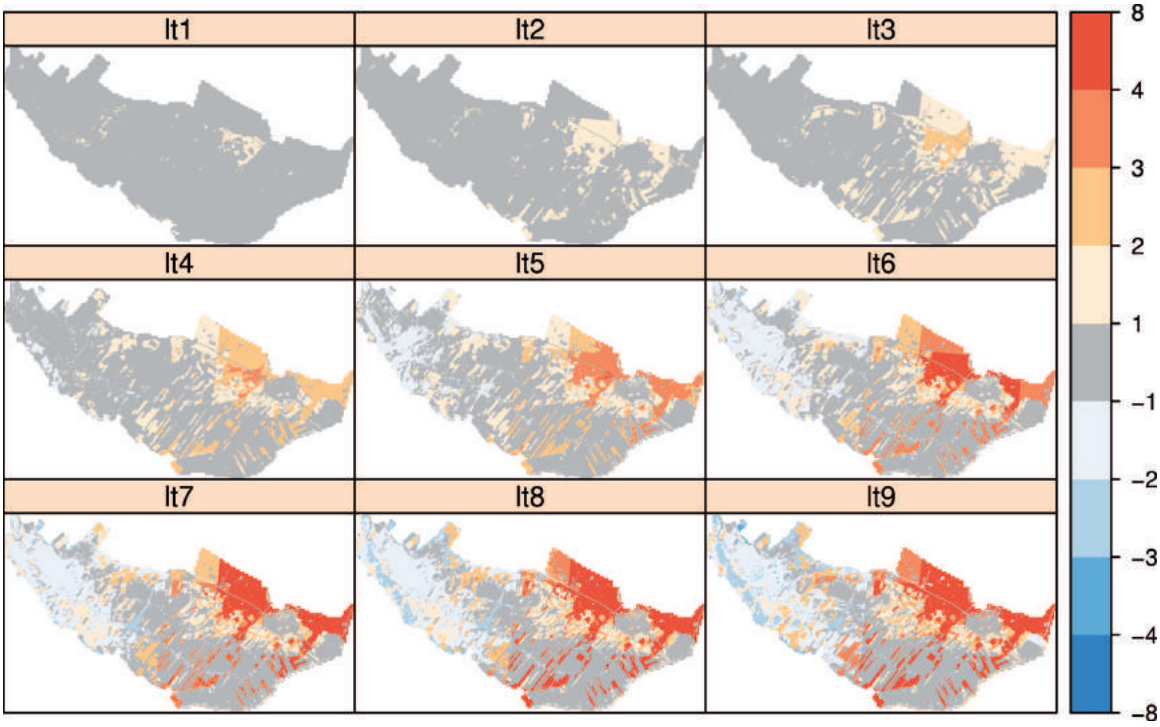

Figure 5.9 Same as Figure 5.8 but then for soil moisture forecast system 2.

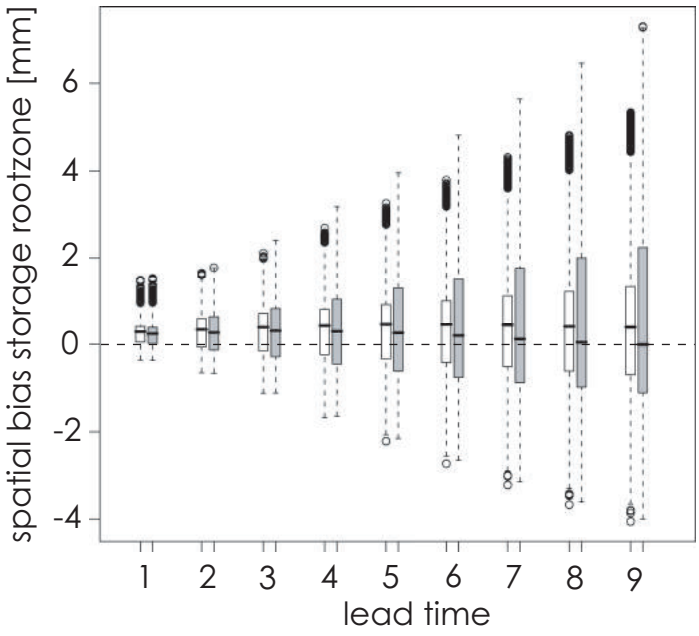

Figure 5.10 Box-and-whisker plots of spatial distribution of bias in root zone storage per lead time for soil moisture forecast system 1 (white) and 2 (grey). The solid boxes range from the lower to the upper quartile, the black line within the box denotes the median, dashed whiskers show the data range. Data that are further than 1.5 times the interquartile range from the nearest quartile are shown as open bullets.

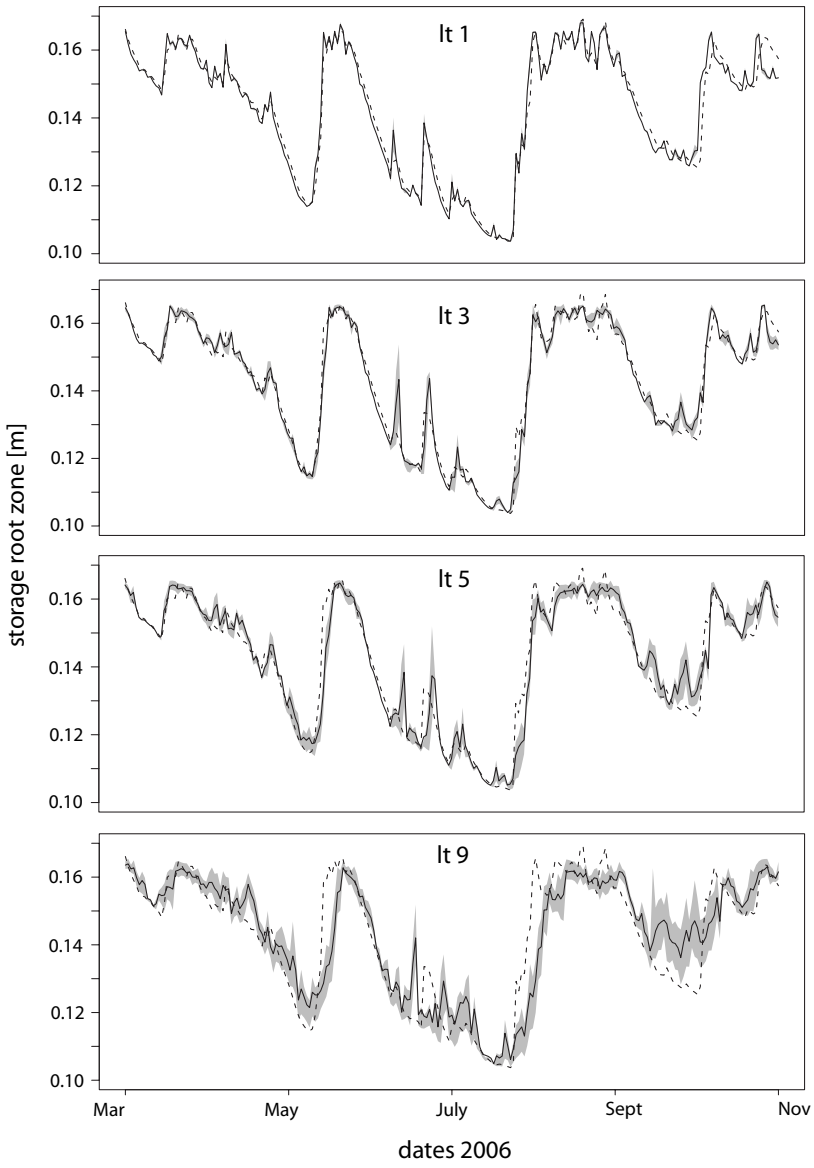

Figure 5.11 Time series of root zone storage [m] for one SVAT-unit during March–November for four different lead times (lt1, lt3, lt5 and lt9). The true run is represented by the dotted line, the ensemble mean by the solid line and the grey boundaries indicate the range between the first and third quartile of the ensemble members (i.e. 50 % of the ensemble members).

Table 5.4: Spatial mean bias, root mean squared error (RMSE) and mean absolute error (MAE) for both soil moisture forecast systems [mm].

lt	bias(1)	bias(2)	RMSE(1)	RMSE(2)	MAE(1)	MAE(2)
1	0.27	0.25	2.35	2.38	1.73	1.74
2	0.28	0.27	3.57	3.61	2.16	2.18
3	0.34	0.35	4.40	4.49	2.61	2.64
4	0.40	0.43	5.26	5.36	3.16	3.19
5	0.45	0.52	6.17	6.32	3.75	3.79
6	0.49	0.59	7.22	7.40	4.45	4.51
7	0.54	0.66	7.93	8.14	5.00	5.07
8	0.58	0.73	8.66	8.91	5.54	5.60
9	0.64	0.81	9.40	9.68	6.15	6.20

of the predicted storage in root zone. As an example we show for one SVAT-unit (location SK in Figure 5.1B) the time series of storage root zone according to the true run (dotted line), according to the ensemble mean (solid line) and the range in storage root zone between the first and third quartile of the ensemble members (i.e. 50 % of the ensemble members, grey bound). Figure 5.11 shows this for 4 lead times (lt1, lt3, lt5 and lt9). This figure shows that the spread of the ensemble members of forecasted root zone storage increases with lead time, i.e. the reliability of forecasted storage in root zone decreases with lead time. Also the correlation between the forecasted and true root zone storage (dotted line) decreases with lead time; both the high and low values of storage root zone from the true run are not reproduced by the forecasts at large lead times and often show a delay.

5.4 Conclusions and outlook

In the following we first list the main conclusions from this study concerning forecasted rainfall and forecasted soil moisture accuracy. Thereafter, the value for operational water management and opportunities for further research are given.

forecasted rainfall accuracy

- The total amount of measured spatial mean rainfall within the study area is forecasted well by the ensemble mean of the rainfall forecast for all lead times (maximum difference 45 mm for lt1). However, the total measured rainfall during March–November 2006 within the study area shows a large spatial variation (200 mm). This spatial variance is not taken into account for forecasted rainfall;
- The measured rainfall (spatial mean) shows a distribution with peaks at 0–1 mm day^{-1} and $>$ 10 mm day^{-1}. These peaks are underestimated by the ensemble mean of the rainfall forecasts and this underestimation increases with lead time. The ensemble members follow more or less the distribution of measured rainfall

for all lead times;

- the modelled uncertainty in rainfall by ECMWF underestimates the true uncertainty for all lead times;
- the number of rainfall events (thresholds 0.1, 0.5 and 1.0 mm day^{-1}) is overestimated ($\sim$ 30 - 40%) by the rainfall forecasts, both with the individual ensemble members as well as with the ensemble mean. This overestimation is constant with lead time for the ensemble members but increases for the ensemble mean with increasing lead time, especially for higher thresholds (up to factor 2–2.5 for lead time 9 days).

forecasted soil moisture accuracy

- Absolute bias values in root zone storage higher than 1 mm begin to show around a lead time of 3 days. The lower- and upper bounds of bias at lead time 9 days are respectively $\sim$ -4 mm to 7 mm;
- The temporal mean bias in root zone storage shows a spatial pattern that strongly resembles the spatial pattern of total measured rainfall. This can be explained by the fact that the true run is forced with spatially variable rainfall while the rainfall forecasts are spatially uniform. As a consequence, areas with less rainfall than spatial average show a negative bias and vice versa;
- Superimposed on the spatial pattern of bias in root zone storage local differences occur, which can be attributed to differences in land use and soil type;
- With increasing lead time mainly the high and low values in root zone storage are not forecasted accurately and often show a delay.

outlook
This study shows that the accuracy of daily ECMWF rainfall forecasts is promising and suggests that the use of these forecasts could be of value for operational water management. The main drawback of using the ECMWF ensemble rainfall forecasts to forecast the spatial distribution of soil moisture is the fact that the rainfall forecasts are spatially uniform for most meso-γ scale (i.e. 2-20 km: Orlanski, 1975) catchments. Insight in the spatial pattern of rainfall is of great importance. Additional information about the spatial structure of rainfall within an area (e.g. due to orographic effects), would make it possible to down-scale the rainfall forecasts, possibly leading to a decrease in the bias of forecasted root zone storage. Besides the spatial pattern in rainfall, this study shows that it is important to have good insight in the actual land use and the soil physical parameters. Finally, the input for reference evapotranspiration was set at observed values. In reality, this should be set at the forecasted values.

This study uses daily rainfall. In The Netherlands rainfall is predominantly stratiform while the hydrological systems are groundwater-dominated with reaction times of several days. This makes a temporal resolution of 24 hours sufficient. However, for

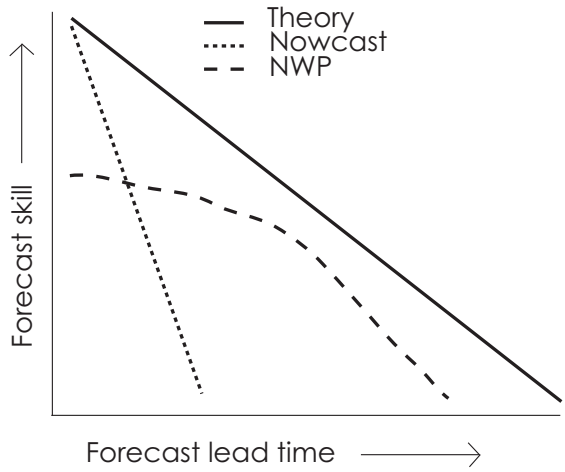

Figure 5.12 Schematic representation of the loss of information content in forecasts as a function of lead time. The solid line represents the theoretical limit of predictability. The dashed line represents NWP models and the dotted line nowcasting methods (after Golding, 1998; Lin et al., 2005).

e.g. mountainous areas the spatio-temporal structures of rainfall are important and the use of 6 hourly rainfall forecasts should be considered and investigated. Besides, for operational rainfall forecast NWPs are not the only source. Extrapolation of radar (or satellite) precipitation patterns for example, also called nowcasting methods, is another one. Nowcasting methods capture the initial information almost perfectly, but as they do not include physics, the skill will decrease rapidly with lead time. NWPs on the other hand capture the physics of large systems very well, but lack local detail because of their limited spatial resolution and have imperfect assimilation algorithms. Therefore their skill is not so high for small lead times but decreases only gradually with increasing lead time (Golding, 1998). Figure 5.12 gives a schematic view of this, in which the line of the theoretical limit is based on the fact that in a chaotic system such as atmosphere there is always loss of skill with increasing lead time. Lin et al. (2005) investigated the cross-over point in time where NWPs start to have more skill than nowcasting methods and found this to be 6 hours after the forecast is initiated. Although this conclusion is based on 3dVAR methods instead of 4dVAR systems (such as that of the ECMWF), qualitatively it is safe to say that in case rainfall forecasts are used in hydrological studies with time steps of for example 1 hour, a combination of nowcasting methods and NWPs should be beneficial.

Acknowledgments:
The authors like to thank the Royal Netherlands Meteorological Institute (KNMI), in particular Kees Kok , Robert Mureau and Daan Vogelezang for their help and for providing us their data. Also, we are grateful to the Water Board Hoogheemraadschap Stichtse Rijnlanden (HDSR) for logistic support with the hydrological model. Paul van Walsum and Ab Veldhuizen (Alterra) are thanked for their support with METASWAP and Judith Snepvangers (TNO/Deltares) with her help with MODFLOW. J.M. Schuurmans is Financially supported by Deltares.

6 Synthesis

Four research questions were formulated for this thesis:

1. What is the added value of meteorological radar with respect to rain gauges?
2. What is the effect of spatial variability of daily rainfall on modelled interior catchment response?
3. Can remotely sensed evapotranspiration improve the prediction of spatially-distributed soil moisture by a distributed hydrological model?
4. Is it feasible to accurately predict the spatial distribution of soil moisture using rainfall forecasts of a numerical weather prediction model as input for a distributed hydrological model, and, if so, up to how many days?

To answer these questions and to test the practical applicability, we performed fieldwork and set up a blueprint of a system that integrates operational hydrometeorological variables into a distributed hydrological model: the Hydrological Now- and Forecasting System (HNFS). In this chapter the four research questions are answered briefly, based on the results of the preceding chapters, and the answers are discussed in a broader perspective. Also ongoing related research is pointed out. Because of the close relationship between the first two research questions these are grouped in one section. Finally, some applications of the HNFS are given as well as some considerations about its use in practice.

6.1 Added value of meteorological radar

Results
The added value of meteorological radar with respect to rain gauges depends on the density of the available rain gauge network. We showed that if a high density rain gauge network (in our case approximately 13 gauges per 100 km^2, i.e. our temporary research network) is available, rain gauge data only will provide accurate high-resolution rainfall fields and the additional value of radar is negligible. However, for areas with a less dense rain gauge network (in our case approximately 1 gauge per 100 km^2, i.e. the currently available network), the combination of rain gauges and radar

gave the best results, followed by bias-corrected radar only and finally rain gauges only.

The second research question addresses the question whether it is important for hydrologists to take into account the spatial variability of rainfall *if* this information is available. We showed that if one is interested in the day-to-day variability of the spatial distribution of soil moisture and groundwater level, it is important to take the spatial variability of rainfall within the catchment into account. However, if one is interested only in the general behavior of the catchment (i.e. groundwater and soil moisture climatology), it is sufficient to accurately know the spatial average of rainfall within the catchment. This holds also for the daily discharge. However, if a catchment is divided into subcatchments, the spatial average of rainfall within the subcatchment is of importance. The use of a single rain gauge, especially when this rain gauge is situated outside the catchment, carries great risk, because the chance that this rain gauge represents the spatial average rainfall is very small. Model results with radar based rainfall as input showed similar results as when the dense network of rain gauges was used as input, suggesting that bias-corrected radar products are ready to be used in operational water management.

Discussion
In practice, a dense network of rain gauges like the research network that was set up for this study is seldom available. Besides, if we want the HNFS to be an online system we need insight in the actual rainfall fields. This means the rain gauges should be equipped with telemetry. Moreover, regular maintenance of the rain gauge is of great importance to secure its accuracy. Because the rainfall fields from meteorological radar proved to be so useful in our study and because they are available almost immediately, we recommend it as input data source for hydrological models. Recently (2007) KNMI renewed the radar software and now produces 1 x 1 km^2 radar images instead of the 2.5 x 2.5 km^2 we used for our research in 2004. However, accurate rain gauge information will still be needed as "ground truth" for calibration of the radar. Firstly, rain gauge information is needed to make a range correction for the radar based rainfall fields. There is a distance related underestimation of surface rainfall by the radar, due to spatial expansion of the radar beam and attenuation of the radar signal. In 2004 only range corrected radar images of 24 hours were available at KNMI, restricted by the temporal resolution of the largest rain gauge network. Nowadays, also 3-hourly radar images are range corrected. Secondly, rain gauge data are needed because radar does not measure rainfall directly but measures reflected electromagnetic waves that are translated to rainfall with the so-called Z-R relationships throughout the year. Which Z-R relationship should be used depends on the rainfall type (i.e. stratiform, convective). Up to now KNMI uses one constant Z-R relationship, which has been found to be most suitable for stratiform dominated rainfall events (which is the case in the Netherlands). Research on using variable Z-R relationships is going on (Uijlenhoet, 2008). This could improve the correlation between rain gauge data and radar based rainfall fields and thus our method to derive high-resolution rainfall fields from a combination of rain gauges and radar.

Ongoing related research
A recent development that could be used to improve radar-based rainfall estimates, or even be another source in rainfall information is the use mobile-telephone networks (that involves electromagnetic waves similar to radar) that can potentially estimate rainfall information. Promising results have been found using these networks (Leijnse et al., 2007; Messer et al., 2006), that are especially dense in urban areas. Main challenge now is to spatially upscale these line-rainfall estimates. Furthermore, a development from which mainly data-poor areas (no radar available) could benefit is the rainfall estimation derived from the geostationary satellite Meteosat (temporal resolution of 15 minutes, highest spatial resolution is 3 x 3 km^2), that covers Europe and Africa (Roebeling et al., 2008; Wolters et al., 2008). This technique is however only applicable during day-time. Another possibility is the use of TRMM (Tropical Rainfall Monitoring Mission), which is the only rain radar in space (Huffman et al., 2007).

6.2 Remotely sensed latent heat fluxes for improving model predictions of soil moisture

Results
We showed with a real case study that remotely sensed ET_{act} is very useful for hydrological model validation. Comparison of the magnitude as well as the spatial distribution of the remotely sensed and hydrological model based ET_{act} helps to detect potential errors in the hydrological model, both flux-related and conceptual errors. In our case study we concluded that (i) in the lower areas the soil moisture of the root zone in our hydrological model is too high, (ii) the reference evapotranspiration that is used in the hydrological model (Makkink) should be replaced with a method that takes into account the aerodynamic part of evapotranspiration (Penman-Monteith) and (iii) the model concept of forest evapotranspiration in areas with deep groundwater levels (no capillary rise from groundwater anymore) should be adjusted.
Besides a comparison, we also assimilated ET_{act} values of SEBAL with METASWAP by performing a linear statistical correction procedure that weighs the SEBAL and METASWAP based ET_{act} values based on their confidence. The newly derived ET_{act} values were translated back to new soil moisture contents of the root zone using the concept of METASWAP that relates evapotranspiration reduction with soil moisture. This resulted in a spatially-distributed adjustment of root zone soil moisture, which we consider to be realistic but which is hard to validate because of the lack of other, spatially-distributed soil moisture data.
Implementation of our data assimilation method also showed that in case the model concept of land-plant-atmosphere interaction (i.e. the linkage between root zone soil moisture and ET_{act}) is not correct, ET_{act} is not a useful variable to update root zone soil moisture. This manifested itself in areas with forest where capillary rise from groundwater did not play a role anymore because the groundwater level is too deep.
As we had both an ASTER images and MODIS image for the same days, we could also compare their relative contribution. In our study the MODIS images, despite their

lower spatial resolution in comparison to ASTER (15 x 15 m^2 for ASTER and 250 x 250 m^2 for MODIS), appeared just as useful as the ASTER images.

Discussion
The advantage of ET_{act} derived from satellites is that it provides us with spatially-distributed information. This in contrast to the commonly available validation data sources for hydrological models, which provide either point information (e.g. observations wells) or area-integrated information (e.g. discharge). However, only during periods with evapotranspiration reduction, there is a linkage between soil moisture and ET_{act}, which makes it useful to use satellite based ET_{act} in order to improve the accuracy of soil moisture as calculated by our hydrological model.
A drawback of ET_{act} derived from polar orbiting satellites (like ASTER and MODIS that were used in this study) is the temporal resolution. Besides the fact that these satellites have a certain return period, the potential temporal resolution is reduced by the fact that cloud free circumstances are needed to gain useful thermal images. This makes it, especially in a often clouded country like The Netherlands, an unreliable data source. Moreover, the future of thermal band is at risk. Up to now, for example NASA has no budget to equip the new Landsat satellite with a thermal instrument. Several memos have been written (e.g. Allen et al., 2006) to express the need for thermal band on the new Landsat satellite. ET_{act} images derived from geostationary satellites like SEVIRI (Spinning Enhanced Visible and Infrared Imager) on Meteosat are much less sensitive to these cloud free restrictions as the temporal resolution is much higher (15 minutes). However, its spatial resolution is much lower in comparison to ASTER and MODIS (at highest 3 x 3 km^2).
Satellite based information must always be translated to hydrological variables using a specific algorithm which involves (i) uncertainty and (ii) a time lag. Measurements of the derived hydrological variables that deliver "ground truth" are essential to be able to judge the relative reliability of either satellite based and hydrological model based results. Automation of the algorithms is needed to reduce the time lag and with that make online adjustment of the hydrological model using data assimilation possible.
Data assimilation updates state variables of the hydrological model but does not solve the underlying cause of error in the hydrological model that leads to the difference between modelled and remotely sensed ET_{act}. Data assimilation should therefore not be considered as a replacement for model calibration.

Ongoing or related research
Besides thermal band satellite images that were used in this thesis, (passive or active) microwave remote sensing data are also commonly applied in hydrology. With these data it is possible to determine the top layer (few cm up to 10 cm) soil moisture. Research is mainly focussing on (i) algorithms to derive root zone soil moisture from microwave remote sensing data (e.g. Owe et al., 2008; De Jeu and Owe, 2003) and (ii) assimilation of microwave derived soil moisture into hydrological models (e.g. Hoeben and Troch, 2000; Pauwels et al., 2007), as microwave derived soil moisture is not representative for the soil moisture within the whole root zone (from which water is extracted for evapotranspiration). Besides, for areas with forest the soil moisture data that are derived with microwave technique are less reliable as it is hard for the

microwave signal to penetrate the canopy.
The spatial resolution of microwave data depends on the type of sensor (active or passive) and the scan-mode of the sensor. In case of an active sensor like ENVISAT ASAR (Loew et al., 2006) spatial resolution varies between 30 x 30 m^2 (high resolution mode with operation time of 30 minutes per orbit and a 30-day return period) up to 1 x 1 km^2 in global mode (5 day return period). Passive systems measure the intensity of microwaves at certain wavelengths radiated by the earth. Due to the weakness of this signal, spatial resolution is much lower than for active systems and is in the order of 50 x 50 km^2 (2-3 days repeat time) in case of for example AMSR-E (Owe et al., 2008). Research within The Netherlands using air-crafts equipped with microwave instruments, which generates higher resolution images, is going on (Miralles, 2008).

6.3 Forecasting spatially-distributed soil moisture

Results
In Chapter 5 we mimicked an online forecast system that provides 9 day ahead forecasts of regional soil moisture for the period March-November 2006. Daily rainfall forecasts from the numerical weather prediction model (NWP) of the European Centre for Medium-Range Weather Forecasts (ECMWF) were used, which were provided by the KNMI. Firstly, the accuracy of the forecasted daily rainfall was determined as function of lead time by comparing the forecasts with high-resolution rainfall fields using both radar and rain gauges. Secondly, the accuracy of forecasted soil moisture was determined by comparing the forecasted soil moisture with the model results that used the high-resolution rainfall fields (the so-called "true run").

We found that the total amount of measured spatial mean rainfall within the study area is forecasted well by the ensemble mean of the rainfall forecast for all lead times (maximum difference 45 mm for lt1). However, the total measured rainfall during March–November 2006 within the study area shows a large spatial variation (200 mm), which is not taken into account for forecasted rainfall. The measured rainfall (spatial mean) shows a distribution with peaks at 0–1 mm day^{-1} and > 10 mm day^{-1}. These peaks are underestimated by the ensemble mean of the rainfall forecasts and this underestimation increases with lead time. The ensemble members however follow more or less the distribution of measured rainfall for all lead times. We also found that the modelled uncertainty in rainfall by ECMWF underestimates the true uncertainty for all lead times. Besides, the number of rainfall events (thresholds 0.1, 0.5 and 1.0 mm day^{-1}) is overestimated ($\sim$ 30 - 40%) by the rainfall forecasts, both with the individual ensemble members as well as with the ensemble mean. This overestimation is constant with lead time for the ensemble members but increases for the ensemble mean with increasing lead time, especially for higher thresholds (up to factor 2–2.5 for lead time 9 days).

Comparison of the spatial distribution of temporal mean soil moisture showed that bias values in root zone storage higher than 1 mm began to show around a lead time of 3 days. The lower- and upper bounds of bias at a lead time of 9 days

were respectively $\sim$ -4 mm to 7 mm (negative values meaning that the forecasted soil moisture is too wet in comparison to the "true run"). We found that the bias in root zone storage showed a spatial pattern that represents the spatial pattern of total rainfall: areas with less rainfall than spatial average show a negative bias and vice versa. For the soil moisture forecasts we used both the individual rainfall ensemble members (system 1) as well as the mean of the rainfall ensemble members (system 2). Because of the non-linear behavior of the unsaturated zone these systems can lead to different outcomes. However, system 1 and 2 showed similar results for the bias in temporal mean soil moisture. The advantage of system 1 is that it makes it possible to show the reliability (i.e. consistency) of the predicted soil moisture per model node and to make probabilistic forecasts. With system 2 this is not possible but its advantage is that the computational demand is much lower.

Discussion
In this study we only investigated the modelled soil moisture uncertainty caused by uncertainty in rainfall forecasts, thereby assuming that the high-resolution rainfall fields were the actually true rainfall within the catchment. Uncertainties due to model errors were not taken into account. Besides, uncertainty due to forecasted evapotranspiration were also not taken into account. In our study we chose to use observed evapotranspiration of that day, so the results should be considered as the upper bound skill of the soil moisture forecast system. However, with the outcomes of the ECMWFit is also possible to take the forecasted evapotranspiration into account.

Ongoing or related research
For operational rainfall forecasts, NWPs are not the only source. Extrapolation in time of radar (or satellite) precipitation patterns for example is another one (the so-called nowcasting methods). Lin et al. (2005) investigated the cross-over point in time where NWPs start to have more skill than nowcasting methods and found this to be 6 hours after the forecast is initiated. Although this conclusion is based on 3dVAR methods instead of 4dVAR systems (such as that of the ECMWF), qualitatively it is safe to say that in case rainfall forecasts are used in hydrological studies with time steps of for example 1 hour, a combination of nowcasting methods and NWPs should be beneficial.

6.4 HNFS: applications and considerations

With the HNFS we are able to show the current as well as the forecasted spatial distribution of several useful hydrological properties that are accounted for in our model METASWAP. Some examples are (1) actual soil moisture in root zone (2) potential storage in unsaturated zone (3) evapotranspiration reduction and (4) irrigation demand of root zone: the amount of water that should be added via irrigation to the root zone in order to resolve evapotranspiration reduction. Figure 6.1 shows this as an example for 17 July 2006. Besides, with HNFS it is also possible to show time series of forecasted soil moisture which is caused by uncertainty in rainfall forecasts, like was done in Figure 5.11.

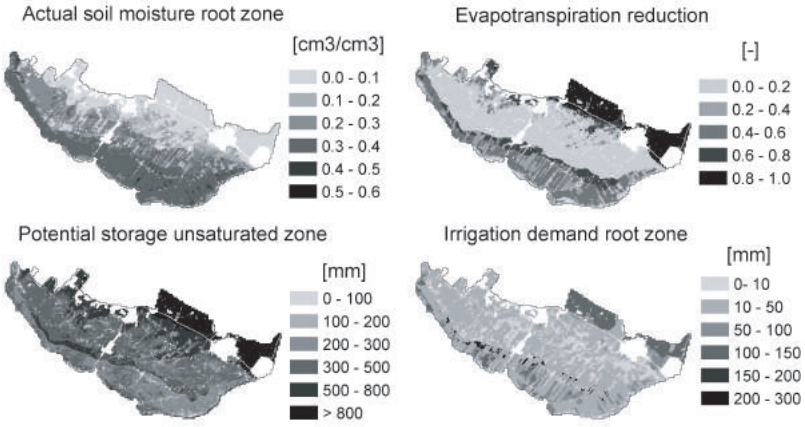

Figure 6.1 Example of practical application of HNFS for 17 July 2006.

The accuracy of our hydrological model outcomes will make or break the value of the above listed practical applications. As mentioned in Chapter 1, spatially-distributed models are developed at ongoing higher spatial resolution due to increasing data availability and computer capacity. Considering the hydrological cycle, as well as the temporal and spatial scales of the hydrological processes, it is clear that the "reality" of our hydrological system is complex. In a recent paper Sivakumar (2008) comes to the conclusion, based on an extensive literature research, that hydrologists have the tendency to (i) make the models more and more complex and (ii) focus on individual mathematical techniques rather than general hydrologic issues.
Are we seeking an answer to a scientific question, thereby searching for a appropriate hydrological model, or are we developing a model an thereby searching for an appropriate question? In other words, is our question leading or is our model leading? This is where the separation between hydrology as science itself and hydrology as an applied science for decision support comes into play. For practical use the main question we should ask ourselves should be: "for what purpose do we want to develop this system?". Although this seems very trivial it is something that is quickly overlooked in our optimism that we are technically capable of building a multi-purpose model that will be useful for e.g. water boards (discharge prediction), farmers (water stress prediction) and drinking water concerns (recharge prediction). To be able to make accurate model predictions, the following four aspects should be considered, which should keep pace with each other.

- model complexity
- input data availability
- calibration and validation measurement availability

- user-friendliness of the model

To make progress in hydrology the "weakest link" of those four aspects should be improved. In the following the current state of these four aspects in The Netherlands is addressed.

With model complexity both increasing detail and improved model concepts are referred to. An example of this is the development of the Netherlands Hydrological Modeling Instrument (Delsman et al., 2008), which is a collaboration between the larger research institutes to couple unsaturated, saturated and surface water model codes. This could lead to better description of the hydrological system. However, there is a danger that coupling of these different modules becomes a (technical) challenge itself, thereby focussing too much on certain model concepts instead of taking advantage of using several model concepts as is encouraged by for example Beven (2006).

The two largest rives in The Netherlands are the Rhine (average annual discharge at the border 2,300 m^3 s^{-1}) and the Meuse (average annual discharge at the border 230 m^3 s^{-1}). Translated to water depth over The Netherlands (41,000 km^3), their yearly budget is 1770 mm respectively 177 mm. So actually there are two rivers in between the Rhine and Meuse: the river "Down" and river "Up". The river Down being rainfall (annual average 800 mm) and the river Up being evaporation (annual average 550 mm). These two main input variables (rainfall and evapotranspiration) of the hydrological system deserve the needed attention. During the last few years the rainfall radar that can detect the spatial distribution of rainfall has improved considerably. In this study we showed the added value of radar and the importance of taking this into account in distributed hydrological models. However, although on average almost 70% of annual rainfall evaporates, good insight into the (spatial distribution) of evaporation lacks. This is maybe due to its latent character. More attention should be payed to this significant flux.

Calibration data are needed to be able to judge which parameters in the hydrological model should be adjusted and validation data are needed to test the accuracy of our hydrological models. What data and on what spatial and temporal resolution goes together with (i) the question for what purpose we developed a model and (ii) the spatial and temporal resolution of our model. However, the basic components of the water balance (i.e. inlets and outlets) of (sub)catchments should always be available. This is not the case at this moment. Even worse, the number of commonly available measurements like observation wells has been cut back over the last few years.

An acknowledged pitfall of hydrological simulation models is that they will always generate an outcome. It is the hydrologist's task to weigh these aspects against each other and prevent the pretence of knowing the hydrological variables at a high resolution. It is the challenge for hydrologists to decide whether outcomes are trustworthy or not and to decide which model parameters should perhaps be adjusted. As model complexity and thus the number of parameters and their interaction increases this becomes a very hard job to deal with. This is what is meant with the user-friendliness: models should not be more complex than what qualified hydrologists can deal with.

Besides, accessibility of the model code together with proper documentation is indispensable to improve the model through experiences from other users.

Possibly, we can learn from our colleagues the meteorologists who struggle with the same kind of problems in their NWPs and more and more decide to focus on the development of model ensembles, rather than on increasing the model complexity. With the use of model ensembles it is possible to gain insight in the model reliability and, in case there are validation sources, also in the model accuracy. Development of model ensembles that are based on perturbations of the initial conditions of the model or, more relevant for hydrological modeling, different parameter combinations is a challenge itself. Another possible consideration is the use of anomalies, which is often done in meteorology.

Appendix 1

Rain gauge calibration

The gauges used in this study have a collecting funnel diameter of 254 mm and were set to measure approximately 0.2 mm of rain per tipping. For most rain gauges the manufacturer provided the average volume per tipping. However, tipping bucket type rain gauges are known to overestimate rainfall at low rainfall intensities and to underestimate rainfall at high rainfall intensities (e.g. Molini, 2005; Habib et al., 2001). Therefore we dynamically calibrated all rain gauges in the laboratory (Figure 2), following Van den Assem (1988). Figure 3 shows the results of this calibration. It was found that the intercept of the linear relationship between tipping volume and rain rate varies between 0.185 and 0.202 mm/tipping, with 83 % of the values being below 0.2 mm/tipping. Considering a rainfall intensity range of 0-100 mm/hour and assuming a tipping volume of 0.2 mm/tipping, the absolute error caused by ignoring the linear relationship is 0-5 % in 47 % of the cases, 5-10 % in 47 % of the cases and 10-15 % in 6 % of the cases.

Figure 2 Photo of rain gauge calibration.

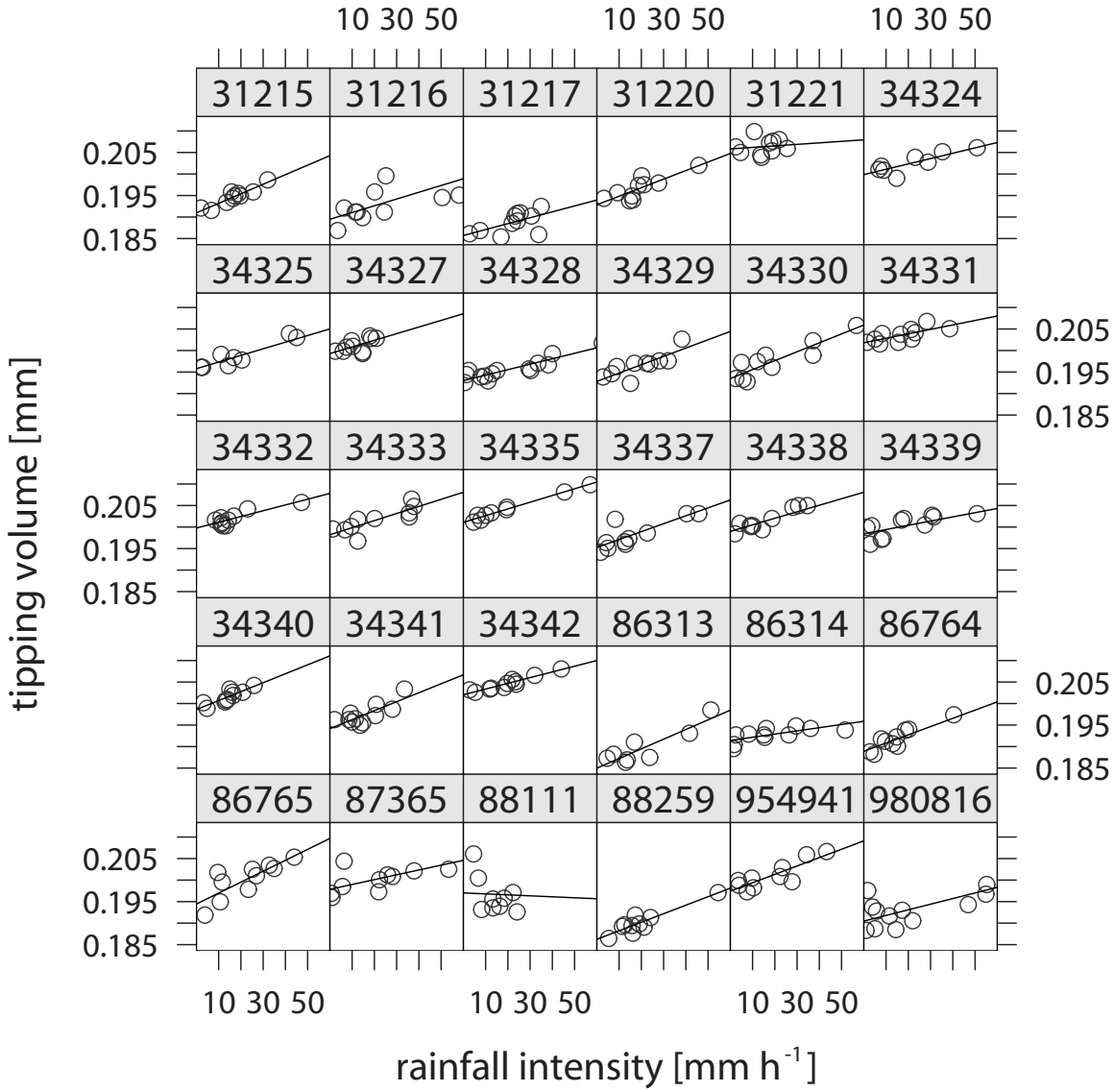

Figure 3 Dependency of tipping volume on rainfall intensity with calibration curves fitted by linear regression for each of the 30 rain gauges (numbers indicate serial numbers).

Appendix 2

Geostatistical Simulation of Daily Rainfall

Prediction techniques such as kriging tend to smooth out the local variability of rainfall, especially further away from the data locations. Kriging variances provide a measure of local uncertainty but give no insight into the joint spatial distribution of rainfall uncertainty. Because the hydrological system is non-linear, the use of smoothed rainfall fields could lead to a biased hydrological response when used as input for hydrological models. Therefore it would maybe be better to stochastically simulate rainfall fields and use an ensemble of simulated rainfall fields as input. Here we show how sequential simulation with colocated cokriging could be used.

Sequential Gaussian Simulation
For the sequential simulation we used the same data set as used for kriging, so the square-root transformed rain gauge data and colocated range corrected radar data. Sequential simulation can be described by the following steps (Goovaerts, 1997):

1. Select randomly a simulation location (usually on a grid) and perform kriging using the rain gauge measurements (original data set), giving a kriging prediction and kriging variance.

2. Draw randomly a number from a Gaussian distribution that has a variance equal to the kriging variance and a mean equal to the kriging prediction. This number will be a conditioning datum for all subsequent drawings.

3. Select randomly another prediction location and repeat step 2, including in the kriging all previously simulated values as observations to preserve the spatial variability as modelled in the variogram.

4. When all prediction locations have been simulated, transform back to the original distribution (in our case by squaring the simulated data). This provides the first simulation field. When simulating another realisation, steps 1-4 are repeated with a new random sequence.

Because all the simulated data are added to the conditioning data, it is necessary to limit the search neighborhood in order to reduce the calculation time. In our case, we used only the 40 nearest data points.

As for the rainfall prediction, we used both ordinary kriging and ordinary colocated cokriging for the simulation of rainfall. However, the "classic" sequential Gaussian simulation algorithm assumes that the mean value or function of the random field under consideration is known. In that respect, it is the simulation-equivalent of respectively simple kriging and simple colocated cokriging. For simple kriging we used the mean of the non-zero square-root transformed rain gauges as the mean. This value was also taken for the mean of the first variable for colocated cokriging. The mean of the square-root transformed radar values within the extent was taken as mean of the secondary variable.

Required Spatial Resolution
With the sequential simulation method we simulated rainfall depths at point locations, which have a small spatial support. In order to produce rainfall fields at a given spatial resolution we have to simulate several points within each pixel. The number of points required depends on the variability of the rainfall process, that is represented by the variogram. However, as a rule of thumb, 16-25 points are sufficient (Goovaerts, 1997). The outcomes of these points within each pixel are averaged, giving the mean rainfall depth for each pixel.

Simulation Results
Figure 4 shows the results of one simulated rainfall field of 1 May 2004 at the small extent, using the ordinary kriging and simple colocated cokriging equivalent of sequential gaussian simulation. Figure 4a shows the simulated rainfall values on a point grid, with a regular spacing of 100 meter. To produce simulated rainfall fields on a spatial resolution of 500 m $\times$ 500 m, the outcomes of the 25 points within each grid 500 m $\times$ 500 m are averaged (Figure 4b).

For two events (4 April 2004 and 1 May 2004) we performed 100 simulations of the rainfall field at small extent, using ordinary kriging and colocated cokriging. For each of the 100 simulations we calculated the cumulative distribution function (cdf) and plotted this together with the cdf of the rain gauge data set. Figure 5 shows that colocated cokriging simulation is more precise (low spread) than the ordinary kriging simulation, especially for 1 May 2004, where the correlation between the rain gauge data and colocated radar values is high (0.84). Figure 5 also shows that the simulations are accurate, reproducing the cumulative distribution function of the rain gauge data.

The simple colocated cokriging equivalent of sequential gaussian simulation enables us to simulate rainfall fields at any required spatial resolution, conditional to both rain gauges and radar fields. The simulated rainfall fields reproduce both high and low rainfall values as well as the spatial correlation of the observed rainfall fields and can be used as an ensemble input for hydrological models.

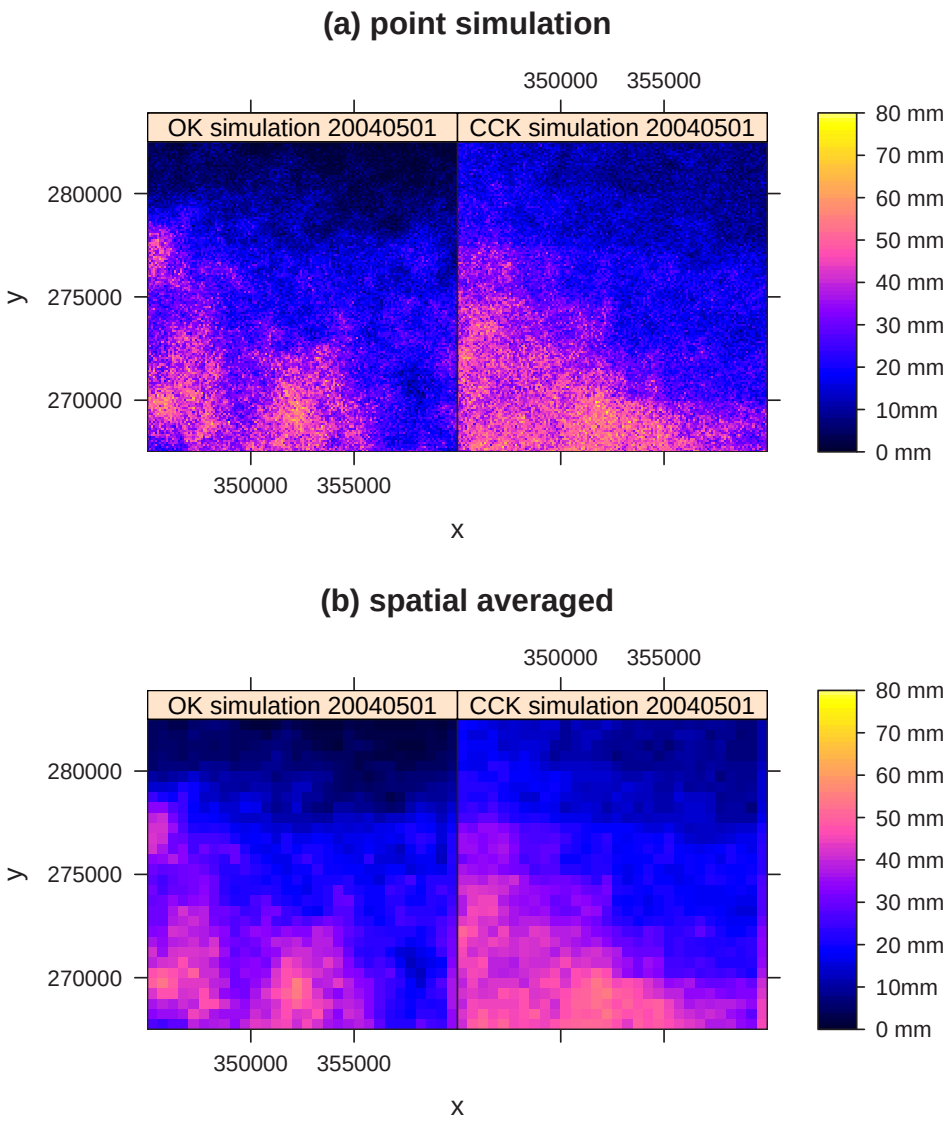

Figure 4 Results of sequential gaussian simulation of rainfall depths at 1 May 2004, using ordinary kriging (OK) and simple colocated cokriging (CCK) on both (a) a point grid and (b) high resolution grid of 500 m $\times$ 500 m.

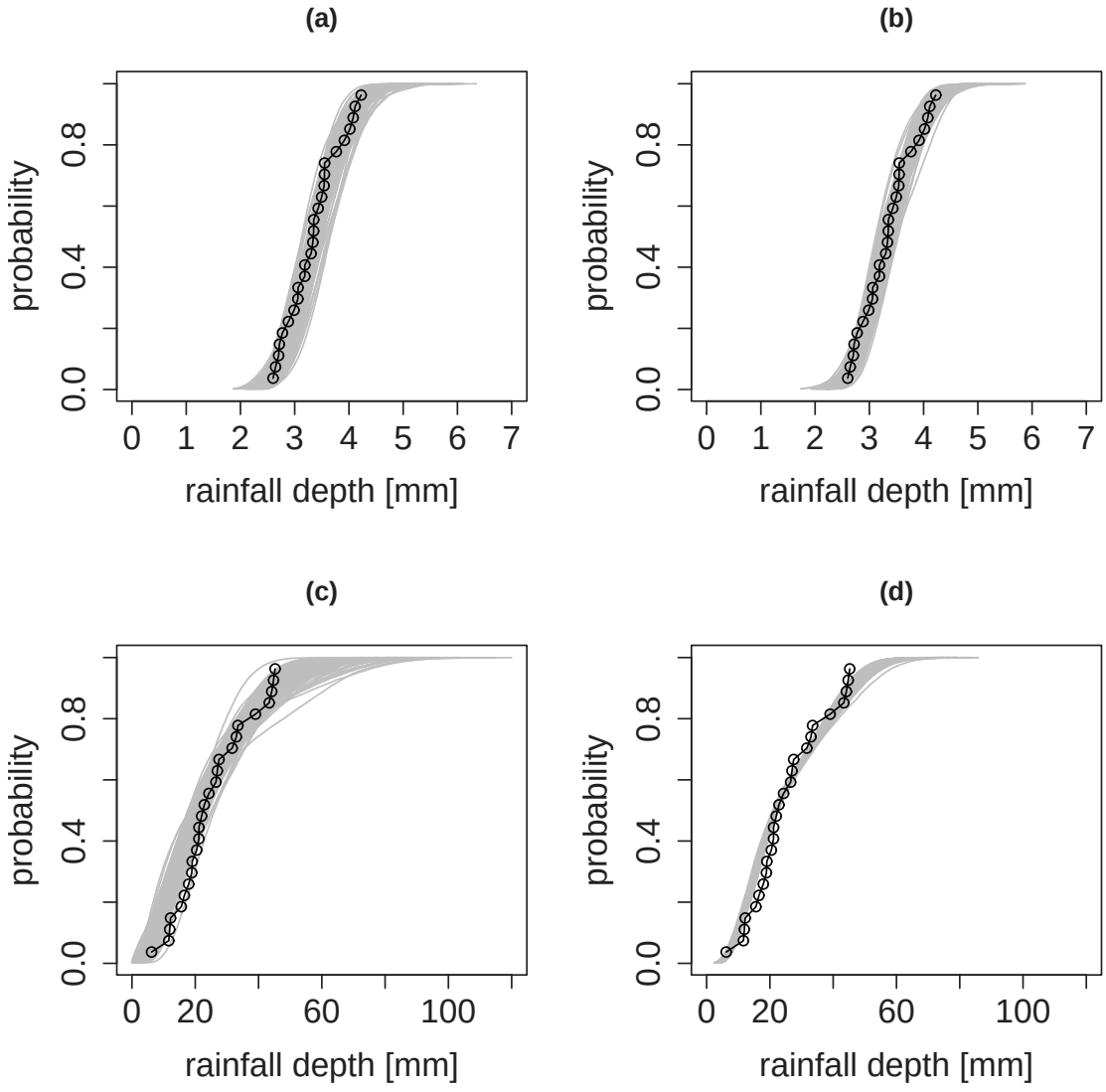

Figure 5 Cumulative distribution function of the simulated rainfall (grey lines) and the rain gauge data (black dots): (a) ordinary kriging simulation for 4 April 2004; (b) colocated cosimulation for 4 April 2004; (c) ordinary kriging simulation for 1 May 2004; (d) colocated cosimulation for 1 May 2004.

Appendix 3

ech$_2$o calibration

In this study we used 20 cm ECH$_2$O probes (EC-20) that use the capacitance technique to derive the dielectric permittivity of a medium (Bogena et al., 2007). For each soil moisture measurement location (Figure 4.1B) we performed a calibration. Tubes with a diameter of 20 cm and 40 cm length were drilled into the ground, nearby the measurement locations at 2 depths: 10 cm and 50 cm. In the laboratory the soil samples were first wetted to approximately field capacity after which the ECH$_2$O probes were inserted into the soil samples, perpendicular to the surface. Then the top of the tubes were cut off to create an area from which moisture could evaporate, a situation that represents actual field conditions (Figure 6). The soil moisture content according to the ECH$_2$O probes was logged every 5 minutes. We weighted the soil samples twice a day in order to get the gravimetric soil moisture content. Figure 7 shows the calibration results of the soil moisture sensors, for each soil moisture measurement location at 10 and 50 cm. The fitted splines were used to calibrate the soil moisture measurements that were taken in the field. Field measurements were done at 5, 15, 30, 50 and 70 cm depth. For field measurements at 5 and 15 cm, the fitted splines of the calibration at 10 cm were used. For field measurement at 30, 50 and 70 cm, the fitted splines of the calibration at 50 cm were used. It must be noted that extrapolation of splines can be very risky, however all the field measurement were within the range that was measured by the ECH$_2$O sensors during calibration.

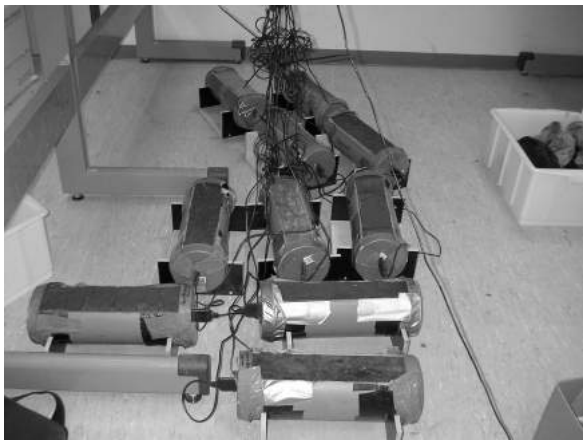

Figure 6 Photo of soil moisture sensor calibration.

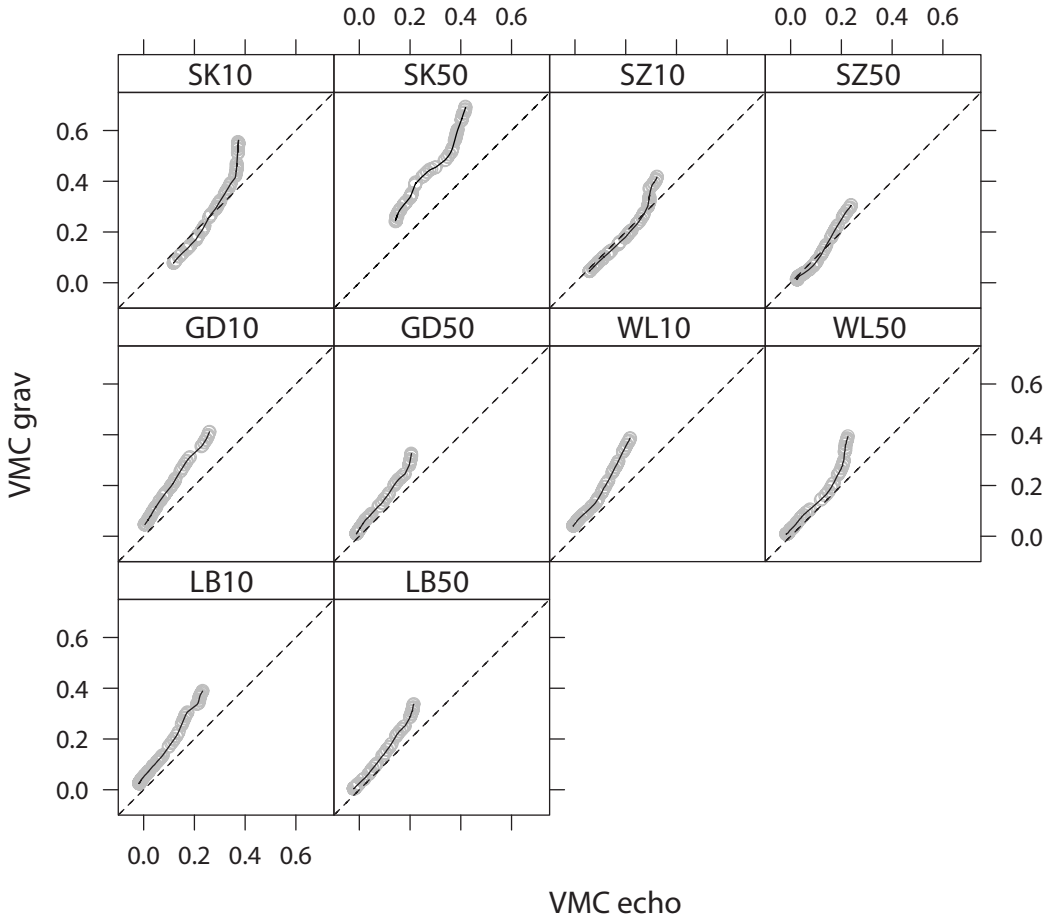

Figure 7 Volumetric moisture content (VMC [cm^3 cm^{-3}]) of gravimetric measurements against VMC of ECH2O sensors for each soil moisture measurement location (Figure 4.1B) at 2 depths: 10 cm and 50 cm. Black lines are the fitted splines, dotted lines represent 1:1 line.

Appendix 4

groundwater model specifications

Our groundwater model is part of an existing groundwater model with a larger spatial extent. The model boundary (Figure 4.1A) is taken from an earlier study of the study area (Hermans et al., 2004). The model boundary is chosen such that wrong boundary conditions have negligible small influence on the study area. The north-east side lies over the ice pushed ridge, the south-east boundary lies south of a river, the south-west side follows a deep canal (Amsterdam-Rijnkanaal) and in the north-west the boundary lies far enough from the study area, considering the northeast-southwest groundwater flow direction. The groundwater model consists of 7 layers (aquifers) separated by aquitards in between (Figure 8). Within the aquifers the Dupuit assumption holds true, which means that there is only lateral flow. Within the aquitards there is only vertical flow. The first aquifer and aquitard together form the confining layer that exists of holocene river sediments and is only present in the south-east part of the study area. Its boundary lies halfway along the study area, coinciding with the boundary between soil type 19 and 12 (Figure 4.1B).

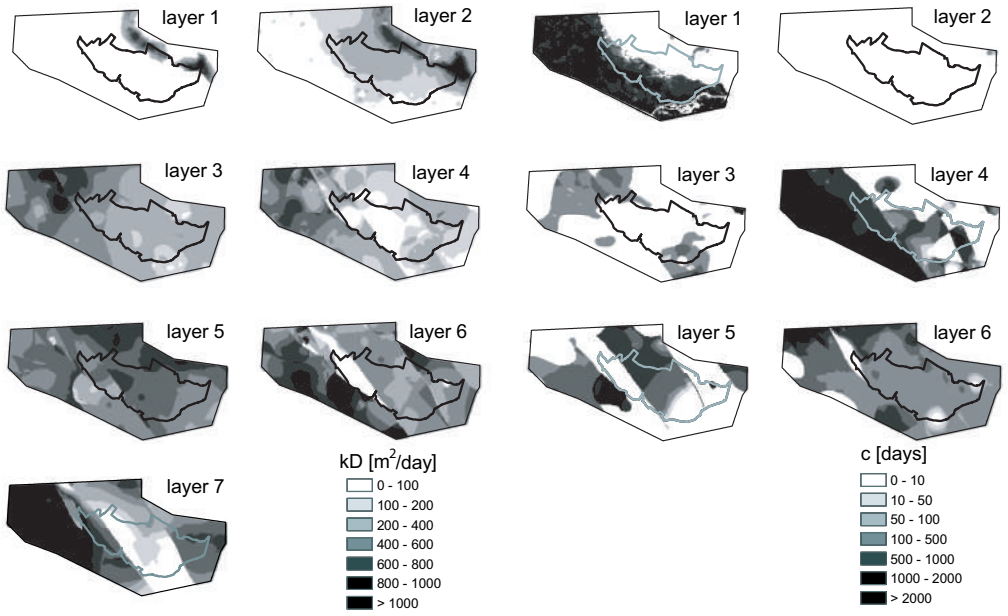

Figure 8 Transmissivity (kD) [m^2 day^{-1}] and resistance (c) [days] values of hydrological model.

Appendix 5

SEBAL

The Surface Energy Balance Algorithm for Land (SEBAL) is based on the surface-energy balance (Bastiaanssen, 1995; Bastiaanssen et al., 2005):

$$R_n = G_0 + H + \lambda\rho E, \tag{1}$$

in which R_n [W m^{-2}] is the net radiation; G_0 [W m^{-2}] is the soil heat flux; H [W m^{-2}] is the sensible heat flux and λE [W m^{-2}] is the latent heat flux that is associated with actual evapotranspiration (ET_{act}) by the latent heat of vaporization (λ) and ρ is the density of water [kg m^{-3}].

From satellite radiances the surface parameters surface albedo (r_0 [-]), Normalized Difference Vegetation Index (NDVI [-]) and surface temperature (T_s [K]) are determined for each satellite pixel.

The instantaneous net radiation $R_{n,i}$ at time of satellite overpass is determined with Equation 2.

$$R_{n,i} = (1 - r_0) \cdot K_{ext,i} \cdot \tau_{sw,i} + L_i^{\downarrow} + L_i^{\uparrow}, \tag{2}$$

with

$$L_i^{\downarrow} = \varepsilon_{atm} \cdot \sigma \cdot T_a^4 \tag{3}$$

and

$$L_i^{\uparrow} = \varepsilon_s \cdot \sigma \cdot T_s^4, \tag{4}$$

in which the emissivity of the atmosphere (ε_{atm}) [-] is an empirical relationship with humidity, the emissivity of the surface (ε_s) [-] is derived from NDVI, σ is the Stefan-Boltzman constant (5.67 e-08 W m^{-2} K^{-4}), T_a [K] is the air temperature (meteorological station data) and T_s [K] the surface temperature (satellite image).

The instantaneous soil heat flux ($G_{0,i}$) is calculated using a sinus relation for soil temperature, a coefficient of heat conductivity and an attenuation depth.

Having $R_{n,i}$ and $G_{0,i}$ the remaining problem is the division between the (instantaneous) sensible (H_i) and the (instantaneous) latent heat flux (λE_i), which can be expressed by the (instantaneous) evaporative fraction (Λ_i [-])

$$\Lambda_i = \frac{\lambda \rho E_i}{R_{n,i} - G_{0,i}} = \frac{\lambda \rho E_i}{\lambda \rho E_i + H_i} = \frac{R_{n,i} - G_{0,i} - H_i}{R_{n,i} - G_{0,i}} \tag{5}$$

If H_i is solved for each satellite pixel, λE_i is the residue of the energy balance. SEBAL computes H_i using a so-called "self calibration" procedure. The coldest pixel is selected in the satellite image, where it is assumed that H_i=0 (and $\lambda E_i = R_{n,i}$-$G_{0,i}$), and the warmest pixel is selected where it is assumed that $H_i = R_{n,i}$-$G_{0,i}$ (and λE_i=0). For this cold and warm pixel the vertical temperature difference ΔT between two reference heights (see Equation 7) is calculated to match the value of H at a given aerodynamic resistance. For the cold pixel ΔT=0, for the warm pixel ΔT is solved iteratively using the Equations 6–11. These equations are based on the Monin-Obukhov Similarity Theory (MOST, Monin and Obukhov (1954)) that describes the flux-profile relationships of wind, temperature, humidity and latent heat flux. The Obukhov length L [m] is the height above the surface where mechanical and convective forces are equal. Holtslag (1987) has shown that MOST is valid in The Netherlands up to a height of 200 m. In the Equations 7 and 8 z_1 is set to the roughness length (z_{om} [m]), that comes in this study from a slightly modified roughness map from the Royal Netherlands Meteorological Institute (KNMI). This map is based on the Dutch national land-cover database LGN (Oort et al., 2007; De Wit and Clevers, 2004), as is the land use map in our hydrological model. The roughness map is slightly modified with an orographic correction and a small time correction for agricultural land use, using NDVI. The parameter z_2 is set to a standard height of 10 m. The wind velocity at height z_2 , u_{z2} [m s^{-1}] in Equation 8 is based on Meteolook data. Meteolook is a physically based regional distribution model for measured meteorological variables and is developed by WaterWatch (Voogt, 2007), and κ is the von Karman constant [-]. Meteolook provides interpolated maps of the routinely measured weather variables air temperature, wind velocity and humidity. This model is also based on the MOST theory as well as on recent research that links meteorological conditions of neighbouring land surface types. Hutjes (1996) and Bink (1996) applied the "bottom-up-top-down" approach, where measurements at a site with given surface characteristics are transformed to values at a height where surface influences are no longer dominantly present (e.g. blending height). For the Netherlands it is found that the blending height is $\sim$ 60 m (Wieringa, 1986; Vermeulen, 2001). In Meteolook a blending height of 100 m is taken.

Now, the sensible heat flux is calculated with:

$$H = \rho_a \cdot c_p \cdot T_* \cdot u_*, \tag{6}$$

in which the specific heat of air (c_p) [J kg^{-1} K^{-1}] is kept constant, the air density (ρ_a) [kg m^{-3}] is a function of elevation, temperature and humidity, T_* [K] is a Temperature scalar given by Equation 7 and u_* the friction velocity [m s^{-1}] given by Equation 8.

$$T_* = \Delta T/[ln(z_2/z_1) - \gamma_h(z_2, L) + \gamma_h(z_1, L)], \tag{7}$$

in which $\Delta T = T_{z_2} - T_{z_1}$ and γ_h is a stability function given by 9.

$$u_* = (k \cdot u_{z2})/[ln(z_2/z_1) - \gamma_m(z_2, L) + \gamma_m(z_1, L)], \tag{8}$$

in which γ_m is a stability function given by 10

$$\gamma_h(\frac{z}{L}) = \begin{cases} L < 0 : 2 \cdot ln(\frac{1+x^2}{2}) \\ L = 0 : 0 \\ L > 0 : -5 \cdot \frac{z}{L} \end{cases} \tag{9}$$

$$\gamma_m(\frac{z}{L}) = \begin{cases} L < 0 : 2 \cdot ln(\frac{1+x}{2}) + ln(\frac{1+x^2}{2}) - 2 \cdot arctan(x) + \frac{\pi}{2} \\ L = 0 : 1 \\ L > 0 : -5 \cdot \frac{z}{L} \end{cases} \tag{10}$$

$$x = \sqrt[4]{1 - 16 \cdot \frac{z}{L}} \tag{11}$$

After solving ΔT for the hot pixel(ΔT=0 for the cold pixel) by solving Equations 6-11 for ΔT, L and H such that $H_i = R_{n,i} - G_{0,i}$, a linear relationship is fitted for the ΔT–T_s relationship, which is thus image specific. Field research has demonstrated that this linear relationship is valid (Wang, 1995; Franks and Beven, 1997). The advantage of this ΔT-T_s relationship is that it eliminates propagation of errors on the energy balance partitioning and the need for atmospheric correction, by band, for short-wave reflection.
With the ΔT-T_s relationship, together with the wind velocity u_{z2} from Meteolook and the site-specific z_1 =z_{om}, the sensible heat flux H can be calculated for each pixel of the satellite image (Equation 6). λE follows from solving the energy balance, Equation 1. This means that the instantaneous evaporative fraction (Λ_i) is known for every satellite pixel. It is assumed in SEBAL that the daily evaporation fraction is the same as the instantaneous evaporation fraction. This means that if the daily net radiation ($R_{n,24}$) and daily soil heat flux ($G_{0,24}$) are known, the daily latent heat flux λE and thus the daily evaporation E is known for each satellite pixel.

To derive the daily soil heat flux ($G_{0,24}$), the sinus relation used to derive the instantaneous soil heat flux is integrated over 24 hours. Furthermore the soil heat flux is attenuated based on NDVI. The more vegetation, the lower G_0 .

The daily net radiation, $R_{n,24}$ can be calculated for each satellite pixel using a simplified formula (De Bruin and Stricker, 2000)

$$R_{n,24} = (1 - r_0) \cdot \tau_{sw} \cdot K^{\downarrow}_{exo} - 110 \cdot \tau_{sw}, \tag{12}$$

in which τ_{sw} is the transmissivity of atmosphere for short wave radiation [-] and $K^{\downarrow}_{exo}$ is the extraterrestrial radiation [W m^{-2}]. τ_{sw} can be calculated for each meteorological station where $K^{\downarrow}$ is measured with pyranometers. In this study a constant τ_{sw} of the nearest meteorological station is used for the satellite images, because the images cover a relatively small area.

$$\tau_{sw} = \frac{K^{\downarrow}}{K^{\downarrow}_{exo}} \tag{13}$$

$K^{\downarrow}_{exo}$ can be calculated as a function of the solar constant (G_{sc}, 1367 [W m^{-2}]), the inverse relative distance between earth and sun d_r [-], the solar declination δ [rad], the latitude φ [rad], the day of year J [-] and the sunset angle ω [rad] (Equations 14-17).

$$K_{exo} = \frac{G_{sc} \cdot d_r}{\pi}[arccos[-tan(\varphi)tan(\delta)]sin(\varphi)sin(\delta) + cos(\delta)cos(\varphi)sin(\omega_s)] \tag{14}$$

$$\delta = 0.409 \cdot sin(\frac{2\pi}{365}J - 1.39) \tag{15}$$

$$d_r = 1 + 0.033 \cdot cos(\frac{2\pi}{365}J) \tag{16}$$

$$\omega_s = arccos[-tan(\varphi)tan(\delta)] \tag{17}$$

Summary

Physically based distributed hydrological computer simulation models are important tools for hydrologists to obtain insight into the hydrologic cycle and to determine how precipitation is distributed over the different hydrological stores (e.g. surface water discharge, soil moisture, groundwater). In the last 30 years the number but also the complexity of hydrological computer models has grown tremendously, due to more powerful computers, geographical information systems (GIS) and remote sensors. As the spatial resolution of these models increases, the amount of available data to provide these models with *input* and *validation* information at the same spatial resolution lacks behind. At the same time hydrometeorological information based on remote sensing techniques has improved over the years and has become more easily available. These data can serve as improved input and validation data for distributed hydrological models. Besides, meteorologists developed numerical weather prediction models (NWP) that can be used to make forecasts of the hydrological system. However, in practice, these remotely sensed and forecasted hydrometeorological variables are not commonly used in hydrological models. The reason for this lack of use are some unresolved research questions about how these hydrometeorological data should be integrated into the hydrological models and whether these data could improve the accuracy of the hydrological models at all.

The scope of this thesis was to investigate (i) whether operational remote sensing data that provide spatially-distributed hydrological information can improve the accuracy of the distributed hydrological models and (ii) whether rainfall forecasts could provide accurate forecasts of the hydrological model. Within the hydrological system the focus was on soil moisture. The operational remotely sensed data were restricted to meteorological rainfall radar and actual evapotranspiration (ET_{act}) derived from satellites.

To test the integration of remotely sensed and forecasted hydrometeorological variables into a hydrological model we set up the Hydrological Now- and Forecasting System (HNFS). By using operational data and hydrological models with real case studies we hoped to show the potentials and limitations of such a system in practice.

To derive high-resolution daily rainfall fields that can serve as input for the hydrological models, we applied geostatistics (Kriging variants) using rain gauge data only, radar data only and a combination of rain gauge and radar data. Results showed that the added value of radar with respect to rain gauges is significant. With the operational rain gauge network in The Netherlands, it was shown that a combination

of rain gauge and radar data gave the best results, followed by radar only and finally rain gauge data only. Only in case of a dense network, like our experimental network (30 rain gauges within an area of 15 km x 15 km), the rain gauges did perform better than radar.

The need to use spatially variable rainfall fields in a distributed hydrological model was tested by using a scenario analysis of different rainfall inputs. Results showed that the need to take into account the spatial variability of rainfall depends on the hydrological modelling objective. If one is interested in the day-to-day variability of distributed soil moisture and groundwater level it is important to take the spatial variability of rainfall into account. However, if one is interested in the general hydrological behavior (i.e. groundwater and soil moisture climatology) it is sufficient to take into account the spatial mean rainfall within the catchment. This holds also for the daily discharge. It was shown that there is a great risk in using one rain gauge only, especially if it is situated outside the study area.

ET_{act} derived from satellites proved to be very useful in the process of model validation, although this is restricted to periods with evapotranspiration reduction. Spatially-distributed ET_{act} data made it possible to indicate areas of potential model error, both flux-related as conceptual model errors. Assimilation of ET_{act} based on satellites into our hydrological model, resulted in a spatial adjustment of modelled soil moisture. We consider this adjustment to be realistic, but this is hard to validate because of the lack of other, spatially-distributed validation data.

Finally, we studied the feasibility of forecasting regionally distributed soil moisture (up to 9 days ahead) by using ensemble rainfall forecasts from the NWP of the European Centre for Medium-Range Weather Forecasts (ECMWF) as input for our hydrological model. As rainfall is one of the most important input variables, the accuracy of the forecasted soil moisture highly depends on the accuracy of the rainfall forecasts. Comparing the forecasted daily rainfall with measured rainfall (combination of rain gauge and radar data) we found that the accumulated rainfall in our study period (March-Nov 2006) was forecasted very well by all lead times. However, the spatial variation shown by measured rainfall is not taken into account by rainfall forecasts. The forecasted spatially-distributed soil moisture was compared to a "true run", which was the same hydrological model with measured rainfall as input. The temporal mean bias in soil moisture gradually increased with increasing lead time. The spatial distribution of the bias in soil moisture resembled the spatial pattern in total rainfall within the study area. Areas with less rainfall than spatial average show a negative bias and vice versa. Using either the individual ensemble members or the ensemble mean of the rainfall forecast as input made hardly any difference in the spatial pattern of temporal mean bias in soil moisture. However, with the individual ensemble members it is possible to show the reliability of predicted soil moisture.

This study has shown how remotely sensed and forecasted hydrometeorological variables can be integrated into distributed hydrological models. As this study is based on real data, it has shown the potentials and limitations of applying a system like the HNFS in practice. Finally, considerations about future implementation of this system are given.

Samenvatting

Hydrologische actuele en kortetermijn voorspellingen
Integratie van operationeel beschikbare hydrometeorologische variabelen verkregen met remote sensing en voorspellingen in ruimtelijk verdeelde hydrologische modellen

De hydrologische cyclus is de voortdurende beweging van water tussen aarde en atmosfeer en speelt een belangrijke rol in ons klimaatsysteem. Computersimulatiemodellen die (een deel van) de hydrologische cyclus simuleren zijn een belangrijk instrument voor hydrologen. Met dergelijke modellen kunnen zij het hydrologische systeem beter begrijpen en beschrijven, zoals de verdeling van neerslag over de verschillende hydrologische compartimenten (bijvoorbeeld afvoer, bodemvocht en grondwaterstand). Als gevolg van de toename van de rekenkracht van computers en het opkomen van geografische informatie systemen, is de complexiteit van deze hydrologische modellen de laatste 30 jaar enorm toegenomen. Terwijl de ruimtelijke resolutie van deze modellen toeneemt, blijft de hoeveelheid beschikbare data op eenzelfde ruimtelijke schaal om deze modellen van invoer en validatiegegevens te kunnen voorzien achter. Tegelijkertijd is de informatie vanuit 'remote sensing' (van afstand waargenomen) technieken de afgelopen jaren sterk verbeterd en is gemakkelijker beschikbaar geworden. Voorbeelden hiervan zijn de neerslagradar en verdampingsbeelden afkomstig van satellietopnamen. Deze remote sensing data kunnen dienen als een verbeterde invoer en validatie bronnen voor de ruimtelijk gedistribueerde hydrologische modellen. Daarnaast hebben meteorologen numerieke weersvoorspellingmodellen ontwikkeld, waarvan de uitkomsten (bijv. neerslag voorspellingen) door hydrologen gebruikt kunnen worden om voorspellingen te maken van het hydrologisch systeem. Echter, in de praktijk worden deze operationele hydrometeorologische variabelen, verkregen met remote sensing en voorspellingen, nog niet algemeen gebruikt in hydrologische modellen. De reden hiervoor is dat er nog onbeantwoorde onderzoeksvragen liggen over hoe deze hydrometeorologische gegevens te integreren in hydrologische modellen en of deze data de nauwkeurigheid van de hydrologische modellen wel verbetert. Nauwkeurigheid in dit proefschrift is gedefinieerd als "representatie van de werkelijkheid", niet in de mathematische zin als "precisie".

Het doel van dit proefschrift was om te onderzoeken of (i) operationele remote sensing data, die ruimtelijk verdeelde hydrologische modellen van informatie kunnen voorzien, de nauwkeurigheid van deze modellen verbeteren en (ii) of neerslagvoorspellingen nauwkeurige voorspellingen van het hydrologische systeem kunnen opleveren. Binnen het hydrologisch systeem lag de focus op bodemvocht. De opera-

tioneel beschikbare remote sensing data is beperkt tot meteorologische neerslag radar en actuele verdamping (ET_{act}) afkomstig van satellietopnamen.

Om de hydrometeorologische variabelen verkregen met remote sensing en voorspellingen in een hydrologisch model te kunnen integreren hebben we het *Hydrological Now and Forecasting System (HNFS)*, oftewel het Hydrologisch Actueel en Kortetermijn Voorspellingssysteem opgezet. Door gebruik te maken van zowel operationele data en hydrologische modellen alsmede praktijkstudies hopen we de mogelijkheden en beperkingen van een dergelijk systeem in de praktijk inzichtelijk te maken.

Om neerslagvelden met een hoge ruimtelijke resolutie te genereren die vervolgens gebruikt kunnen worden als invoer voor hydrologische modellen hebben we geostatistiek (Kriging varianten) toegepast. Hierbij is gebruik gemaakt van enkel regenmeter data, enkel radar data en een combinatie van regenmeter en radar data. De radar data is afkomstig en geleverd door het Koninklijk Nederlands Meteorologisch Instituut (KNMI). Resultaten lieten de toegevoegde waarde van radar zien bij het genereren van neerslagvelden. Het bleek dat met het huidige nationale netwerk van regenmeters de combinatie van regenmeter data met radar data de meest nauwkeurige neerslagvelden opleverde, gevolgd door enkel radar data en uiteindelijk enkel regenmeter data. Slechts in het geval van een dicht netwerk van regenmeters, zoals ons experimentele netwerk (30 regenmeters in een gebied van 15 km x 15 km), leverde regenmeters beter dan de radar.

De noodzaak om ruimtelijk variabele neerslagvelden te gebruiken in een hydrologisch model is getest door een scenario analyse uit te voeren met verschillende neerslaginvoerscenario's. Resultaten lieten zien dat de noodzaak om ruimtelijk verdeelde neerslag mee te nemen afhangt van de doelstelling van de hydrologische modellering. Indien men is geïnteresseerd in de van dag-tot-dag variabiliteit van ruimtelijk verdeeld bodemvocht of grondwaterstand is het belangrijk om de ruimtelijke verdeling van neerslag mee te nemen. Echter, indien men is geïnteresseerd in het algemene gedrag van een stroomgebied (bijv. grondwater en bodemvocht klimatologie), is het voldoende om het ruimtelijk gemiddelde van de neerslag binnen het stroomgebied mee te nemen. Dit geldt ook voor dagelijkse afvoer. Het is aangetoond in deze studie dat het gebruik van een enkele regenmeter groot risico met zich meebrengt, met name als deze buiten het gebied is gesitueerd.

ET_{act} afgeleid uit satelliet opnamen bleek zeer bruikbaar in het proces van model validatie. Dit is echter beperkt voor perioden waarin er verdampingsreductie optreedt. Ruimtelijk verdeelde ET_{act} data maakte het mogelijk om gebieden met potentiële modelfouten op te sporen. Deze fouten waren zowel flux-, als conceptgerelateerd. Assimilatie (het laten opgaan van twee variabelen in een nieuwe variabele) van ET_{act} afgeleid uit satelliet opnamen in ons hydrologische model, resulteerde in een ruimtelijke aanpassing van gemodelleerd bodemvocht. Deze aanpassing beschouwen wij als realistisch maar is moeilijk te verifiëren als gevolg van het gebrek aan andere, ruimtelijk verdeelde validatiedata.

Ten slotte hebben we de haalbaarheid bestudeerd om het ruimtelijk verdeelde bodemvocht te kunnen voorspellen (tot 9 dagen vooruit). Hierbij is gebruik gemaakt

van het numerieke weersvoorspellingmodel van het Europese Centrum voor Middellangetermijn Weersvoorspellingen (ECMWF) in Reading (Verenigd Koninkrijk). Deze data zijn enigszins bewerkt en geleverd door het KNMI. Omdat neerslag een van de meest belangrijke invoer variabelen is, zal de nauwkeurigheid van het voorspelde bodemvocht sterk afhangen van de nauwkeurigheid van de neerslagvoorspellingen. Uit de vergelijking van voorspelde dagelijkse neerslag met gemeten neerslag (combinatie van regenmeters met radar) bleek dat de totale neerslag tijdens onze studieperioden (maart-november 2006) goed werd voorspeld voor alle voorspeltermijnen (1 tot 9 dagen vooruit). Echter, de ruimtelijke variatie van gemeten neerslag wordt niet meegenomen in de neerslagvoorspellingen. De voorspelde ruimtelijke verdeling van bodemvocht is vergeleken met een "werkelijke situatie". Deze werkelijke situatie is hetzelfde hydrologische model waarbij de gemeten neerslag als invoer is gebruikt. De tijdgemiddelde afwijking tussen voorspeld en werkelijk bodemvocht nam geleidelijk toe met toenemende voorspeltermijn. De ruimtelijke verdeling van deze afwijking liet een patroon zien dat overeenkomt met het ruimtelijk patroon van de totale neerslag in het gebied. Gebieden waar minder neerslag viel dan ruimtelijk gemiddeld lieten in de voorspelling een onderschatting zien van het bodemvocht en vice versa. Het gebruik van hetzij de individuele neerslagvoorspellingen (50 per dag), hetzij het gemiddelde van deze 50 neerslagvoorspellingen vertoonde weinig verschil in het ruimtelijk patroon van de bodemvocht afwijking. Echter, door gebruik te maken van de individuele neerslagvoorspellingen is het mogelijk om de betrouwbaarheid (oftewel de consistentie) van het voorspelde bodemvocht te laten zien.

Deze studie heeft laten zien hoe hydrometeorologische variabelen verkregen met remote sensing en voorspellingen gebruikt kunnen worden in ruimtelijk verdeelde hydrologische modellen. Omdat deze studie is gebaseerd op werkelijke data en modellen heeft het de mogelijkheden en beperkingen van het toepassen van een systeem zoals het HNFS in de praktijk aangetoond. Tot slot zijn aandachtspunten aangegeven voor de toepassing van een dergelijk systeem in de praktijk.

Bibliography

Allen, R.G. (2006), The Need to Continue High Resolution Thermal Imagery (i.e., Land Surface Temperature) on the next Landsat Satellite System for Water Resources Management. University of Idaho.

Allen, R. G., L.S. Pereira, D. Raes & M. Smith (1998), Crop evapotranspiration: Guidelines for computing crop water requirements. FAO Irrigation and drainage paper 56. FAO-Food and Agriculture Organization of the United Nations Rome.

Arnaud, P., C. Bouvier, L. Cisner & R. Dominguez (2002), Influence of rainfall spatial variability on flood prediction. J. Hydrol. 260, pp. 216–230.

Bastiaanssen, W. G. M. (1995), Regionalization of surface flux densities and moisture indicators in composite terrain. A remote sensing approach under clear skies in Mediterranean climates. Ph.D. thesis, Landbouwuniversiteit Wageningen, Wageningen.

Bastiaanssen, W. G. M., E. J. M. Noordman, H. Pelgrum, G. Davids, B. P. Thoreson & R. G. Allen (2005), SEBAL model with remotely sensed data to improve water-resources management under actual field conditions. J. Irrig. Drain. E-ASCE. 131: 85–93.

Battan, L. J. (1973), Radar Observations of the Atmosphere. University of Chicago Press.

Bell, V. A. & R. J. Moore (2000), The sensitivity of catchment runoff models to rainfall data at different spatial scales. Hydrol. Earth Syst. Sci., 4 (4), pp. 653–667.

Berendsen, H. J. A. & E. Stouthamer (2000), Late Weichselian and Holocene palaeogeography of the Rhine-Meuse delta, The Netherlands. Palaeogeogr. Palaeocl., 161 (3-4), pp. 311-335.

Bergström, S & L. P. Graham (1998), On the scale problem in hydrological modelling. J. Hydrol. 211, pp. 253–265.

Beven, K. (2006), On undermining the science? Hydrol. Processes 20, pp. 3141–3146.

Beven, K. (1989), Changing ideas in hydrology-The case of physically-based models. J. Hydrol. 105, pp. 157–172.

Bierkens, M., P. Finke & P. de Willigen (2000), Upscaling and Downscaling Methods for Environmental Research. Kluwer Academic Publishers.

Bink, N. J. (1996), The structure of the atmospheric surface layer subject to local advection. PhD. thesis, Landbouwuniversiteit Wageningen, Wageningen.

Blöschl, G. & M. Sivapalan (1995), Scale issues in hydrological modelling - a review. Hydr. Proc. 9 (3-4), pp. 251–290

Bogena, H. R., J. A. Huisman, C. Oberdörster & H. Vereecken (2007), Evaluation of a low-cost soil water content sensor for wireless network applications. J. Hydrol. 344, pp. 32-42.

Busschers, F. S., C. Kasse, R. T. van Balen, J. Vandenberghe, K. M. Cohen, H. J. T. Weerts, J. Wallinga, C. Johns, P. Cleveringa, F. P. M. Bunnik (2007), Late Pleistocene evolution of the Rhine-Meuse system in the Southern North Sea basin: imprints of climate change,

sea-level oscillation and glacio-isostacy. Quaternary Sci. Rev. 26, pp. 3216-3248.
Caldwell, M. M., T. E. Dawson & J. H. Richards (1998), Hydraulic lift: consequences of water efflux from the roots of plants. Oecologia, 113, 151–161.
Carpenter, T. M., K. P. Georgakakos & J. A. Sperfslagea (2001), On the parametric and NEXRAD-radar sensitivities of a distributed hydrological model suitable for operational use. J. Hydrol. 253, pp. 169–193.
Cressie, N. A. C. (1993), Statistics for spatial data, Revised Edition. John Wiley & Sons, Inc.
Creutin, J. D., G. Delrieu & T. Lebel (1988), Rain measurements by rain gauge-radar combination: a geostatistical approach. J. Atmos. Oceanic Technol., 5, pp. 102–115.
Czarnomski, N. M., G. W. Moore, T. G. Pypker, J. Licata & B. J. Bond, B.J. (2005), Precision and accuracy of three alternative instruments for measuring soil water content in two forest soils of the Pacific Northwest. Can. J. For. Res. 35, pp. 18671876.
Dawson, T. E. (1996), Determining water use by trees and forests from isotopic, energy balance, and transpiration analyses: The role of tree size and hydraulic lift. Tree Physiol., 16, 263–272.
De Bruin, H. A. R. (1987), From Penman to Makkink. In: Proc. and Inf. Vol. 39. TNO Committee on Hydrological Research, pp. 5–31.
De Bruin, H. A. R., & J. N. M. Stricker (2000), Evaporation of grass under non-restricted soil moisture conditions, Hydrol. Sci. J., 45(3), 391–406.
De Jeu, R. A. M., & M. Owe (2003), Further validation of a new methodology for surface moisture and vegetation optical depth retrieval, Int. J. Remote Sensing, 24, 4559-4578.
Delsman, J., A. Veldhuizen & J. Snepvangers (2008), Netherlands Hydrological Modeling Instrument, Proc. Modflow and more 2008: Ground water and public policy, May 18-21, 2008, Colorado.
De Roo, A., B. Gouweleeuw, J. Thielen, J. Bartholmes, P. Bongioannini-Cerlini, E. Todini, P. Bates, M. Horritt, N. Hunter, K. Beven, F. Pappenberger, E. Heise, G. Rivin, M. Hils, A. Hollingworth, B. Holst, J. Kwadijk, P. Reggiani, M. van Dijk, K. Sattler & E. Sprokkereef (2003), Development of a European flood forecasting system. Int. J. River Basin Manag., 1, pp. 49–59.
Deutsch, C. & A. Journel (1998), GSLIB. Geostatistical software library and user's guide. Oxford University Press.
De Wit, A. J. W. & J. G. P. W. Clevers (2004), Efficiency and accuracy of per-field classifcation for operational crop mapping. Int. J. Remote Sens., 25(20), pp. 4091-4112.
Diggle, P. J., J. A. Tawn & R. A. Moyeed (1998), Model-based geostatistics. J. R. Stat. Soc. Ser. C-Appl. Stat., 47, pp. 299–326.
Feddes, R. A., H. Hoff, M. Bruen, T. Dawson, P. de Rosnay, P. Dirmeyer, R. B. Jackson, P. Kabat, A. Kleidon, A. Lilly & A. J. Pitman (2001), Modeling root water uptake in hydrological and climate models. B. Am. Meteorol. Soc. 82(12), 2797–2810.
Feddes, R. A., P. J. Kowalik & H. Zaradny (1978), Simulation of field water use and crop yields. Simulation monographs. University of Wageningen, Pudoc.
Feddes, R. A. (1987), Crop factors in relation to Makkink reference- crop evapotranspiration. Comm. Hydrol. Res. TNO, The Hague. Proc. and Inf. 39, pp. 33-44.
Fiorucci, P., P. La Barbera, L. G. Lanza & R. Minciardi (2001), A geostatistical approach to multisensor rain field reconstruction and downscaling. Hydrol. Earth Syst. Sci., 5 (2), pp. 201–213.
Franks, S. W. & K. J. Beven (1997), Estimation of evapotranspiration at the landscape scale: A fuzzy disaggregation approach. Water Resour. Res. 33(12), pp. 2929–2938.
Gekat, F., P. Meischner, K. Friedrich, M. Hagen, J. Koistinen, D. B. Michelson & A. Hu-

uskonen (2004), Weather Radar, Principles and Advanced Applications. Springer, Berlin, Germany, Ch. The State of Weather Radar Operations, Networks and Products.
Golding, B. W. (1998), Nimrod: A system for generating automated very short range forecasts, Meteorol. Appl., 5, pp. 1–16.
Goodrich, D. C., J. M. Faures, D. A. Woolhiser, L. J. Lane & S. Sorooshian (1995), Measurements and analysis of small-scale convective storm rainfall variability. J. Hydrol. 173, pp. 283–308.
Goovaerts, P. (1997), Geostatistics for Natural Resources Evaluation. Oxford University Press.
Goovaerts, P. (2000), Geostatistical approaches for incorporating elevation into the spatial interpolation of rainfall. J. Hydrol., 228, pp. 113–129.
Gouweleeuw, B. T., J. Thielen, G. Franchello, A. P.J. De Roo & R. Buizza (2005), Flood forecasting using medium-range probabilistic weather prediction, Hydrol. Earth Syst. Sci., 9, pp. 365–380.
Grayson, R. B. & G. Blöschl (2000), Spatial patterns in catchment hydrology: observations and modelling. Cambridge University Press, Cambridge.
Habib, E., W. F. Krajewski, & G. J. Ciach (2001), Estimation of rainfall interstation correlation. J. Hydrometeor., 2(6), pp. 621–629.
Hermans, A. G. M., P. E. V. Van Walsum, J. Runhaar & P. J. T. Van Bakel (2004), Model construction, calibration and determination of actual ground- and surface water regime (In Dutch). Alterra report 914. Alterra, Wageningen.
Hoeben, R. & P.A. Troch (2000), Assimilation of active microwave observation data for soil moisture profile estimation. Water Resour. Res., 36(10), pp. 2805-2819.
Holleman, I. (2003), Rainfall analysis from radar and groundstation measurements. In Dutch. Royal Netherlands Meteorological Institute (KNMI), Tech. Rep. Technical report TR-272.
Holleman, I. (2004), VPR adjustment using a dual CAPPI technique. Proc. of ERAD, vol. 2, Copernicus GmbH, pp. 25–30.
Holleman, E. T., W. J. Zaadnoordijk, N. H. Meuter, A. S. Roelandse & A. Veldhuizen (2005), Wateropgave HDSR-West. In Dutch. Tech. Rep. Reference: 9M8931/R00002/HTD/Rott1, Royal Haskoning.
Holtslag, A. A. M. (1987), Surface fluxes and boundary layer scaling. Scientific report WR 87-2, Royal Netherlands Meteorological Inst. (KNMI). De Bilt.
Huffman, G. J., R. F. Adler, D. T. Bolvin, G. Gu, E. J. Nelkin, K. P. Bowman, Y. Hong, E. F. Stocker & D. B. Wolff (2007), The TRMM Multisatellite Precipitation Analysis (TMPA): Quasi-Global, Multiyear, Combined-Sensor Precipitation Estimates at Fine Scales. J. Hydrometeor. 8(1), pp. 38–55.
Hutjes, R. W. A. (1996), Transformation of near-surface meteorology in a small-scale landscape with forest and arable land. Ph.D. thesis, Rijksuniversiteit Groningen, Groningen.
Isaaks, E. H. & R. M. Srivastava (1989), Applied Geostatistics. Oxford University Press.
Immerzeel, W. W. & P. Droogers (2008), Calibration of a distributed hydrological model based on satellite evapotranspiration. J. Hydr. 349, pp. 411–424.
Jarvis, P.G. (1976), The Interpretation of the Variations in Leaf Water Potential and Stomatal Conductance Found in Canopies in the Field. Philosophical Transactions of the Royal Society of London. Series B, Biological Sciences, Vol.273, No. 927, pp. 593-610.
Johnson, L. E. & B. G. Olson (1998), Assessment of Quantitative Precipitation Forecasts, Weather. Forecast., 13, pp. 75–83.
Journel, A. & C. Huijbregts (1978), Mining geostatistics. Academic Press.
Krajewski, W. F. (1987), Cokriging radar-rainfall and rain gage data. J. Geophys. Res.-

Atmos., 29, pp. 9571–9580.
Krajewski, W. F., V. Lakshmi, K. Georgakakos & S. Jain (1991), A monte carlo study of rainfall sampling effect on a distributed catchment model. Water Resour. Res. 27 (1), pp. 119–128.
Krajewski, W. F., A. Kruger & V. Nespor (1998), Experimental and numerical studies of small-scale rainfall measurements and variability. Water Sci. Technol., 37 (11), pp. 131–138.
Krajewski, W. F. & J. A. Smith (2002), Radar hydrology: rainfall estimation. Adv. Water Resour. 25 (8-12), pp. 1387–1394.
Krajewski, W. F., G. J. Ciach & E. Habib (2003), An analysis of small-scale rainfall variability in different climatic regimes. Hydrological Sciences Journal-Journal Des Sciences Hydrologiques, 48 (2), pp. 151–162.
Lee, J. E., R. S. Oliveiria, T. E. Dawson & I. Fung (2005), Root functioning modifies seasonal climate. P. Natl. Acad. Sci. USA 102, pp. 17576–17581.
Leijnse, H., R. Uijlenhoet & J.N.M. Stricker (2007), Rainfall measurement using radio links from cellular communication networks. Water Resour. Res. 43, W03201, doi:10.1029/2006WR005631.
Lin, C., S. Vasic, A. Kilambi, B. Turner, & I. Zawadzki (2005), Precipitation forecast skill of numerical weather prediction models and radar nowcasts, Geophys. Res. Lett., Vol. 32, L14801, doi:10.1029/2005GL023451.
Loew, A., R. Ludwig & W. Mauser (2006), Derivation of surface soil moisture from ENVISAT ASAR wide swath and image mode data in agricultural areas. IEEE T Geosci. Remote Vol. 44, Issue 4, pp. 889-899.
Makkink, G. F. (1957), Testing the Penman formula by means of lysimeters. J. Int. Water England, 11, pp. 277–288.
McDonald, M. G. & A. W. Harbaugh (1983), A modular three-dimensional finite-difference ground-water flow model, Open-File Report 83-875. U.S. Geological Survey, 528 pp.
Messer, H., A. Zinevich, & P. Alpert (2006), Environmental monitoring by wireless communication networks, Science 312, 713.
Molini, A., L. Lanza, & P. La Barbera (2005), The impact of tipping-bucket rain gauge measurement errors on design rainfall for urban-scale applications. Hydrol. Processes, 19, pp. 1073–1088.
Miralles, D.G. (2008), Surface Soil Moisture Mapping over Utrecht (NL) with an Aircraft-Based Passive Microwave Instrument. MSc. Thematic Research Thesis, Internal Report, VU University Amsterdam, 18 pp.
Monin, A. S. & A. M. Obukhov (1954), Basic laws of turbulent mixing in the ground layer of the atmosphere. T. Geophys. Inst. of the Soviet Acad. Scie., S.S.S.R., 24, pp. 163–187.
Moore, R. J., D. A. Jones, D. R. Cox & V. S. Iham (2000), Design of the HYREX rain gauge network. Hydrol. Earth Syst. Sci., 4 (4), pp. 523–530.
Mualem, Y. (1976), A new model predicting the hydraulic conductivity of unsaturated porous media. Water Resour. Res. 12, 513-522.
Obled, C., J. Wending & K. Beven (1994), The sensitivity of hydrological models to spatial rainfall patterns: an evaluation using observed data. J. Hydrol. 159, pp. 305–333.
O'Connell, P. E. & E. Todini (1996), Modelling of rainfall, flow and mass transport in hydrological systems: an overview. J. Hydrol. 175, pp. 3–16.
Olsson, J. & G. Lindström (2008), Evaluation and calibration of operational hydrological ensemble forecasts in Sweden, J. Hydrol., 350, pp. 14–24.
Oort, P .A. J. van, Bregt, A. K., Bruin, S. de & A. J. W. de Wit (2004), Spatial variability in classification accuracy of agricultural crops in the Dutch national land-cover database.

Int. J. Geogr. Inf. Sci. vol. 18, no. 6, september 2004, pp. 611-626.
Orlanski, I. (1975), A rational subdivision of scales for atmospheric process. Bull. Amer. Met. Soc., 56 (5), pp. 527–530.
Owe M., R. de Jeu, & T. Holmes (2008), Multisensor historical climatology of satellite-derived global land surface moisture, J. Geophys. Res., 113, F01002, doi:10.1029/2007JF000769.
Pappenberger, F., K. J. Beven, N. M. Hunter, P. D.Bates, B. T. Gouweleeuw, J. Thielen & A. P. J. de Roo (2005), Cascading model uncertainty from medium range weather forecasts (10 days) through a rainfall-runoff model to flood inundation predictions with the European Flood Forecasting System (EFFS), Hydrol. Earth Syst. Sci., 9, pp. 381–393.
Pauwels, V. R. N., N. E. C. Verhoest, G. J. M. De Lannoy, V. Guissard, C. Lucau, and P. Defourny (2007), Optimization of a coupled hydrology-crop growth model through the assimilation of observed soil moisture and leaf area index values using an ensemble Kalman filter. Water Resour. Res., 43, W04421, doi:10.1029/2006WR004942.
Pebesma, E. J. (2004), Multivariable geostatistics in S: the gstat package. Comput. Geosci., 30, pp. 683–691.
Persson, A. (2001), User guide to ECMWF forecast products, Meteor. Bulletin M3.2, ECMWF.
Pipunic, R. C., J. P. Walker, & A. Western (2008), Assimilation of remotely sensed data for improved latent and sensible heat flux prediction: A comparative synthetic study. Remote Sens. Environ. 112, pp. 1295–1305.
Querner, E. P. (1997), Description and application of the combined surface and groundwater flow model MOGROW. J. Hydrol. 192, pp. 158–188.
R Development Core Team (2004), R: A language and environment for statistical computing, R Foundation for Statistical Computing, Vienna, Austria, ISBN 3-900051-07-0.
Reed, S. M., V. I. Koren, M. B. Smith, Z. Zhang, F. Moreda, D.-J. Seo & DMIP Participants (2004), Overall Distributed Model Intercomparison Project results. J. Hydrol. 298, pp 27–60.
Refsgaard, J.C. & H. J. Henriksen (2004), Modeling guidelines-terminology and guiding principles. Adv. Water Resour. 27, pp. 71–82
Refsgaard, J.C. (1997), Parameterisation, calibration and validation of distributed hydrological models. J. Hydrol.198, pp. 69–97.
Refsgaard, J. C. (1996), Terminology, modelling protocol and classification of hydrological models codes. In: Abbott, M.B., Refsgaard, J.C. (Eds.), Distributed Hydrological Modelling. Kluwer Academic Publishers, Dordrecht, pp. 17-39.
Roebeling R. A., H. M. Deneke & A. J. Feijt (2008), Validation of cloud liquid water path retrievals from SEVIRI using one year of CloudNET observations, J. of Appl. Met. and Clim., 47, pp. 206-222.
Roulin, E. (2007), Skill and relative economic value of medium-range hydrological ensemble predictions, Hydrol. Earth Syst. Sci., 11, pp. 725–737.
Roulin, E. & S. Vannitsem (2005), Skill of medium-range hydrological ensemble predictions, J. Hydrometeor., 6, pp. 729–744.
Schuurmans, J. M, M. F. P. Bierkens, E. J. Pebesma & R. Uijlenhoet (2007), Automatic prediction of high-resolution daily rainfall fields for multiple extents: the potential of operational radar. J. Hydrometeor. 8, pp. 1204–1224.
Schuurmans, J. M., Bierkens, M. F. P. (2007), Effect of spatial distribution of daily rainfall on interior catchment response of a distributed hydrological model. Hydrol. Earth Syst. Sci., 11, pp. 677-693.
Schuurmans, J. M., P. A. Troch, A. A. Veldhuizen, W. G. M. Bastiaanssen & M. F. P.

Bierkens (2003), Assimilation of remotely sensed latent heat flux in a distributed hydrological model. Adv. Water Res., 26, pp. 151-159.

Sivakumar, B. (2008), Undermining the science or undermining Nature?. Hydrol. Process. 22, pp. 893–897.

Seo, D. J., W. F. Krajewski, A. Azimizonooz & D. S. Bowles (1990b), Stochastic Interpolation of Rainfall Data from Rain Gauges and Radar Using Cokriging. 2. Results. Water Resour. Res., 26 (5), pp. 915–924.

Seo, D. J., W. F. Krajewski & D. S. Bowles (1990a), Stochastic Interpolation of Rainfall Data from Rain Gauges and Radar Using Cokriging. 1. Design of Experiments. Water Resour. Res., 26 (3), pp. 469–477.

Shah, S. M. S., P. E. O'Connel & J. R. M. Hosking (1991), Modelling the effects of spatial variability in rainfall on catchment response. 2. Experiments with distributed and lumped models. J. Hydrol. 175, pp. 89–111.

Steiner, M., R. A. Houze & S. E. Yuter (1995), Climatological characterization of three-dimensional storm structure from operational radar and rain gauge data. J. Appl. Meteor., 34, pp. 1978–2007.

Steiner, M., J. Smith, S. Burges, C. Alonso & R. Darden (1999), Effect of bias adjustment and rain gauge data quality control on radar rainfall estimation. Water Resour. Res., 35 (8), pp. 2487–2503.

Su, Z. (2002), The Surface Energy Balance System (SEBS) for estimation of turbulent heat fluxes. Hydrol. Earth Syst. Sci., 6, pp. 85-100.

Taylor, S. A. & G. L. Ashcroft (1972), Physical edaphology. T218p W. H. Freeman & Co., San Francisco. 533 p.

5Biological and Irrigation Engineering, Utah State Univ.

Uijlenhoet, R. (2008), Precipitation physics and rainfall observation. In (M.F.P. Bierkens. A.H. Dolman and P.A. Troch editors) Climate and the Hydrology Cycle. IAHS Special Publications 8, IAHS Press, Wallingord, UK.

Van Dam, J. C. (2000), Field-scale water flow and solute transport. SWAP model concepts, parameter estimation, and case studies. PhD-thesis, Wageningen University, Wageningen, The Netherlands, 167 p., English and Dutch summaries.

Van den Assem, S. (1988), Calibration of tipping bucket rain- gauges (in Dutch). Landbouwuniversiteit Wageningen, Research report nr. 85, The Netherlands.

Van de Kassteele, J. & A. Stein (2006), A model for external drift kriging with uncertain covariates applied to air quality measurements and dispersion model output. Environmetrics, 17, pp. 309–322.

van Genuchten, M. Th. (1980), A closed-form equation for predicting the hydraulic conductivity of unsaturated soils. Soil Sci. Soc. Am. J. 44, 892-898.

Van Walsum, P. E. V. & P. Groenendijk (2008), Quasi steady-state simulation of the unsaturated zone in groundwater modeling of lowland regions, Vadose Zone J. 7, 769–781.

Vermeulen, J. P. L. (2001), The atmospheric boundary layer over a heterogeneous vegetated landscape. Ph.D. thesis, Vrije Universiteit te Amsterdam, Amsterdam.

Voogt, M. P. (2007), Meteolook: a physically based regional distribution model for measured meteorological variables. M.Sc. thesis, Delft University of Technology.

Wang, J., Y. Ma, M. Menenti ,W. G. M. Bastiaanssen & Y. Mitsuta (1995), The scaling up of land surface processes over a heterogeneous landscape with satellite observations. J. Meteorol. Soc. Jpn. 73(6), pp. 1235–1244.

Warren, J. M. , F. C. Meinzer, J. R. Brooks, J. C. Domec & R. Coulombe (2007), Hydraulic redistribution of soil water in two old-growth coniferous forests: quantifying patterns and controls, New Phytologist, 173, pp. 753–765.

Wessels, H. R. A. & J. H. Beekhuis (1997), Stepwise procedure for suppression of anomalous ground clutter. COST-75 Seminar on Advanced Radar Systems, EUR 16013 EN, pp. 270–277.

Wieringa, J. (1986), Roughness-dependent geographical interpolation of surface wind speed averages. Q. J. Roy. Meteor. Soc. 112, pp. 867–889.

Winter, T. C., D. O. Rosenberry & A. M. Sturrock (1995), Evaluation of 11 equations for determining evaporation for a small lake in the North Central United States. Water Resour. Res. 31 (4), pp. 983–993.

Wolters, E.L.A., R.A. Roebeling & A.J. Feijt (2008), Evaluation of cloud phase retrieval methods for SEVIRI onboard METEOSAT-8 using ground-based lidar and cloud radar data J. Appl. Meteor., (accepted).

Wösten, J. H. M., F. De Vries, J. Denneboom & A. F. Van Holst (1988), Generalization and soil physical translation of the Dutch soil map, 1:250.000, on behalf of the PAWN-study (In Dutch). Report nr. 2055, Stichting voor Bodemkartering, Wageningen.

Zaadnoordijk, W. J. (2003), Analytic expression for output reliability: Verifying automated calibration and confidence calculations of a groundwater flow simulator. Water Resour. Res. 39 (12), pp. 1351.

Dankwoord

Dan is het nu tijd om het dankwoord te schrijven. In de laatste fase van mijn aioschap liet ik mijn gedachten wel eens afdwalen naar dit moment. Het zou betekenen dat alles echt af was. Nu is het dan echt zover om het, waarschijnlijk meest gelezen stuk van dit proefschrift, te schrijven!

Hoe het begon: 5 maart 2003, mijn verjaardag, maar ook de dag dat Marc Bierkens zijn inaugurele rede als professor bij de Universiteit Utrecht hield. Het was Peter Troch, professor bij Universiteit Wageningen en mijn toenmalige afstudeerbegeleider, die tijdens de receptie de legendarische woorden uitsprak (ik sta niet in voor het letterlijke citaat): 'Als je nog overweegt aio te worden, Marc zoekt nog mensen'. Hoewel ik op dat moment een vaste betrekking had bij ingenieursbureau Grontmij en het daar goed naar mijn zin had, liet deze opmerking me niet los en ik besloot te solliciteren. En zo begon het aio-avontuur dat 'aiomon' heette!

Marc, als eerste wil ik jou heel erg bedanken. Uiteraard voor het mogelijk maken van dit onderzoek maar ook voor je enthousiasme en vertrouwen gedurende de afgelopen jaren. Toen ik begon waren Reinder en ik je enige promovendi en had je nog veel tijd om ons op weg te helpen en ook je stempel op het onderzoek te drukken. Ondertussen heb je talloze aio's onder je hoede en hebben we mijns inziens onderling een werkrelatie opgebouwd die hoort bij een aio in de laatste fase. Je betrokkenheid bij mijn onderzoek is altijd gebleven en je commentaar was altijd scherp en bovendien snel. Frans van Geer, mijn copromotor, wil ik als tweede hartelijk danken. Vooral in de tweede fase hebben we regelmatig goed contact gehad, wat samenhing met mijn meer frequentere aanwezigheid bij TNO (ondertussen Deltares). Bedankt voor je waardevolle commentaar en hulp. Peter Troch heb ik al eerder genoemd. Zonder genoemde opmerking destijds was ik misschien nooit aio geworden en was dit proefschrift er niet geweest. Grote dank ben ik jou verschuldigd aan de tijd dat je mijn afstudeerbegeleider bent geweest in Wageningen. Mijn enthousiasme voor dit onderwerp heb jij aangewakkerd en onder jouw hoede heb ik mijn eerste wetenschappelijke artikel geschreven. Helaas is je verhuizing naar de Universiteit van Arizona een te grote stap gebleken om uiteindelijk voor mij als copromotor op te treden, wat in eerste instantie de bedoeling was.

Naast mijn promotoren wil ik als eerste EdzeR Pebesma heel erg bedanken. Toen ik als aio begon was 'R' voor mij gewoon een letter uit het alfabet. Nu ben ik ook een volgeling (citaat Edzer: 'R kan alles, behalve een lekker menu voor je koken') en zelfs uitdrager. Je enthousiaste begeleiding bij (geo-) statistiek en R-programmeren

waren zeer waardevol. Ik hoop dat het je nu goed bevalt als professor in Münster en dat je met je band 'de nieuwe Galukken' nog vaak mag optreden in Amersfoort tijdens de jazz-dagen! Een andere persoon aan wie ik veel dank ben verschuldigd is Remko Uijlenhoet. Regenmeters bestellen, een keer mee het veld in, de nodige tijd besteed om me de 'ins en outs' van de regenradar te leren: mijn dank daarvoor. Je enthousiasme werkt aanstekelijk en je bent voor mij het voorbeeld hoe je 'lusten en lasten' in de wetenschap met elkaar kunt verenigen. Het radar congres in Gotland staat met stip op nummer 1!

Voor dit onderzoek waren veel meteorologische data nodig. Het KNMI heeft hier een geweldige bijdrage aan geleverd en ik ben dit instituut dan ook enorm dankbaar. Allereerst wil ik Ton Donker en Iwan Holleman hartelijk danken. Ton, de data werden dankzij jou altijd uitstekend geleverd en gestroomlijnd. Ik hoop dat je nu geniet van je pensioen! Iwan, heel erg bedankt voor je hulp en uitleg over de regenradar en je interesse in mijn onderzoek. Het radaroverleg wat je samen met Remko Uijlenhoet bent gestart heb ik altijd zeer inspirerend en leerzaam gevonden. Hartelijk dank voor de leerzame presentaties en discussies aan de volgende personen in willekeurige volgorde: Hidde Leijnse, Adri Buishand, Hans Beekhuis, Han Stricker, Paul Torfs, Aart Overeem, Remco van de Beek (jij ook bedankt voor samenwerking in het veld!) en Pieter Hazenberg. Kees Kok, Robert Mureau en Daan Vogelezang van het KNMI: jullie wil ik enorm bedanken voor de data (en bijbehorende uitleg) die ik in de laatste fase van mijn proefschrift heb gebruikt: neerslagvoorspellingen. Kees, ook hartelijk dank voor het doorlezen en van commentaar voorzien van mijn conceptartikel!

Het Hoogheemraadschap De Stichtse Rijnlanden (HDSR), met name Joost Heijkers, dank ik voor de logistieke en financiële hulp bij diverse data en hydrologische modellen. Wouter Meijninger en Wim Bastiaanssen van WaterWatch wil ik hartelijk danken voor het leveren en bewerken van de satellietbeelden.

Alle collega's van het departement Fysische Geografie: super bedankt voor de unieke werksfeer de afgelopen jaren! De meest uiteenlopende zaken zijn besproken in de koffiehoek: van wetenschappelijke discussies tot persoonlijke gesprekken met daartussen heel veel grappen. Als je even in een dip zat was er altijd wel iemand te vinden om dit gevoel mee te delen. Geweldig, hou het zo en ik zal jullie absoluut missen! Persoonlijk wil ik mijn ex-kamergenoten Marc Vissers en Daniel Mourad bedanken. In onze mediterrane (vanwege de werktijden) kamer vond regelmatig uitwisseling plaats van muziek (Marc, dankzij jou heb ik nu een verantwoorde muziekcollectie), politieke meningen (Daniel, heb ik van jou de tik soms iets te vaak op nu.nl te kijken?) en aio-perikelen. Uiteraard wil ook mijn latere en 'huidige' kamergenoot Arien Lam heel erg bedanken. Onze muzieksmaak kwam niet overeen (op Ella Fitzgerald na: bij jou het meest moderne, bij mij ongeveer het oudste) maar dat werd ruimschoots gecompenseerd door andere overeenkomsten zoals ouderschap. Ik wens jou nog heel veel succes toe met het afronden van je promotieonderzoek en sorry dat ik de laatste tijd een minder trouwe kamergenoot was omdat ik veel tijd bij TNO/Deltares doorbracht. Alle (ex-) medewerkers van het technisch lab van fysische wil ik ook hartelijk danken. Theo, bedankt voor het meedenken; Hassan, bedankt voor het uitlenen van divers veldwerk materiaal; Marcel, altijd weer bereid de zoveelste kapotte regenmeter

te repareren; Chris, je hulp in het veld was geweldig en zelfs kolfapparaten zijn jou toevertrouwd; Bas, dankzij jou kwamen de KNMI data ook echt tot mijn beschikking en ging het niet verloren. Verder dank ik 'mijn' afstudeerstudente Inger de Groot voor haar hulp tijdens het verzamelen van veldwerkgegevens en het vergroten van mijn didactische vaardigheden. Geomedia wil ik hartelijk danken voor het ontwerpen van de kaft en uitnodiging.

Alle collega's van TNO/Deltares, jullie ook bedankt! Het combineren van twee werkplekken vond ik in het begin erg lastig maar aan het eind heb ik me goed thuis gevoeld. Ate en Esther, jullie waren fijne kamergenoten! Judith Snepvangers wil ik danken voor de hulp bij het MODFLOW modelleren. Ab Veldhuizen en Paul van Walsum van Alterra dank ik hartelijk voor alle hulp bij MetaSwap!

I am grateful to the members of the examination committee. Thank you very much for taking the effort to read this thesis. Susanne (mijn kolfmaatje) en broer Wytze: bedankt voor al jullie tips, hulp en opmerkingen. Ik ben blij dat jullie mijn paranimfen willen zijn!

Gelukkig was er de afgelopen jaren meer dan alleen werk. Francis, Fred, Joost, Karen, Koen, Linda, Roos, Stef, oftewel 'De Hoeksteen' dank jullie wel voor de nodige afleiding! Primaire vriendinnetjes Bregje, Brigit, Karen, Mariska, Marieke en Nicole bedankt voor de weekendjes weg, etentjes, boottochtjes en eindeloze mail conversaties. Floor, dank je wel voor je geweldige vriendschap! Iedereen ook dank voor het begrip dat ik de laatste tijd niet overal meer aan meedeed.

Lieve pa en ma, ik wil jullie enorm bedanken voor jullie steun, interesse en stimulans tijdens deze afgelopen jaren! Bij jullie vond ik altijd een luisterend oor en geruststellende woorden (ma, je woorden 'als je maar rustig blijft' zijn altijd blijven hangen). Pa ook bedankt voor het meehelpen bij het plaatsen van de eerste regenmeters en het aanschaffen van de beschermende omheiningen. Bedankt ook, zeker ook mijn schoonouders, voor het feit dat Akke altijd bij jullie terecht kon als we met werk in de knoop kwamen. En verder al mijn broers, zussen, zwagers en schoonzussen, neven en nichten: Jaap, Saskia, Eva, Jan-Brecht, Margreet, Paul, Mees, Zeger, Wytze, Joke, Jaap, Manuel, Akke, Matthijs, Dirk-Jan, Elske, Johannes, Jan, Debby, Alfred, Ingrid, Arien, Karin, Nico, Lieke en Jochem. Leuk dat jullie meegeleefd hebben en ja, ik ben nu echt afgestudeerd!

En *last but certainly not least*: Koen, Akke en Per. Het was (en is) altijd zo fijn thuiskomen bij jullie! Koen, dank je wel voor al je liefde, geduld, interesse, steun en relativerende woorden. En uiteraard ook dank voor je hulp bij het graven van de kuilen voor de bodemvochtmeters. Akke, dankzij jou werden mijn werkdagen efficiënter en bovendien bracht je geweldige afleiding en vreugde. Elke morgen heb jij weer zo'n zin in de dag en dat werkt aanstekelijk! En kleine Per, je hebt de laatste fase van dit promotieonderzoek in de buik meegemaakt (hopelijk zonder al teveel stress) maar nu ben je er gelukkig gezond en wel. Je komst was een goede stok achter de deur om alles op tijd af te ronden. Ik kijk ernaar uit nog heel lang van elkaar te mogen genieten!

Amersfoort, oktober 2008.

Publications

Peer reviewed papers - published

Schuurmans, J.M, M.F.P. Bierkens, E.J. Pebesma & R. Uijlenhoet (2007), Automatic prediction of high-resolution daily rainfall fields for multiple extents: the potential of operational radar. J. Hydrometeor. 8, pp. 1204–1224.

Schuurmans, J.M & M.F.P. Bierkens (2007), Effect of spatial distribution of daily rainfall on interior catchment response of a distributed hydrological model. Hydrol. Earth Syst. Sci., 11, pp. 677–693.

Schuurmans, J.M., P.A. Troch, A.A. Veldhuizen, W.G.M. Bastiaanssen & M.F.P. Bierkens (2003), Assimilation of remotely sensed latent heat flux in a distributed hydrological model. Adv. Water Resour., 26, pp. 151–159.

Peer reviewed papers - accepted

Schuurmans, J.M & M.F.P. Bierkens (2008), Ability to forecast regional soil moisture with a distributed hydrological model using ECMWF rainfall forecasts. accepted for publication in J. Hydrometeor.

Peer reviewed papers - submitted

Schuurmans, J.M, F.C. van Geer & M.F.P. Bierkens (2008), Remotely sensed latent heat fluxes for improving modelled soil moisture predictions: a case study. submitted to Remote Sens. Environ.

Other papers

Schuurmans, J.M, F.C. van Geer & M.F.P. Bierkens (2008), Actuele en korte termijn voorspellingen voor operationeel waterbeheer (in Dutch). Stromingen.

Schuurmans, J.M. & M.F.P. Bierkens (2007), Belang van betere neerslaginformatie voor hydrologen (in Dutch). H2O, 40(12), pp. 27–29.

Conference abstracts

Schuurmans, J.M. & M.F.P. Bierkens (2008), Value of ECMWF ensemble rainfall forecasts for forecasting catchment spatially distributed soil moisture. Catchment-scale Hydrological Modelling & Data Assimilation International Workshop III (CAHMDA III). Melbourne–Australia.

Schuurmans, J.M, M.F.P. Bierkens, E.J. Pebesma & R. Uijlenhoet (2004), Simulating high resolution rainfall fields for operational water management using meteorological radar and rain gauges. In Third European Conference on Radar in Meteorology and Hydrology (ERAD) together with the COST 717 seminar. Visby–Island of Gotland–Sweden.

Schuurmans, J.M, M.F.P. Bierkens, E.J. Pebesma & R. Uijlenhoet (2004), Estimating high resolution rainfall fields based on meteorological radar and rain gauges for operational water management. In Geophysical Research Abstracts 6 - 1st General Assembly. Nice–France: European Geosciences Union (EGU).

Schuurmans, J.M, M.F.P. Bierkens, P.A. Troch & Geer, F.C. van Geer (2004), Nowcasting for operational water management using reduced hydrological models and data assimilation. In Geophysical Research Abstracts 6- 1st General Assembly. Nice–France: European Geosciences Union (EGU).

Curriculum Vitae

Johanna Magritha (Hanneke) Schuurmans was born on 5 March 1977 in Harderwijk, The Netherlands, completing the family of six children. In 1995 she did her VWO exam at Lingecollege in Tiel. After that she started her study 'Soil, Water and Atmosphere' at Wageningen University and chose the specialization hydrology. For her first master thesis she worked at the waterboard 'De Maaskant' in Oss, The Netherlands. There she implemented the just released WATERNOOD method (groundwater controlled surface water management) in a part of the waterboard area. In 2000 she went for half a year to the International Water Management Institute (IWMI) in Sri Lanka. There she studied, in collaboration with a fellow student, the effect of several irrigation scenarios on plant growth and nutrient outflow. Back in the Netherlands she finished her study with a master thesis at Alterra, studying the implementation of remotely sensed evapotranspiration into a spatially-distributed hydrological model. This study resulted in the publication of Schuurmans et al. (2003). After her studies Hanneke worked for two years at the consultancy and engineering firm Grontmij in Houten as advisor hydrology. She exchanged her permanent position to start as PhD student at the department of Physical Geography of Utrecht University. Starting January 2009, Hanneke will be working at Future Water, a research and advisory company that works throughout the world to combine scientific research with practical solutions for water management, as researcher/advisor hydrology.